Thesis

on

Optimization and Analysis of Photovoltaic Systems under Uniform and Partial Shading Conditions

Shashank Kumar

Roll No.: 156102030

Supervisor: Dr. Sisir Kumar Nayak

DEPARTMENT OF ELECTRONICS AND ELECTRICAL ENGINEERING

INDIAN INSTITUTE OF TECHNOLOGY GUWAHATI

GUWAHATI - 781039

October 2024

Dedicated to

To

My Supervisor

Dr. Sisir Kumar Nayak

and

To

My parents,

My brothers and relatives for their support

Certificate

This is to certify that the thesis entitled "Optimization and Analysis of Photovoltaic Systems Under Uniform and Partial Shading Conditions," submitted by Shashank Kumar (156102030), a research scholar in the Department of Electronics and Electrical Engineering, Indian Institute of Technology Guwahati, for the award of the degree of Doctor of Philosophy, is a record of an original research work carried out by him under my supervision and guidance. The thesis has fulfilled all the requirements as per the regulations of the institute and in my opinion has reached the standard needed for submission. The results embodied in this thesis have not been submitted to any other University or Institute for the award of any degree or diploma.

Date:

Place: Guwahati.

Dr. Sisir Kumar Nayak
Professor
Dept. of Electronics and Electrical Engg
Indian Institute of Technology Guwahati
Guwahati - 781 039, Assam, India.

Acknowledgements

First and foremost, I consider it a privilege to express my sincere gratitude to my supervisor, Dr. Sisir Kumar Nayak, for his guidance and motivation throughout my study. I am particularly thankful for his assistance in teaching me about research paper writing.

I am also grateful to my current and former doctoral committee members, Dr. Sanjib Ganguly, Dr. A. Ravindranath, Dr. Praveen Kumar, and Dr. Praveen Tripathy, for dedicating their valuable time to evaluate the progress of my work. Their suggestions have been invaluable. I would like to express my thanks to Prof. Sukumar Mishra from IIT Delhi for providing access to their experimental facility and to Surya Prakash for his assistance in these experiments.

Furthermore, I would like to thank the Head of the Department and the other faculty members for their support in conducting this work. My thanks also go to Dr. Himanshu Sekhar Sahu, my senior, for his guidance and for introducing me to various concepts, ongoing research, and technical problems in the field of photovoltaic technology. This includes the concept of the double diode photovoltaic module and the problems associated with it. I am also grateful to Mr. Ridib Bharali and some other technical and non-technical staff for their support during this work.

I would like to thank Sandeep Kumar Sahoo, along with several juniors and seniors, and the research scholars of the Power Control Laboratory at IIT Guwahati, for their support. I extend my gratitude to my parents and to my brothers, Shashi Shekhar and Shitanshu Shekhar, for their support.

Shashank Kumar

Abstract

This thesis presents a new approach for converting the implicit current-voltage (I-V) expression of a photovoltaic (PV) module into an explicit expression of current as a function of voltage. The maximum power point (MPP) of a double diode model (DDM) PV module is estimated directly from the explicit I-V expression of a module under different environmental conditions (DECs). The extension of use of explicit I-V expression to estimate the MPP of a DDM PV module under different shading conditions is also carried out. Since the explicit I-V expression is used for the estimation of the MPP of a DDM PV module under both uniform and non-uniform irradiance conditions, the proposed method is simple, accurate, and efficient. A comparison of the MPP of a DDM PV module, as extracted using the proposed method, with that obtained from different existing methods under various irradiance conditions, is presented. The MPP of the DDM PV array at non-STC (Standard Test Condition), as determined by the proposed method, is verified through experimental measurements and MATLAB simulations. The results show that the estimation of the MPP of a DDM PV module using the proposed method is more accurate and computationally efficient. The explicit I-V expression of a module, used for estimating the MPP, will be useful to PV professionals.

This thesis also presents a novel generalized model of the series-parallel (S-P) connected PV array, along with its circuit equation, and an algorithm for estimating its global maximum power point (GMPP) under partial shading conditions (PSCs). A set theory-based approach is proposed to develop equations in terms of the voltage and current of strings and arrays in the generalized model of the S-P PV configuration under PSCs. Furthermore, a mathematical expression for the iteration voltage is derived based on a generally observed property of local maximum power point (LMPP). The proposed GMPP estimation algorithm converges quickly by simultaneously eliminating non-potential sections and subsections of the power-voltage (P-V) curve of an array. Robustness of the proposed method for GMPP estimation is tested by considering 2,000 random shading patterns generated by MATLAB for two different PV arrays. Comparisons with other existing methods in terms of GMPP estimation accuracy and computational time demonstrate

the competitiveness of the proposed method. Experimental validation of the proposed method was conducted using a box with halogen lights to measure the I-V characteristics of a PV array. Both simulation and experimental results demonstrate the superiority of the proposed GMPP estimation method for PV arrays under PSCs, making it valuable for PV professionals.

A novel approach is proposed for estimating the operating point of a photovoltaic (PV) source directly connected to single or multiple loads. This proposed algorithm divides the PV with load system into two components: PV without series resistance, and series resistance with load. The estimation of the operating point for the PV and load combination, using the proposed technique, is carried out by matching the I-V characteristics between the PV without series resistance and the series resistance with load, employing a novel method. As this proposed method is free from derivatives and does not require any prediction of the initial value, the estimation technique is notably simple in terms of computational complexity and applicability. The estimated results obtained from this technique closely match the actual results. Furthermore, the outcomes of this technique surpass those of other methods in terms of computational time. This proposed estimation technique will be beneficial for the design, operation, and maintenance of standalone PV systems, as well as for the energy management of various types of storage systems, such as thermal, mechanical, and chemical, connected to the PV source.

Finally, this thesis introduces a novel algorithm to estimate the parameters of a DDM PV module. Moreover, the bisection method is employed to identify the discrepancy between the MPP voltage obtained and the MPP voltage specified in the datasheet. This iterative process aids in determining the independent parameters, and subsequently, the other dependent parameters.

Contents

List of Tables

List of Figures

List of Acronyms

PV	Photovoltaic
DDM	Double Diode Model
SDM	Single Diode Model
I-V	Current-Voltage
P-V	Power-Voltage
MPP	Maximum Power Point
MPPT	Maximum Power Point Tracking
STC	Standard Test Condition
DEC	Different Environmental Condition
PS	Pattern Search
GS	Gauss Siedel
NR	Newton Raphson
LM	Levenberg Marquardt
PSC	Partial Shading Condition
S-P	Series-Parallel
LMPP	Local Maximum Power Point
GMPP	Global Maximum Power Point
GA	Genetic Algorithm
PSO	Particle Swarm Optimization
MVP	Most Valuable Player
F-SVR	Field Support Vector Regression

List of Symbols

G	Irradiance of light falling on the PV source in W/m^2
T	Temperature of the PV source in K
I_{sc}	Short circuit current of PV module
V_{oc}	Open-circuit voltage of PV module
I_{ph}	Photo-current of DDM PV module
I_{o1} and I_{o2}	Dark saturation currents of both diodes of a DDM PV module
R_s	Series resistance of DDM PV module
R_{sh}	Shunt resistance of DDM PV module
A_1 and A_2	Ideality factors of both diodes of DDM PV module
V_t	Thermal voltage at T Kelvin
N_s	Number of cells in the PV module
V	Voltage of the PV source
I	Current of the PV source
S_I	Function of which zeroes to be found for getting current of PV module at given V
F_i	Exponential part of function S_I which is to be approximated for getting explicit expression
P_{S_I}	A function whose zero approximates the current of the PV module at a given voltage V
I_L	Explicit expression of I using linear approximation of F_i between points (0, $F_i(0)$) and (I_{ph}, $F_i(I_{ph})$)
I_T	Explicit expression of I by approximating function F_i as a tangent line at point (0,$F_i(0)$)
I_G	Better explicit expression of I by approximation of F_i as first order order polynomial
I_{ij}	Current in the j^{th} group of i^{th} string
V_{ij}	Voltage of the bypass diode of the j^{th} group in i^{th} string
$I_{ph_{ijk}}$	Photo-current of unit PV source (group of series connected cells i.e., cell string, PV module) in the k^{th} subgroup in the j^{th} group of i^{th} string
$I_{o1_{ijk}}$ and $I_{o2_{ijk}}$	Dark saturation currents of unit PV source in the k^{th} subgroup in the j^{th} group of

	i^{th} string
V_{ijk}	Voltage of unit PV source in the k^{th} subgroup in the j^{th} group of i^{th} string
I_{ijk}	Current of unit PV source in the k^{th} subgroup in the j^{th} group of i^{th} string
G_{ijk}	Irradiance of unit PV source in the k^{th} subgroup in the j^{th} group of i^{th} string
T_{ijk}	Temperature of unit PV source in the k^{th} subgroup of the j^{th} group of i^{th} string
N_{ijk}	Number of unit PV source of the k^{th} subgroup of the j^{th} group of i^{th} string
T_{ij}	Temperature of the bypass diode of j^{th} group in the i^{th} string
$A_{1_{ijk}}$ and $A_{2_{ijk}}$	Ideality factors of unit PV source in the k^{th} subgroup of the j^{th} group of i^{th} string
$N_{s_{ijk}}$	Number of cells in unit PV source in the k^{th} subgroup of the j^{th} group of i^{th} string
$R_{s_{ijk}}$	Series resistance of unit PV source in the k^{th} subgroup of the j^{th} group of i^{th} string
$R_{sh_{ijk}}$	Shunt resistance of unit PV source in the k^{th} subgroup of the j^{th} group of i^{th} string
$A_{bp_{ij}}$	Ideality factor of the bypass diode of j^{th} group in the i^{th} string
$V_{t_{ij}}$	Thermal voltage of the bypass diode of j^{th} group in the i^{th} string
$I_{o_{ij}}$	Dark saturation current of the bypass diode of j^{th} group in the i^{th} string
q_{ij}	Number of the subgroups of j^{th} group in the i^{th} string
A_{bl_i}	Ideality factor of the blocking diode of the i^{th} string
V_{t_i}	Thermal voltage of the blocking diode of the i^{th} string
I_i	Current through the i^{th} string
V_i	Voltage of the i^{th} string
R_i	Equivalent resistance of the connecting wires in the i^{th} string
$R_{c_{i(i+1)}}$	Equivalent resistance of the connecting wires between the i^{th} and $(i+1)^{th}$ string
I_{o_i}	Dark saturation current of the blocking diode in the i^{th} string
V_{b_i}	Voltage across the blocking diode in the i^{th} string
V_S	Row matrix to store starting values of voltages of present eligible sections
V_S^{Pre}	Row matrix to store the initial values of voltages of previous eligible sections
I_S	Row matrix to store starting values of currents of present eligible sections
I_S^{Pre}	Row matrix to store starting values of currents of previous eligible sections

P_S	Row matrix to store starting values of power of present eligible sections
P_S^{Pre}	Row matrix to store starting values of power of previous eligible sections
V_F	Row matrix to store the final values of voltages of present eligible sections
V_F^{Pre}	Row matrix to store the final values of voltages of previous eligible sections
I_F	Row matrix to store the final values of currents of present eligible sections
I_F^{Pre}	Row matrix to store the final values of currents of previous eligible sections
P_F	Row matrix to store the final value of powers of present eligible sections
P_F^{Pre}	Row matrix to store the final values of powers of previous eligible sections
M	Maximum power among currently known points
N_{ES}	Number of eligible sections
N_{ES}^{next}	Number of eligible section for next iteration
f_L	Explicit current expression of electrical load as function of V
f_{PV}	Explicit current expression of PV without R_s, unit as function of V_{sh}
F_L	Explicit current expression of load with R_s, unit as function of V_{sh}
I_{SC}	Rated short circuit current at STC of PV module
V_{OC}	Rated open-circuit voltage at STC of PV module
V_{MP}	Rated maximum power point voltage at STC of PV module
I_{MP}	Rated maximum power point current at STC of PV module

Chapter 1

Overview

Contents

1.1 Introduction

Electricity can be generated from solar energy primarily through two methods: Solar Thermal Energy Systems and Photovoltaics (PV), as illustrated in Figure 1.1. The first one, Solar Thermal Energy System, uses solar energy to heat some kind of fluid which drives an electrical generator to get the electricity. The latter, i.e., PV, directly converts the solar radiation to electrical energy. The working of PV can be explained by the photovoltaic effect. Due to the absence of any moving part, it requires very little maintenance. Further, it has the advantage of high scalability, allowing its use from home installations to GW-level solar plants. Also, due to environmental concerns and the falling cost, the PV generator is becoming the highly favorable source of electricity.

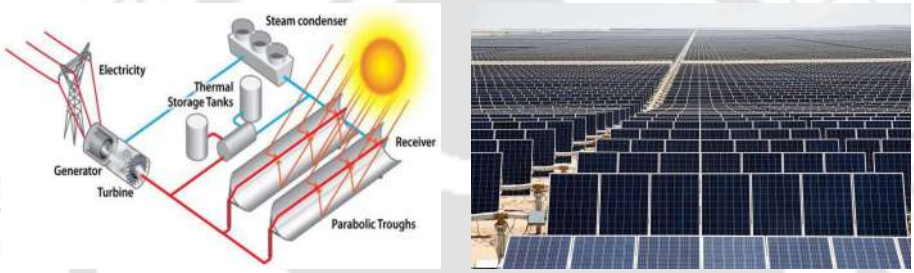

(a) Solar Thermal Power Plant (b) Solar Photovoltaic Power Plant

Figure 1.1: Both types of solar power plants. (a) Solar thermal power plant (Source: MDPI, available at https://www.mdpi.com/1996-1073/12/13/2454). (b) Solar photovoltaic power plant (Source: Recharge News, available at https://www.rechargenews.com/transition/-solar-to-be-world-s-largest-power-source-by-2050-as-cost-halves/2-1-558127).

The PV cell is the smallest unit of a PV generator. Most of the solar cells available on the market are manufactured using silicon, as shown in Figure 1.2. To achieve a usable output voltage, given that the open circuit voltage of a PV cell is quite low, many cells are connected in series or in a series and parallel (S-P) combination, forming what is known as a PV module. Furthermore, the combination of different modules is called a PV array. The current-voltage (I-V) characteristic of a PV generator is implicit in nature. This complexity complicates the analysis of a PV generator's behavior under specific parameters in given environmental conditions. The expression relating I-V in a PV generator is crucial for studying the behavior of PV generators under different environmental conditions. Furthermore, it plays a significant role in designing components for systems utilizing PV technology. Estimating the maximum power point (MPP)

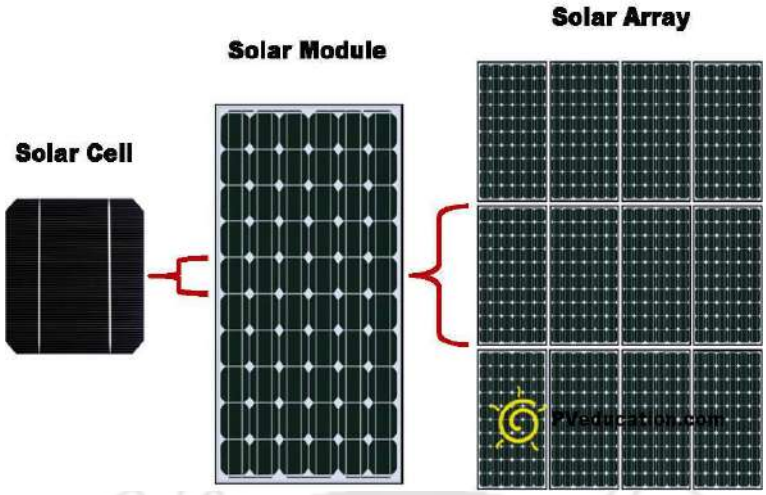

Figure 1.2: PV cell, module, and array (Source: PV Education, available at https://pveducation.com/solar-concepts/solar-cells-modules-arrays/).

is crucial for forecasting the maximum energy output of a PV plant. This estimation also facilitates the maximum power point tracking (MPPT), as PV generators operate at their peak power output only at a specific operating point.

Figure 1.3: Partial shading in a real-life situation (Source: Solar Panels Melbourne Victoria, available at http://www.solarpanelsmelbournevictoria.com.au/about-us/).

Certain environmental conditions in some locations can lead to the soiling of PV array modules, resulting in an uneven distribution of sunlight across the modules. Additional factors, such as differing orientations, uneven mounting surfaces, proximity to trees, and nearby buildings, can also contribute to an uneven distribution of solar irradiance on the solar PV array, a phe-

nomenon known as partial shading, as shown in Figure 1.3. The accurate estimation of the global maximum power point (GMPP) of a PV array under partially shaded conditions poses a greater challenge than under uniform irradiance conditions due to the presence of multiple peaks or local maximum power points (LMPPs) in the power-voltage (P-V) curve. Due to multiple peaks, most algorithms that can accurately estimate the MPP under uniform irradiance may not find the GMPP in partially shaded conditions. They may become stuck at a local peak that is not the GMPP. Therefore, a specialized algorithm is required to identify the highest peak among all local peaks and accurately determine the GMPP in partially shaded condition.

Estimating the operating point for a PV system connected to a specific load is crucial for analyzing fault scenarios in the integration of PV systems with grids (such as nano grids, micro grids, and mini grids). Furthermore, this estimation is valuable in the design of systems that incorporate PV technology. Simulation tools like SPICE are generally used to solve circuits, including PV systems connected to an electrical load or loads. However, these software programs generate circuit equations using the Modified Nodal Analysis (MNA) technique. Subsequently, multi-variable equations are solved using the multidimensional Newton-Raphson (NR) method. Nonetheless, during this process, MNA introduces unnecessary variables for forming the equations, and the use of the multidimensional NR method increases computational complexity and decreases robustness.

Parameter estimation is necessary to accurately simulate a PV model under varying environmental conditions. Parameter estimation algorithms can be divided into three main categories: analytical, iterative, and population search-based methods. Analytical methods use additional equations, approximations, and information to estimate the parameters. Iterative algorithms essentially solve the error minimization problem using iterative techniques. The population search-based methods for parameter estimation start with many initial values for a parameter and find the optimal population of parameters using various techniques. The estimation of PV parameters is of great importance in analyzing the behavior of PV systems under different environmental conditions. Furthermore, it plays a significant role in accurately estimating the MPP and determining the optimal operating point for PV systems.

Although PV technology offers several advantages, it also presents challenges that must be addressed. These challenges include the implicit I-V expression of PV systems, the complexity of determining the operating point, the MPP, and parameter estimation. These complexities arise from the implicit I-V expression of PV systems and the presence of multiple LMPPs in PV arrays under partially shaded conditions.

Therefore, this research aims to contribute significantly to the advancement and optimization of solar energy utilization by investigating various aspects of PV systems. This includes exploring different modeling approaches, developing efficient methods for MPP estimation, parameter estimation, and operating point determination under both uniform and partially shaded conditions.

1.2 Literature survey

1.2.1 Explicit expression of DDM PV module and the estimation of MPP in uniform and Partially Shaded Conditions

There are two main types of mathematical models for studying the I-V characteristics of a PV source: (1) the Single Diode Model (SDM) and (2) the Double Diode Model (DDM), both of which present the I-V relationship in implicit form. The circuit representations of both models are given in Fig. 1.4. I_{ph}, I_D, R_{sh}, R_s, V, and I are the photocurrent, diode current, shunt resistance, series resistance, voltage, and current of the SDM as shown in Fig. 1.4(a). Meanwhile, I_{ph}, I_{D1}, I_{D2}, R_{sh}, R_s, V, and I are the photocurrent, current in Diode 1, current in Diode 2, shunt resistance, series resistance, voltage, and current of the DDM as shown in Fig. 1.4(b).

The DDM is known to have better accuracy at certain conditions [1, 2]. Lumped-circuit models with multiple diodes have been broadly accepted to accurately describe the I–V characteristics [3]. The SDM is particularly inaccurate in describing cell behavior at low illuminations [4]. While the DDM is consistent with the underlying physics of the electrical characteristics and should give an accurate description of the real solar cell for low-level- injection conditions [5]. In [6], some assumptions have been made in deriving the explicit I-V expression of the DDM PV module based on the Lambert-W function. These assumptions are not accurate and introduce

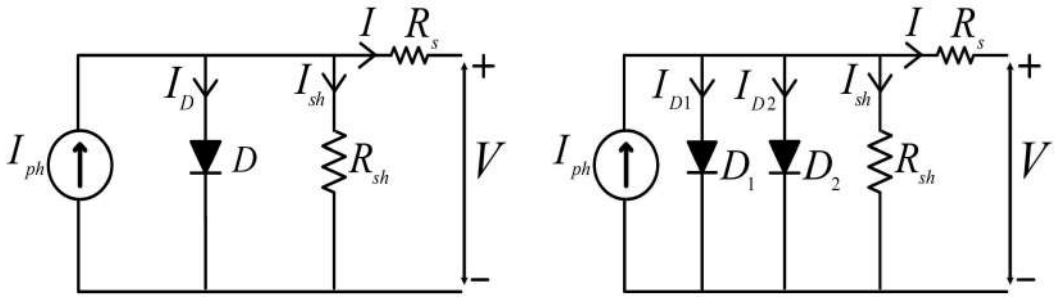

Figure 1.4: Main mathematical models of a PV module (a) Single Diode Model (SDM) and (b) Double Diode Model (DDM)

error. In [7], an exact representation of the conversion from implicit to explicit form using the Lambert-W function for DDM is shown. However, the Lambert-W function-based approximation requires more computational time because the Lambert-W function is not an elementary function and utilizes approximate series expansions for obtaining values.

For MPP estimation of PV systems, there is extensive literature available. In [8], two simple and powerful maximum power-point tracking techniques (based on computational methods) known as voltage-based MPPT (VMPPT) and current-based MPPT (CMPPT) are simulated, constructed, and compared. These two methods only require I_{sc} and V_{oc} of the PV module at the given environmental conditions. The MPP values obtained using these methods are V_{MPP}=$M_V V_{oc}$ and I_{MPP}=$M_C I_{sc}$, where V_{MPP}, I_{MPP}, M_V and M_C represent the MPP voltage, MPP current, voltage factor and current factor, respectively. This simplicity facilitates straightforward implementation, yet the accuracy of these methods is relatively low. Estimating the MPP of a PV array under various environmental conditions involves using modified Gauss-Seidel (GS), Newton-Raphson, Levenberg-Marquardt, and other iterative techniques. However, these methods may not always achieve convergence. Levenberg-Marquardt (LM) algorithm is used to estimate the MPP of a DDM PV module under different environmental conditions [9]. However, the LM method requires manually inputted initial values, dependent on the situation for the solution and the acceleration coefficient. If chosen arbitrarily, the method may fail to converge. This issue is also encountered with the GS and NLS methods, with the GS method being notably slower than the LM method.

In [10], the authors proposed an empirical expression for determining the value of the MPP voltage as a function of temperature. This expression was obtained through regression analysis of experimental data from various modules tested under different environmental conditions. However, this expression is not considered reliable and yields significant errors in many cases. Conversely, [1] presents a more accurate empirical expression for predicting the GMPP of a partially shaded PV array. Nevertheless, it does not achieve high accuracy for all types of modules and shading conditions.

1.2.2 Analysis of generalized series-parallel PV arrays under partial shading: I-V and P-V curves, MPP estimation challenges

The mathematical formulations for calculating the $I-V$ and $P-V$ characteristics of partially shaded photovoltaic (PV) arrays are presented in [11–14]. However, these studies fail to minimize the number of variables and equations by not assuming identical current and voltage variables for the PV submodules and bypass diodes under the same environmental conditions, specifically irradiance and temperature, for a partially shaded array. This absence of minimization results in equations that require more time to solve and demand additional storage in the system. Moreover, all these formulations are confined to the S-P PV array configuration and presuppose uniform irradiance levels across all cells in a submodulean assumption that may not always be valid, as not all cells within a submodule might be exposed to the same environmental conditions. Additionally, these studies overlook the resistances of connecting wires, omitting a crucial aspect that would offer a more accurate depiction of the PV array's operational dynamics.

The estimation of the MPP for a PV generator under partial shading conditions (PSCs) presents more difficulties than it does under conditions of uniform irradiance, attributable to the emergence of multiple peaks. Such complexity significantly complicates the task of accurately determining the global maximum power point (GMPP) of a PV array when subjected to PSC, necessitating the adoption of advanced algorithms or methodologies for precise estimation.

In response to this challenge, authors have developed simplified approximate formulas to estimate the GMPP [15], [10], [1]. The effectiveness and accuracy of these methods hinge on the

specific shading parameters of partial shading, namely the irradiance levels and the number of modules at each irradiance level.

In [16], authors present a novel Psim-based piece-wise linear macro-model. Psim is a software for simulating power electronic system. The new model can be used to predict PV module characteristics for various operating conditions and understand the behaviours of a long PV string and a large-scale PV array under any PSC patterns on Psim platform. Furthermore, analyses of the I-V and P-V curves of a PV string under PSC of several shading cases were conducted in [17]. These studies have provided significant observations regarding the MPP of a PV string in PSCs. In [18], several rules for general shading patterns of PV array are unveiled. Such insights are crucial for approximating the LMPP and, consequently, the GMPP. However, it should be noted that these methods are not universally robust and may yield incorrect results in different cases of partial shading. In [19], authors propose a field-support vector regression (F- SVR) based MPPE approach for estimating the MPP in PSC. In this, a conventional SVR is applied to study the mapping relationship between PV electrical characteristics and the MPP locus.

Maximum power point tracking (MPPT) algorithms for identifying the global maximum power point (GMPP) have been proposed in various studies, including [20], [21], and [22]. These algorithms primarily employ intelligent strategies to reduce the regions of the P-V curve that need to be investigated for the GMPP. However, even with the reduction of certain regions, these methods still necessitate small step perturbations in voltage to precisely identify the GMPP. Consequently, this approach could potentially extend the time required for GMPP estimation. Thus, employing these techniques may lead to longer durations for GMPP estimation.

1.2.3 Operating point estimation of a PV plus load system

To solve the $I - V$ characteristic equation at a specific situation (i.e., at a particular voltage or load), iterative methods such as Newton-Raphson (NR), Levenberg-Marquardt (LM) [23–26], among others, are employed. However, it is often observed that these algorithms experience convergence failure.

The Wave method [12] has been proposed for estimating the operating point of a PV system with a resistive load. In this method, authors apply the single dimension NR on a modified function incorporating two extra independent parameters and a single variable, namely, voltage, to determine the operating point voltage and current for a given load resistance connected to a PV system. Due to the modified expression being more complex and requiring three manual initializations and derivative calculations, it is more computationally intensive. Furthermore, the Wave method necessitates a good initial guess to converge within a reasonable timeframe. However, this method is not suitable for all types of loads.

Conversely, artificial intelligence methods [27,28] require a substantial amount of datasets for training and implementation. Accumulating such datasets poses a challenge for PV installers. Moreover, processing these large datasets increases computational complexity and can lead to issues with computer memory.

1.2.4 Parameter estimation of a DDM PV module

Parameter estimation algorithms can be divided into three main categories: analytical, iterative, and population search-based methods. Analytical methods utilize extra equations, approximations, and information to estimate parameters. For example, the analytical methods in [29] use datasheet information.

Iterative algorithms, such as nonlinear least squares (NLS) [30], essentially solve the error minimization problem. In [26], an LM based iterative method is used for parameter estimation. A pattern search-based algorithm is proposed in [31] for parameter estimation of PV modules. On the other hand, population search-based methods for parameter estimation start with many sets of randomly generated parameters and use various techniques to find the optimal set. Differential evolution algorithm is a heuristic, population-based method [32]. Many nature inspired algorithms are reviewed in [33]. In [34,35] population based methods which utilize GA are used. However, population-based methods produce different values in each run and is not very reliable.

A separable non-linear least square search (SNLSS) is proposed in [36] to estimate the PV parameters. For a fixed value of R_s, the least square algorithm is applied to minimize the

error and determine the other four linear parameters. The parameter R_s is optimized using the Nelder-Mead algorithm, which is an iterative method.

1.3 Motivation

Considering the aforementioned limitations, the motivation of this research work are as follows:

- The literature review reveals that the DDM of a PV module is more complex than the SDM due to the presence of two exponential terms in its implicit characteristic equation, which renders the DDM PV module computationally inefficient for simulation. Due to this complexity, very few attempts have been made to accurately convert the implicit characteristic equation of the DDM into an explicit form. Therefore, an explicit $I - V$ characteristic equation that approximates the DDM PV module is needed to simulate a PV system with the accuracy of the DDM while reducing the computational challenges.

- The review also highlights that the available MPP estimation algorithms lack accuracy and computational efficiency, thereby increasing computational complexity. Additionally, many estimation techniques require an initial value of the solution, which depends on human experience with the system. Thus, a fast and accurate MPP estimation technique that does not rely on human-based input is necessary.

- Some authors have proposed empirical expressions for determining the GMPP value of a partially shaded PV array. However, these expressions, based on regression analysis of experimental data from PV arrays with different types of PV modules under various shading conditions, sometimes yield erroneous results. An exact mathematical method is therefore required to accurately estimate the GMPP of a partially shaded PV array.

- It is observed that methods for drawing $I-V$ and $P-V$ curves involve numerous variables and equations, which are not computationally efficient. These mathematical models are valid only when all cells in a submodule are under the same environmental conditions, i.e., identical irradiance and temperature. Moreover, the models do not account for the

resistance of connecting wires, which is crucial for accurately estimating the MPP of a PV system. Therefore, a model of the PV array under PSCs that considers the resistance of connecting wires is required.

- The literature indicates that authors have developed algorithms employing intelligent strategies to reduce the regions of the P-V curve requiring investigation for the GMPP. However, even after narrowing down specific regions, these methods still use small step perturbations in voltage to identify the GMPP, potentially prolonging the time needed for GMPP estimation. Therefore, a fast algorithm to precisely estimate the GMPP values for a partially shaded PV array is needed.

- It is noted that population search-based algorithms necessitate significant memory for storing and accessing fitness values for population members. Meanwhile, many existing iterative parameter estimation techniques require manual initialization. The iterative estimation techniques relying solely on datasheet values must incorporate an additional equation, namely that the rate of change in power with respect to voltage is zero ($\frac{dP}{dV} = 0$) at the MPP voltage.

1.4 Objective

- To convert the implicit double diode model (DDM) PV module expression into an explicit form.

- To develop a fast and accurate maximum power point (MPP) estimation technique for PV systems, independent of case-based manual input.

- To formulate a mathematical model for a specific case of a series-parallel (S-P) PV array, incorporating bypass and blocking diodes.

- To construct a mathematical model to depict the $I - V$ and $P - V$ characteristics of a generalized model of an SP partially shaded PV array, taking into account the resistances of connecting wires.

- To devise a rapid method to precisely estimate the global maximum power point (GMPP) of a general case of an SP partially shaded PV array, accommodating any shading pattern and including the resistance of connecting wires.

- To develop a fast iterative algorithm that consistently converges to estimate the operating point of a PV system directly connected to a load.

- To create a fast iterative parameter estimation technique that eliminates the need for case-based manual initialization and the additional equation derived from the derivative at the MPP.

1.5 Contributions of the thesis

The contributions of this thesis are summarized as follows:

- The third order partial derivative of the exponential component of the implicit $I - V$ equation with respect to I, for the double diode model (DDM) of nearly all commercially available PV sources under all irradiances and temperatures commonly found on Earth, is approximately zero for $0 \leq I \leq I_{\text{ph}}$ and $V \in [0, V_{\text{oc}}]$. Furthermore, this partial derivative of the exponential component decreases further with an increase in the order of derivative.

- Utilizing the property described above, it is found that the exponential component of the implicit I-V equation for the DDM PV module can be accurately approximated by second-order or higher-order polynomials in terms of I (where $0 \leq I \leq I_{\text{ph}}$) at a given voltage $V \in [0, V_{\text{oc}}]$. Furthermore, the root-mean-square (rms) of the approximation error generally decreases as the order of the polynomial used for approximating the exponential term increases. This trend is consistent for most commercially available PV sources under typical environmental conditions on Earth. However, the RMS error between the polynomial approximation and the exponential term may increase beyond a certain order in many cases. The fact that the exponential component can be approximated by a polynomial in terms of I (where $0 \leq I \leq I_{\text{ph}}$) of order two or higher at a given voltage is further

utilized to derive a second-order polynomial approximation-based explicit expression for the current in the DDM PV module, expressed solely in terms of voltage.

- Development of an accurate, robust, and fast maximum power point (MPP) estimation algorithm that eliminates the need for case-specific manual input.
- Creation of an algorithm that estimates the global maximum power point (GMPP) of a special case of series-parallel connected partially shaded PV array using a genetic algorithm.
- Formulation of an accurate, robust, and fast MPP estimation algorithm for the GMPP of a general case of series-parallel connected partially shaded PV array.
- Introduction of a parabola-based iterative algorithm that consistently converges to estimate the operating point of a PV system directly connected to a load without requiring case-specific manual input.
- Establishment of a fast iterative parameter estimation technique that obviates the need for case-specific manual initialization and the additional equation derived from the power derivative with respect to voltage at the MPP.

1.6 Organization of the Thesis

This thesis is organized into the following chapters:

- Chapter 2 discusses the derivation of an explicit $I - V$ expression from the implicit $I - V$ expression for the double diode model (DDM) of a PV module. This chapter also explores the use of this expression for estimating the maximum power point (MPP) of a PV array. It proposes a fast, accurate, and robust method for MPP estimation, based on the properties of an isosceles triangle. Moreover, a genetic algorithm-based technique is introduced for estimating the global maximum power point (GMPP) for a special case of a series-parallel PV array under partial shading conditions.

- Chapter 3 introduces a novel method for estimating the $I-V$ characteristics of a generalized model of a series-parallel PV array. It also presents a rapid, reliable, and precise technique for GMPP estimation. This technique is designed to ensure fast and accurate GMPP estimation under various shading conditions.

- Chapter 4 proposes a new technique using a parabola-based approach for fast and accurate estimation of the operating point of a PV-load system. This method aims to enhance the efficiency and precision in determining the operating conditions of the system.

- Chapter 5 unveils a rapid iterative parameter estimation technique that removes the need for manual initialization and the reliance on an additional equation derived from the derivative of power with respect to voltage at the MPP. This technique provides a swift and efficient means of parameter estimation without the conventional requirements.

- Chapter 6 offers conclusions and extensions from the conducted research, discussing the implications and findings of the study. It also outlines potential avenues for further research and development in the field.

Chapter 2

MPP estimation of a double diode model PV module from explicit I-V characteristic

Contents

2.1 Introduction

Nowadays, pollution and limitations of conventional fuels have given rise to the need for renewable energy sources. Photovoltaic (PV) power system is growing rapidly in the present scenario, because the solar energy source is free from environmental pollution and has low maintenance [37]. Proper modeling of PV cells, as well as the modules, are required to understand the behavior of the PV systems.

In the literature, two different ways for modeling of a PV cell or module such as single diode model (SDM) and double diode model (DDM) are proposed. The DDM is known to have better accuracy, especially at low irradiance level [2]. Lumped-circuit models with multiple diodes have been broadly accepted to accurately describe the I–V characteristics [3]. The SDM is particularly inaccurate in describing cell behavior at low illuminations [4]. While the DDM is consistent with the underlying physics of the electrical characteristics and should give an accu- rate description of the real solar cell for low-level- injection conditions [5].

The current-voltage (I-V) relationships of SDM and DDM PV module are generally in implicit form. However, the implicit expression can be solved using an iterative method and difficult to estimate the current value at a particular voltage. Therefore, the conversion of implicit expression to the explicit expression of current is needed for both SDM and DDM. An explicit expression of current to estimate the MPP for SDM PV module has been considered by Saloux, Teysseduo, and Sorin[38]. Since this model considers ideal case of a photovoltaic module, it is less accurate. In [15] and [39], an explicit expression of current in terms of voltage using Lambert-W function is described for an SDM of a PV module. In [6] and [7], Lambert-W based representation for current of DDM PV module is presented. The biggest obstacle to get the Lambert-W function based exact representation of DDM is the presence of two exponential terms [7]. In [6], some assumptions have been made in the derivation of the explicit I-V expression of the DDM PV module based on the Lambert-W function. Due to these assumptions the explicit expression of current is less accurate for some cases. For estimation of current at a given voltage, the Pade approximation, series expansion, and asymptotic expression are considered. Hence, if these ap-

proximations are used, then the Lambert-W based expression of current produces more error in estimating the current at a particular voltage. Therefore, this chapter presents an explicit I-V expression of a DDM PV module which shows less % error and less computational complexity. The values of diode quality factors are generally greater than or equal to 1 as also taken in [40]-[41]. The aforementioned fact is useful in the development of explicit expression of current as seen later.

In literature, many methods have been reviewed for MPPT of a PV module[42]. Hill climbing/P&O based methods [43] and[44] are used to track the MPP of a PV module. Pattern search (PS) algorithm is used in [31] to estimate the parameters of a PV module. In an artificial intelligence method, MPP is estimated after training of a neural network. Fuzzy logic [27] is used for MPPT. In [28], a three layer feed-forward neural network is used: an input, a hidden and an output layer to estimate MPP voltage and power of PV array. Due to the requirement of data for training, these methods comparatively require more human intervention and its accuracy depends on the quality of the data and feedback provided by human.

The indirect methods (quasi seeks) [45] have the particular feature that the MPP is estimated from the measures of the PV generators voltage and current, the irradiance, or using empirical data, by mathematical expressions of numerical approximations. In [8], two simple and powerful MPPT techniques (based on computational methods) known as VMPPT and CMPPT are simulated, constructed, and compared. These two methods only require I_{sc} and V_{oc} of the PV module at the given environmental conditions. These are also simple in implementation. However, the accuracy of the above two methods is not good. In [46], Newton-Raphson (NR) method is employed for estimation of the MPP of a PV source. The estimation of MPP of a PV source under different environmental conditions is carried out using modified Gauss-Seidel (GS) in [47]. Levenberg-Marquardt (LM) algorithm is used to estimate the MPP of a DDM PV module under different environmental conditions [9]. But, these itterative methods in some cases may not converge. In order to reduce complexity, increase robustness and accuracy, a novel MPP estimation technique is proposed which uses the explicit expression of current. This method for estimation of MPP of a DDM PV module ensures the accuracy, computational efficiency, and robustness.

In large PV plant, many modules are connected in series-parallel. However, the modules of the PV array receive different irradiance in the many real-time scenario. This scenario causes mismatch loss within the PV array. To reduce the mismatch losses, bypass diodes are used in parallel with the PV modules. However, the P-V curve of a PV array contains multiple peaks due to bypass diodes under non-uniform irradiation condition. Hence, it is difficult to estimate GMPP in partially shaded PV array. Some authors have proposed the empirical expressions of GMPP of a partially shaded PV array [10] and [1]. However, these expressions are not robust for all types of modules and environmental conditions.

To address the problem of estimation of the GMPP, a novel mathematical formulation of a partially shaded PV array has been proposed which is optimized to the GMPP using genetic algorithm (GA) in this thesis.

2.2 Conversion of implicit into explicit I-V expression of a DDM PV module

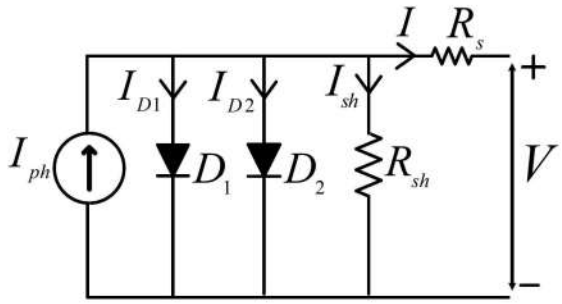

Figure 2.1: Equivalent circuit of DDM of the PV module.

The electrical equivalent of a DDM PV module is given in Fig. 2.1. The I-V characteristics of a PV module using DDM can be written as follows:

$$I = I_{ph} - I_{o1}\left\{\exp\left(\frac{V+IR_s}{A_1N_sV_t}\right)-1\right\} - I_{o2}\left\{\exp\left(\frac{V+IR_s}{A_2N_sV_t}\right)-1\right\} - \frac{V+IR_s}{R_{sh}} \tag{2.1}$$

$$I = I_{ph} - I_{o1}\left\{\exp\left(\frac{V+IR_s}{A_1N_sV_t}\right)\right\} + I_{o1} - I_{o2}\left\{\exp\left(\frac{V+IR_s}{A_2N_sV_t}\right)\right\} + I_{o2} - \frac{V+IR_s}{R_{sh}} \tag{2.2}$$

Here, I_{ph}, I_{o1}, I_{o2}, A_1, A_2, R_s, R_{sh}, N_s, and V_t represent the photocurrent, dark saturation

current 1, dark saturation current 2, diode quality factor 1, diode quality factor 2, series resistance, shunt resistance, number of cells, and thermal voltage of a DDM PV module, respectively.

Now assuming F_i is given as follows:

$$F_i = I_{oi}\left\{\exp\left(\frac{V+IR_s}{A_iN_sV_t}\right)\right\}_{i=1,2} \tag{2.3}$$

$\frac{\delta F_i}{\delta I}$ is written as follows:

$$\frac{\delta F_i}{\delta I} = I_{oi}\left(\frac{R_s}{N_sA_iV_t}\right)\exp\left(\frac{V+IR_s}{A_iN_sV_t}\right) \tag{2.4}$$

$$\frac{\partial^2 F_i}{\partial I^2} = I_{oi}\left(\frac{R_s}{N_sA_iV_t}\right)^2\exp\left(\frac{V+IR_s}{A_iN_sV_t}\right) \tag{2.5}$$

$$\frac{\partial^3 F_i}{\partial I^3} = I_{oi}\left(\frac{R_s}{N_sA_iV_t}\right)^3\exp\left(\frac{V+IR_s}{A_iN_sV_t}\right) \tag{2.6}$$

similarly,

$$\frac{\partial^n F_i}{\partial I^n} = I_{oi}\left(\frac{R_s}{N_sA_iV_t}\right)^n\exp\left(\frac{V+IR_s}{A_iN_sV_t}\right) \tag{2.7}$$

For $n \geq 3$, $A_i \geq 1$, $V \in [0, V_{\text{oc}}]$, $I \in [0, I_{\text{ph}}]$, and for typical values of I_{oi}, R_s, N_s, V_t, V_{oc}, and I_{ph}, which are found in commercially available PV sources under commonly found environmental conditions on Earth,

$$\frac{\partial^n F_i}{\partial I^n} \approx 0 \tag{2.8}$$

According to Lagrange's error formula for polynomial approximation:

If

$$P_i = C_{i(n-1)}I^{n-1} + C_{i(n-2)}I^{n-2} + \ldots + C_{i0} = \sum_{k=1}^{n} C_{i(k-1)}I^{k-1}$$

matches

$$F_i \text{ at } I_1(=0), I_2, \ldots, I_n(=I_{ph}), \text{ at a constant } V, \quad \forall V \in [0, V_{oc}],$$

then, $\forall I \in [0, I_{ph}], \forall V \in [0, V_{oc}]$, and for any $n \geq 3$:

$$F_i(I) - P_i(I) = \frac{1}{n!}\left(\left.\frac{\partial^n F_i(I)}{\partial I^n}\right|_{I=\xi}\right)\prod_{q=1}^{n}(I - I_q) \approx 0$$

at a constant V. The above equation is valid for some $\xi \in [0, I_{ph}]$.

Therefore, for $n \geq 3$, the function F_i is approximated as follow:

$$F_i = C_{i(n-1)}I^{n-1} + C_{i(n-2)}I^{n-2} + ... + C_{i0} \tag{2.9}$$

where $C_{i(n-1)}$, $C_{i(n-2)}$, ...and, C_{i0} are coefficients of different orders of I which are I^{n-1}, I^{n-2}, I^{n-3},.....and, I^0. To find the these coefficients, any n values for I are taken from the arithmetic progression series 0, $\frac{I_{ph}}{2(n-1)}$,.....and, I_{ph}, which is discussed further. The term $\left(\frac{R_s}{N_s A_i V_t}\right)$ is less than one for the typical values of R_s,N_s,A_i and V_t. The reason behind the above fact is that, in any good PV source series resistance per cell $\left(\frac{R_s}{N_s}\right)$ is less than the value of V_t (i.e., 0.0229) at a temperature of -10^oC and the value of A_i is always greater than or equal to one. Therefore, $\frac{\partial^n F_i}{\partial I^n}$ decreases with increase in the order of differentiation 'n' and comes more close to zero with increase in 'n'. Therefore, the accuracy of the polynomial approximation generaly increases with increase in 'n' for nearly all commercially available PV sources under typical irradiance and temperature conditions on Earth. However, it is possible that the RMS error between the polynomial used for approximation and the exponential term may increase beyond a certain higher order in many cases, even when $\frac{\partial^n F_i}{\partial I^n}$ decreases with n, primarily due to the effect of $\prod_{q=1}^{n}(I - I_q)$ in many of those cases.

In this chapter, F_i is approximated by a second-order polynomial (considering $n = 3$ in equation (2.9)). This approximation is valid even for $n = 2$ (first-order polynomial), provided F_i is approximated over an appropriately reduced interval, a subset of $[0, I_{ph}]$. These facts are also generally applicable to the exponential term in the single diode model (SDM). A significant portion of this chapter is devoted to the second-order polynomial approximation of F_i.

Taking second-order approximation, the polynomial, F_i is written as follows:

$$F_i \approx C_{i2}I^2 + C_{i1}I + C_{i0} = \sum_{k=1}^{3} C_{i(k-1)}I^{(k-1)} \tag{2.10}$$

To find the coefficients C_{i2}, C_{i1} and C_{i0}, the values of $F_{i(i=1,2)}$ in (2.3) are matched with approximated quadratic polynomial in (2.10) at three points $(V, 0)$, (V, I_{ph}) and $\left(V, \frac{I_{ph}}{2}\right)$ for all $V \in [0, V_{oc}]$.

By taking point $(V, 0)$ for $(V,\ I)$

Substituting $(V, 0)$ in (2.3) and (2.10) and equating, following equation is obtained as follows:

$$C_{i0} = I_{oi} \exp\left(\frac{V}{A_i N_s V_t}\right) \tag{2.11}$$

By taking point (V, I_{ph}) for $(V,\ I)$

Substituting (V, I_{ph}) in (2.3) and (2.10) and equating, following equation is obtained as follows:

$$C_{i2}{I_{ph}}^2 + C_{i1} I_{ph} + C_{i0} = I_{oi} \exp\left(\frac{V + I_{ph} R_s}{A_i N_s V_t}\right) \tag{2.12}$$

Substituting C_{i0} from (2.11) in (2.12),

$$C_{i2} I_{ph} + C_{i1} = \left(\frac{I_{oi}}{I_{ph}}\right)\left\{\exp\left(\frac{V + I_{ph} R_s}{A_i N_s V_t}\right) - \exp\left(\frac{V}{A_i N_s V_t}\right)\right\} \tag{2.13}$$

By taking point $\left(V, \frac{I_{ph}}{2}\right)$ for $(V,\ I)$

Substituting $\left(V, \frac{I_{ph}}{2}\right)$ in (2.3) and (2.10) and equating, following equation is obtained as follows:

$$C_{i2}\left(\frac{I_{ph}}{2}\right)^2 + C_{i1}\left(\frac{I_{ph}}{2}\right) + C_{i0} = I_{oi} \exp\left(\frac{V + \left(\frac{I_{ph}}{2}\right) R_s}{A_i N_s V_t}\right) \tag{2.14}$$

Substitute C_{i0} from (2.11) in (2.14),

$$0.5 I_{ph} C_{i2} + C_{i1} = \frac{2 I_{oi}}{I_{ph}}\left\{\exp\left(\frac{V + 0.5 I_{ph} R_s}{A_i N_s V_t}\right) - \exp\left(\frac{V}{A_i N_s V_t}\right)\right\} \tag{2.15}$$

By subtracting (2.15) from (2.13), C_{i2} is obtained as follows:

$$C_{i2} = \frac{2 I_{oi}}{{I^2}_{ph}}\left\{\exp\left(\frac{V + I_{ph} R_s}{A_i N_s V_t}\right) + \exp\left(\frac{V}{A_i N_s V_t}\right) - 2\exp\left(\frac{V + 0.5 I_{ph} R_s}{A_i N_s V_t}\right)\right\} \tag{2.16}$$

Substituting C_{i2} in (2.13), C_{i1} is obtained as follows:

$$C_{i1} = \left(\frac{I_{oi}}{I_{ph}}\right)\left\{-\exp\left(\frac{V + I_{ph} R_s}{A_i N_s V_t}\right) - 3\exp\left(\frac{V}{A_i N_s V_t}\right) + 4\exp\left(\frac{V + 0.5 I_{ph} R_s}{A_i N_s V_t}\right)\right\} \tag{2.17}$$

After substituting the quadratic expression (2.10) instead of exponential expression in (2.3), following equation is obtained:

$$I_{ph} - \left(C_{12} I^2 + C_{11} I + C_{10}\right) + I_{o1} - \left(C_{22} I^2 + C_{21} I + C_{20}\right) + I_{o2} - \left(\left(V + I R_s\right)/R_{sh}\right) - I = 0 \tag{2.18}$$

Simplified (2.18) is written as follows:

$$I_{ph} - \left(\sum_{i=1}^{2} C_{i2}\right) I^2 - \left(\left(\sum_{i=1}^{2} C_{i1}\right) + \left(R_s/R_{sh}\right) + 1\right) I - \left(\sum_{i=1}^{2}\left(C_{i0} - I_{oi}\right)\right) - \left(V/R_{sh}\right) = 0 \tag{2.19}$$

$$\left(\sum_{i=1}^{2} C_{i2}\right) I^2 + \left(\left(\sum_{i=1}^{2} C_{i1}\right) + (R_s/R_{sh}) + 1\right) I + \left(\left(\sum_{i=1}^{2} (C_{i0} - I_{oi})\right) + (V/R_{sh}) - I_{ph}\right) = 0 \quad (2.20)$$

Solving the quadratic expression of I in (2.20), the explicit expression of the current is as follows:

$$I = \frac{-\left(\sum_{i=1}^{2} C_{i1}+1 + R_s/R_{sh}\right) + s_{qt}}{2\left(\sum_{i=1}^{2} C_{i2}\right)} \quad (2.21)$$

where

$$s_{qt} = \sqrt{\left(\sum_{i=1}^{2} C_{i1}+1 + R_s/R_{sh}\right)^2 - 4D} \quad (2.22)$$

and

$$D = \left(\sum_{i=1}^{2} C_{i2}\right)\left(V/R_{sh} + \sum_{i=1}^{2} (C_{i0} - I_{oi}) - I_{ph}\right) \quad (2.23)$$

Hence, (2.21) is the proposed explicit expression of the current using auxilliary expressions (2.22) and (2.23) along with the coefficients, C_{i0}, C_{i1} and C_{i2} given in (2.11), (2.17), and (2.16). The coefficients, C_{i0}, C_{i1} and C_{i2} in the proposed current expression are the function of voltage of the PV system.

As it is seen in (2.21), the proposed explicit expression of the current, I is expressed as the only root with positive sign infront of 's_{qt}'. The reason is explained as follows:

Let α and β are the two roots of (2.20) for 'I' which are expressed as:

$$\alpha = \frac{-\left(\sum_{i=1}^{2} C_{i1}+1 + R_s/R_{sh}\right) + s_{qt}}{2\sum_{i=1}^{2} C_{i2}} \quad (2.24)$$

and

$$\beta = \frac{-\left(\sum_{i=1}^{2} C_{i1}+1 + R_s/R_{sh}\right) - s_{qt}}{2\sum_{i=1}^{2} C_{i2}} \quad (2.25)$$

So from (2.20), $\alpha\beta$ is expressed as:

$$\alpha\beta = \frac{\sum_{i=1}^{2} (C_{i0} - I_{oi}) + (V/R_{sh}) - I_{ph}}{\sum_{i=1}^{2} C_{i2}} \quad (2.26)$$

Analysis of numerator of (2.26): Substituting (2.11) and $V = V_{oc}$ in the numerator of (2.26),

Numerator $= I_{o1}\left\{\exp\left(\frac{V_{oc}}{A_1 N_s V_t}\right)\right\} - I_{o1} + I_{o2}\left\{\exp\left(\frac{V_{oc}}{A_2 N_s V_t}\right)\right\} - I_{o2} + \frac{V_{oc}}{R_{sh}} - I_{ph}$

Now substituiting $(V_{oc}, 0)$ for (V, I) in (2.2), following equation is obtained,

$$I_{o1}\left\{\exp\left(\frac{V_{oc}}{A_1 N_s V_t}\right)\right\} - I_{o1} + I_{o2}\left\{\exp\left(\frac{V_{oc}}{A_2 N_s V_t}\right)\right\} - I_{o2} + \frac{V_{oc}}{R_{sh}} - I_{ph} = 0 \tag{2.27}$$

Case I: For $V < V_{oc}$, (2.27) is written as:

$$I_{o1}\left\{\exp\left(\frac{V}{A_1 N_s V_t}\right)\right\} - I_{o1} + I_{o2}\left\{\exp\left(\frac{V}{A_2 N_s V_t}\right)\right\} - I_{o2} + \frac{V}{R_{sh}} - I_{ph} < 0 \tag{2.28}$$

Hence, it is seen from (2.28) that for $V < V_{oc}$, the numerator of (2.26) is written as:

$$\sum_{i=1}^{2}(C_{i0} - I_{oi}) + V/R_{sh} - I_{ph} < 0 \tag{2.29}$$

Case II: For $V > V_{oc}$, (2.27) is written as:

$$I_{o1}\left\{\exp\left(\frac{V}{A_1 N_s V_t}\right)\right\} - I_{o1} + I_{o2}\left\{\exp\left(\frac{V}{A_2 N_s V_t}\right)\right\} - I_{o2} + \frac{V}{R_{sh}} - I_{ph} > 0 \tag{2.30}$$

Hence, it is seen from (2.30) that for $V > V_{oc}$, the numerator of (2.26) is written as:

$$\sum_{i=1}^{2}(C_{i0} - I_{oi}) + V/R_{sh} - I_{ph} > 0 \tag{2.31}$$

Analysis of denominator of (2.26): Simplifying (2.16), C_{i2} is written as:

$$C_{i2} = \frac{2I_{oi}}{I^2{}_{ph}} \exp\left(\frac{V}{A_i N_s V_t}\right)\left\{\exp\left(\frac{0.5 I_{ph} R_s}{A_i N_s V_t}\right) - 1\right\}^2 \tag{2.32}$$

Therfore, for all real valued V and all real-positive values of DDM parameters,

$$C_{i2} > 0 \Rightarrow \sum_{i=1}^{2} C_{i2} > 0 \tag{2.33}$$

Substituting (2.29), (2.31), and (2.33) in (2.26), it is observed that $\alpha\beta < 0$ for $V < V_{oc}$ and $\alpha\beta > 0$ for $V > V_{oc}$. From (2.24) and (2.25), it is observed that $\alpha > \beta$ (since $\sum_{i=1}^{2} C_{i2} > 0$ and sqt > 0). So for $V < V_{oc}$, $\alpha > 0$ and $\beta < 0$ but $\alpha < 0$ (since α will continue to follow I-V characteristics expressed by (2.1)) and $\beta < 0$ (as $\alpha\beta > 0$) for $V > V_{oc}$. Therefore, it is seen that only α is positive for voltage from '0' to 'V_{oc}' and negative for voltage greater than V_{oc}. Thus , it

matches the I-V characteristics of a PV module. Therefore, only α is choosen for the proposed explicit expression of I.

2.2.1 Validation of approximated quadratic function and explicit *I-V* expression

In this section, validation of the explicit expression of current with implicit current expression and the approximated quadratic function with actual exponential function is carried out for three different DDM PV modules of rating 140, 250 and 335 W from CSG PVTECH. Table 2.1 and 2.2 are showing datasheet values and estimated double diode model parameters, respectively. Also, the approximated quadratic function (2.10) and the actual function (2.3) are plotted with respect to current, I at a temperature of 25°C for different value of voltages. Implicit current expression is solved using MATLAB for implicit I-V expression plot. For current, $I \in [0, I_{ph}]$, $F_1 \sim I$ and $F_2 \sim I$ are plotted for $V \in \left[\left(\frac{4}{5}\right) V_{oc}, V_{oc}\right]$ and $V \in \left[\left(\frac{3}{4}\right) V_{oc}, V_{oc}\right]$, respectively.

Table 2.1: Datasheet values of CSG PVTECH PV modules

Parameters	140 W module	250 W module	335 W module
I_{SC} (A)	8.30	8.76	9.49
V_{OC} (V)	22.20	37.7	46.50
V_{MP} (V)	18.10	30.90	38.20
I_{MP} (A)	7.73	8.09	8.77
N_s	36	60	72

Table 2.2: Estimated values of DDM PV parameters

Parameters	140 W module	250 W module	335 W module
I_{ph} (A)	8.31	8.76	9.50
I_{o1} (nA)	0.29	0.27	0.095
I_{o2} (μA)	3.49	0.73	5.36
R_s (Ω)	0.1645	0.2929	0.2558
R_{sh} (Ω)	204.30	733.98	302.85

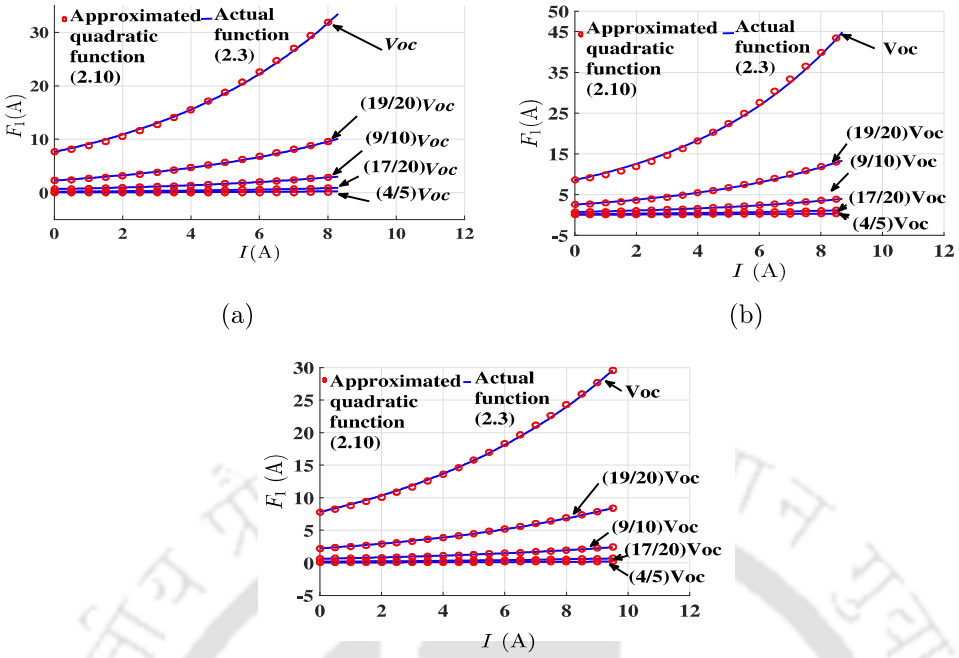

Figure 2.2: Quadratic approximation and actual plots of $F_1 - I$ in the current range from 0 to I_{ph} at a constant value of voltage (at any voltage from 0 to V_{oc}) for (a) 140 , (b) 250 and (c) 335 W DDM PV module.

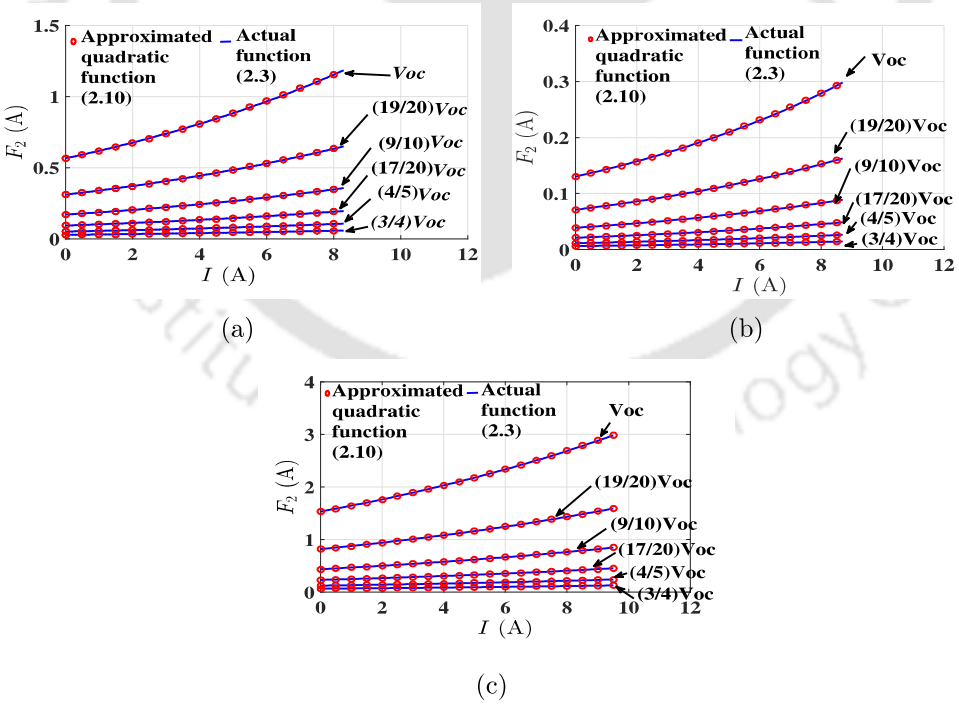

Figure 2.3: Quadratic approximation and actual plots of $F_2 - I$ in the current range from 0 to I_{ph} at a constant value of voltage (at any voltage from 0 to V_{oc}) for (a) 140 , (b) 250 and (c) 335 W DDM PV module.

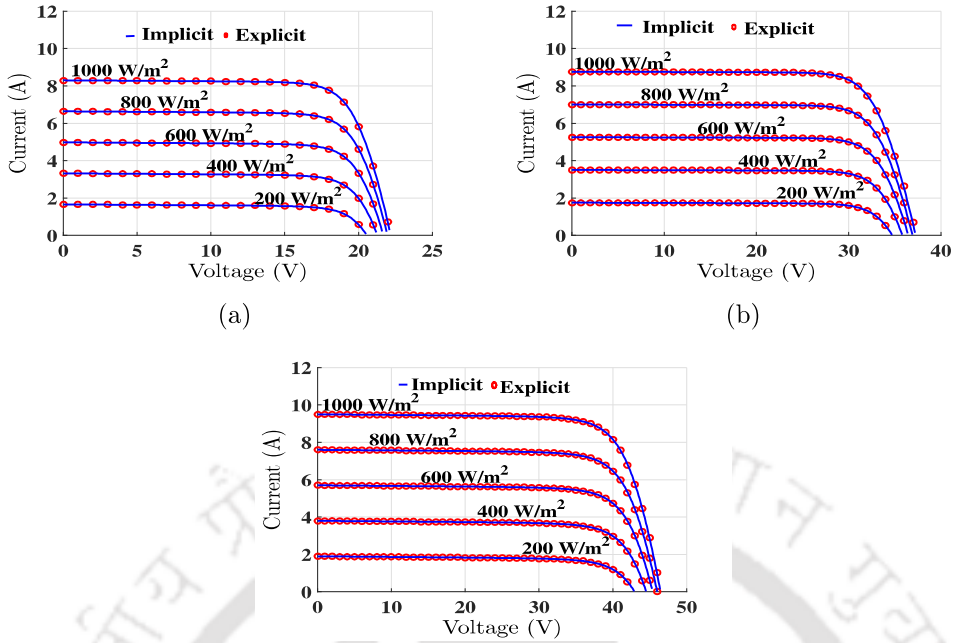

Figure 2.4: *I-V* characteristics of a (a) 140, (b) 250 and (c) 335 W DDM PV modules under different irradiation with a fixed temperature of 25°C.

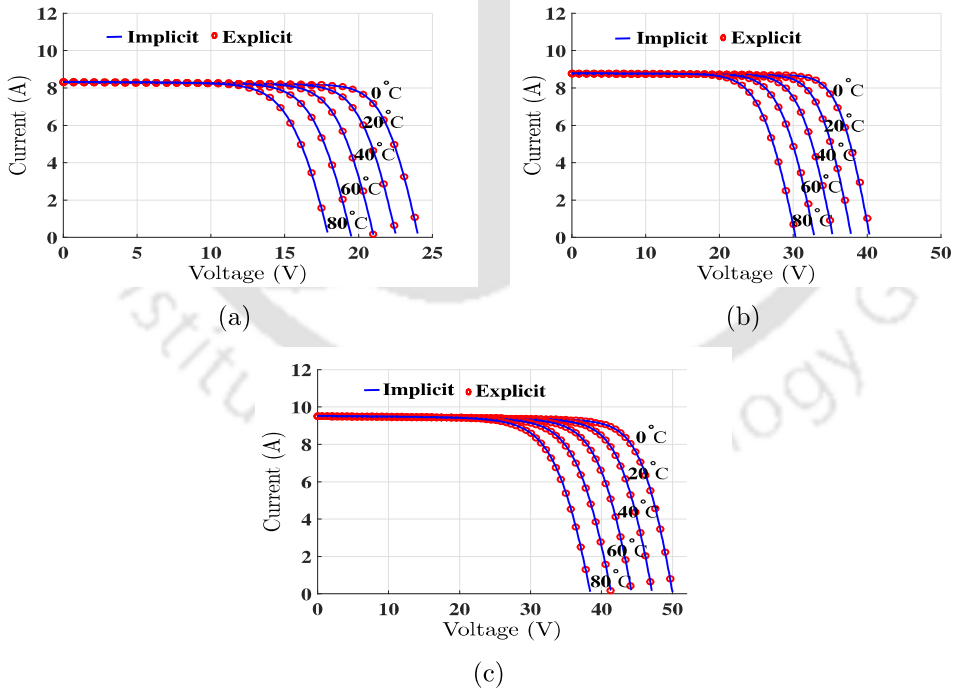

Figure 2.5: *I-V* characteristics of a (a) 140 , (b) 250 and (c) 335 W DDM PV modules under different temperature with a fixed irradiation of 1000 W/m^2.

Table 2.3: Values of I_{o1} and $\left(\frac{R_s}{A_1 N_s V_t}\right)^3$ for different rating of DDM PV modules

PV module	I_{o1}	$\left(\frac{R_s}{A_1 N_s V_t}\right)^3$	$I_{o1}\left(\frac{R_s}{A_1 N_s V_t}\right)^3$	$\frac{\partial^3 F_1}{\partial I^3}\Big\vert_{(V=V_{mp},I=I_{mp})}$
140 W	2.90×10^{-10}	5.4×10^{-3}	1.57×10^{-12}	1.5×10^{-3}
250 W	2.68×10^{-10}	6.6×10^{-3}	1.77×10^{-12}	2.3×10^{-3}
335 W	9.55×10^{-11}	2.6×10^{-3}	2.43×10^{-13}	5.31×10^{-4}

Table 2.4: Values of I_{o2} and $\left(\frac{R_s}{A_2 N_s V_t}\right)^3$ for different rating of DDM PV modules

PV module	I_{o2}	$\left(\frac{R_s}{A_2 N_s V_t}\right)^3$	$I_{o2}\left(\frac{R_s}{A_2 N_s V_t}\right)^3$	$\frac{\partial^3 F_2}{\partial I^3}\Big\vert_{(V=V_{mp},I=I_{mp})}$
140 W	3.48×10^{-6}	6.78×10^{-4}	2.36×10^{-9}	7.38×10^{-5}
250 W	7.28×10^{-7}	8.27×10^{-4}	6.03×10^{-10}	2.18×10^{-5}
335 W	5.36×10^{-6}	3.18×10^{-4}	1.70×10^{-9}	7.98×10^{-5}

In $F_1 \sim I$ plot, $(3/4)V_{oc}$ is omitted for better visualization. In this case, the values of I_{ph} and V_{oc} are taken at STC and plots of $F_1 \sim I$ and $F_2 \sim I$ are shown in Figs. 2.2 and 2.3 respectively. From the figures, F_1 and F_2 with I, it is seen that the approximated quadratic function (2.10) closely matches with actual non-linear exponential function (2.3) for different types of modules. Also, the explicit and implicit I-V curves are plotted for various type of DDM PV modules at different irradiation and different temperature conditions as shown in Figs. 2.4 and 2.5 respectively. From these figures, it is seen that the explicit I-V characteristic closely matches with the implicit I-V characteristics under DEC. From Tables 2.3 and 2.4, it is observed that the values of $\frac{\partial^3 F_i}{\partial I^3}$ for $(i = 1,2)$ at (V_{mp}, I_{mp}) are nearly equal to zero and hence it ensures the validity of approximation.

2.3 Proposed MPP estimation method

Flowchart for the proposed method to estimate the MPP of a DDM PV module is described in the Fig. (2.6). In this method, two boundary voltages are taken and these are considered in such a way that the MPP always falls between them. After that two sides of an isosceles triangle are drawn through these voltages. The isosceles triangle is formed in P-V curve in such a way that its base is on x-axis and height of vertex from x-axis is 'h', where 'h' should be chosen in such a way that it is always greater than the maximum power. In this report 'h' is chosen as $V_{oc}I_{ph}$

which is always greater than the maximum power as shown in Fig. (2.7(a)). The x-coordinate of the vertex of the isosceles triangle is the next iteration point in this method. Then depending on the sign of the slope of the tangent of the P-V curve at this voltage, the next boundary voltage is updated. These processes repeat until both boundary voltages come closer to the given tolerance.

The principle of operation of the proposed method is shown in Fig. (2.7(a)). Initially, boundary points V_i and V_f are initialized as 0 and V_{oc}, i.e., ${V_i}^{(0)} = 0$ and ${V_f}^{(0)} = V_{oc}$ as they include MPP voltage (V_{mp}). In the next step, two equal sides of an isosceles triangle are drawn through the points $\left({V_i}^{(0)}, 0\right)$ and $\left({V_f}^{(0)}, 0\right)$ (which are the corresponding points of initial boundary points on P-V curve) with base on x-axis. The triangle forms a vertex at M_1 whose corresponding point on P-V curve and x-coordinate are Pt_1 and ${V_i}^{(1)}$, respectively. Since the slope of the tangent at Pt_1 turns out to be positive, V_i is updated as ${V_i}^{(1)}$. Therefore, a line is drawn through Pt_1 such that it forms an isosceles triangle of vertex, M_2 with side drawn through point $(V_{oc}, 0)$. The x-coordinate of M_2 is found to be ${V_i}^{(2)}$ whose corresponding point on P-V curve is Pt_2. Again, slope of tangent at Pt_2 is checked which is positive and therefore, V_i is updated as ${V_i}^{(2)}$. The same process is repeated and the new side of isosceles triangle passes through Pt_2 and forms vertex at M_3 whose corresponding point on P-V curve is Pt_3. As the slope of tangent at Pt_3 is positive, V_i is updated as ${V_i}^{(3)}$. Therefore, the side of the next isosceles triangle passes through Pt_3 and forms vertex at M_4 whose corresponding point on P-V curve and x-coordinate are Pt_4 and ${V_f}^{(1)}$, respectively. Since the slope of tangent at Pt_4 is negative, V_f is updated as ${V_f}^{(1)}$. In this process, both boundary points approach to MPP, and the process is repeated till $|V_i - V_f| \leq$ tolerance.

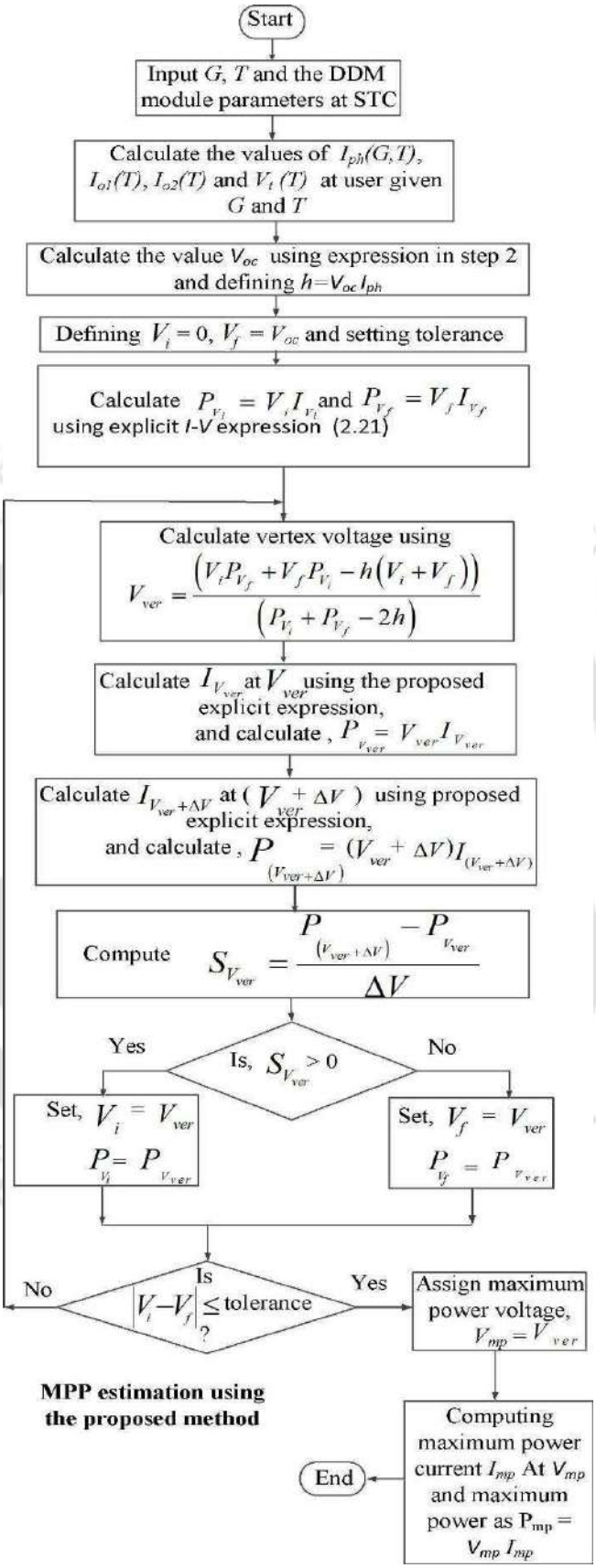

Figure 2.6: Algorithm for estimation of MPP using the proposed method.

The steps to obtain MPP of a module using the proposed method are as follows :

- Environment-dependent parameters such as $I_{ph}\,(G,T)$, $I_{o1}(T)$, $I_{o2}\,(T)$ and $V_t\,(T)$ are estimated using estimated parameters at STC of a DDM PV module.

- For the estimation of MPP using the proposed method, the boundary voltages V_i and V_f are initialized to 0 and $(A_1N_sV_t)\ln\left(\frac{I_{ph}}{I_{o1}}+1\right)(\approx V_{oc})$, respectively. The expression $(A_1N_sV_t)\ln\left(\frac{I_{ph}}{I_{o1}}+1\right)$ is the approximated value of V_{oc} which is slightly greater than real V_{oc} and gives power slightly lesser than zero. It is taken as boundary point here as it encloses MPP.

- The output power of the PV module, P_{V_i}=$V_iI_{V_i}$ and P_{V_f}=$V_fI_{V_f}$ at voltages, V_i and V_f are calculated. Currents I_{V_i} and I_{V_f} at voltages V_i and V_f are obtained using an explicit expression as presented in (2.21).

- The x-coordinate of the vertex of k^{th} isosceles triangle is determined as:

  Let the two points, $(V_i^{(k)}, P_{V_i}^{(k)})$ and $(V_f{}^{(k)}, P_{V_f}^{(k)})$, through which two sides of k^{th} isosceles triangle pass. The height of the vertex from the base is 'h'. The x-coordinate of vertex is $V_{ver}{}^{(k)}$ as shown in Fig. (2.7(b)). If the slope of one side is '$m^{(k)}$' then slope of the other side is '$-m^{(k)}$'. The equations for set of lines forming an isosceles triangle with vertex at height 'h' and base at x-axis are written as follows:

$$P = m^{(k)}V + C^{(k)} \tag{2.34}$$

$$P = -m^{(k)}V + \left(2h - C^{(k)}\right) \tag{2.35}$$

  Satisfying (2.34) and (2.35) at points $(V_i^{(k)}, P_{V_i}^{(k)})$ and $(V_f{}^{(k)}, P_{V_f}^{(k)})$, respectively, (2.34) and (2.35) are expressed as follows:

$$P_{V_i}^{(k)} = m^{(k)}V_i^{(k)} + C^{(k)} \tag{2.36}$$

$$P_{V_f}^{(k)} = -m^{(k)}V_f{}^{(k)} + \left(2h - C^{(k)}\right) \tag{2.37}$$

  Solving (2.36) and (2.37), $m^{(k)}$ and $C^{(k)}$ are derived as follows:

$$m^{(k)} = \frac{\left(P_{V_i}^{(k)} + P_{V_f}^{(k)} - 2h\right)}{\left(V_i^{(k)} - V_f{}^{(k)}\right)} \tag{2.38}$$

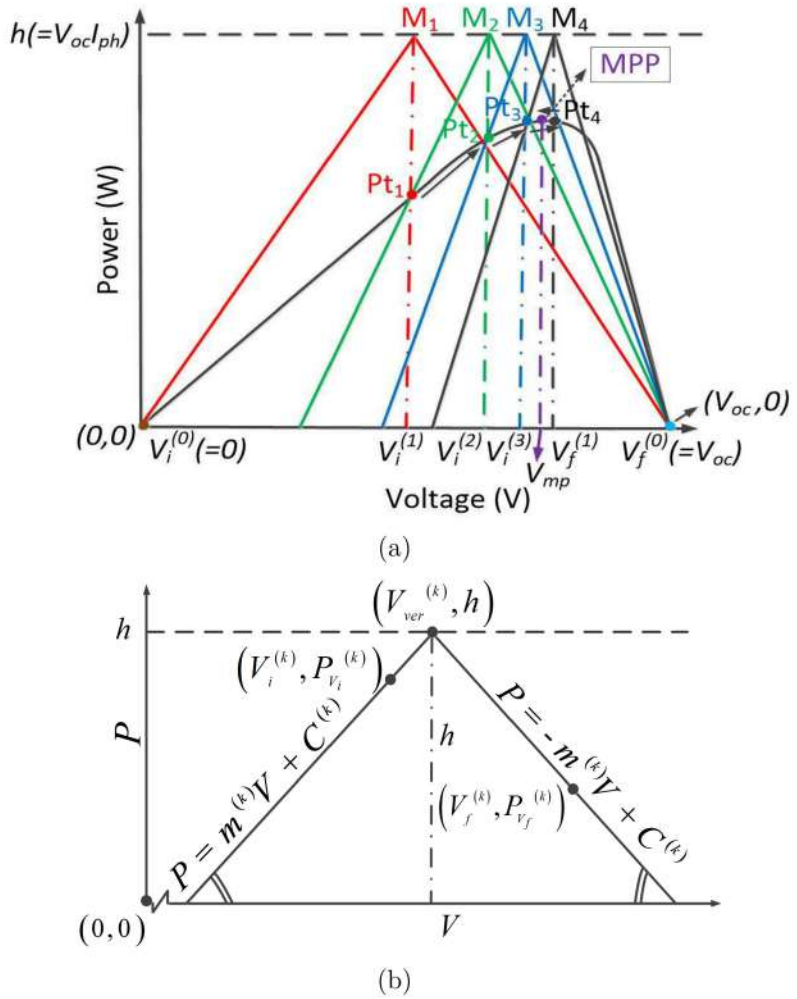

Figure 2.7: (a) Working of the proposed method and (b) k^{th} isosceles triangle.

$$C^{(k)} = \frac{\left(2V_i{}^{(k)}h - P_{V_i}^{(k)}V_f{}^{(k)} - V_i{}^{(k)}P_{V_f}^{(k)}\right)}{\left(V_i{}^{(k)} - V_f{}^{(k)}\right)} \tag{2.39}$$

The x-coordinate of vertex of isosceles triangle obtained by solving (2.34) and (2.35) is given as follows:

$$V_{ver}{}^{(k)} = \frac{\left(h - C^{(k)}\right)}{m^{(k)}} \tag{2.40}$$

Substituting (2.38) and (2.39) in (2.40), the x-coordinate of the vertex is obtained as follows:

$$V_{ver}{}^{(k)} = \frac{\left(V_i{}^{(k)}P_{V_f}^{(k)} + V_f{}^{(k)}P_{V_i}^{(k)} - h\left(V_i{}^{(k)} + V_f{}^{(k)}\right)\right)}{\left(P_{V_i}^{(k)} + P_{V_f}^{(k)} - 2h\right)} \tag{2.41}$$

- Using the proposed explicit expression, the current $I_{V_{ver}}{}^{(k)}$ and hence power $P_{V_{ver}}{}^{(k)}=V_{ver}{}^{(k)}I_{V_{ver}}{}^{(k)}$ are calculated.

- The current and power are estimated for the perturbed voltage, i.e., ${V_{ver}}^{(k)} + \Delta V$, selection of ΔV depends on user and required accuracy for slope calculation.
- The sign of slope of tangent at voltage ${V_{ver}}^{(k)}$ of P-V curve, i.e., ${S_{V_{ver}}}^{(k)} \left(= \frac{{P_{(V_{ver}{}^{(k)} + \Delta V)}} - {P_{V_{ver}{}^{(k)}}}}{\Delta V} \right)$ is calculated and hence boundary voltages are updated as follow:
  - Case 1: if ${S_{V_{ver}}}^{(k)} > 0 \Rightarrow {V_{ver}}^{(k)} < V_{mp}$ So, $\quad {V_i}^{(k+1)} = {V_{ver}}^{(k)}$ and ${P_{V_i}}^{(k+1)} = {P_{V_{ver}}}^{(k)}$.
  - Case 2: if ${S_{V_{ver}}}^{(k)} < 0 \Rightarrow {V_{ver}}^{(k)} > V_{mp}$ So, $\quad {V_f}^{(k+1)} = {V_{ver}}^{(k)}$ and ${P_{V_f}}^{(k+1)} = {P_{V_{ver}}}^{(k)}$.
- If $|V_i - V_f| \leq$ tolerance, then goto next step, otherwise update, $k \leftarrow k+1$ and goto step (4).
- The converged algorithm estimates the V_{mp}.
- The MPP current, I_{mp} is estimated using (2.21) and hence maximum power P_{mp} $(= V_{mp} I_{mp})$ is obtained at DEC.

2.4 Mathematical modelling of a partially shaded PV array using the proposed explicit *I-V* expression

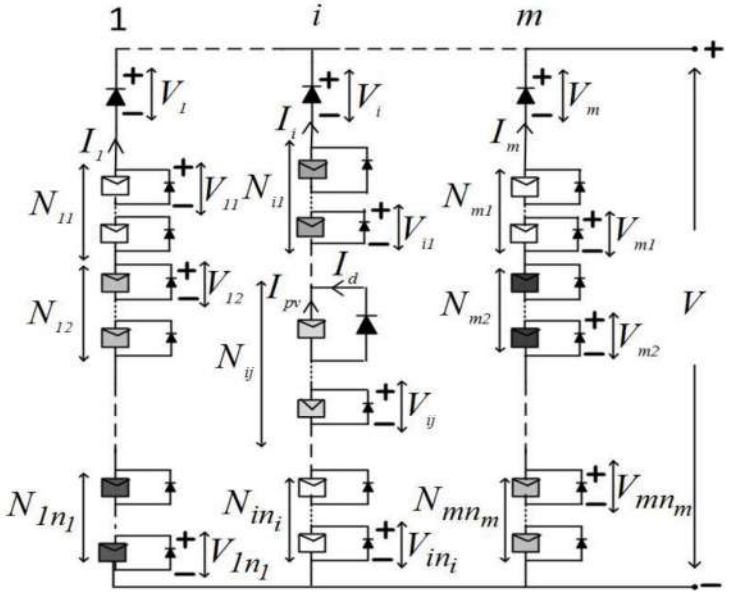

Figure 2.8: PV array in partial shading condition.

To estimate the MPP of a PV array under PSCs using the proposed explicit expression, a PV array of 'm' strings connected in parallel is considered. In each string, the PV modules are grouped based on the irradiance level under PSCs. In the present analysis, N_{ij} is the number of modules at j^{th} irradiance-index of i^{th} string as shown in Fig. 2.8. In this case, irradiance-index denotes the group of solar modules in series in a string which are in the same irradiance level and temperature. The maximum value of irradiance-index in the i^{th} string is n_i. The voltage of each module at the j^{th} irradiance-index in the i^{th} string is V_{ij} and current in the i^{th} string is I_i. The currents of PV module and bypass diode at the j^{th} irradiance-index in the string are I_{pv} and I_d, respectively. The $I_{od_{ij}}$ and Vt_{ij} are the dark saturation current and thermal voltage of the bypass diodes connected with the PV module at the j^{th} irradiance-index in the i^{th} string, respectively. Since these two parameters depend on temperature, these are constant for all the modules in an irradiance index in the present analysis. The voltage across blocking diode is denoted as V_i. The dark saturation current and thermal voltage of blocking diode are denoted as I_{od_i} and Vt_i, and these parameters depend on the temperature of blocking diode. The ideality factor of both, bypass and blocking diode is denoted as η. The function which explicitly describes I_{pv} in terms of V_{ij} is denoted as F_{ij}. The parameters of this function depend on the irradiance and temperature level of the module of the j^{th} irradiance-index in the i^{th} string.

Applying Kirchhoff's current law at the node of any PV module and its bypass diode at the j^{th} irradiance-index in the i^{th} string, the I_i is obtained as follows:

$$I_i = I_{pv} + I_d \tag{2.42}$$

$$I_i = F_{ij}\left(V_{ij}\right) + I_{od_{ij}}\left(e^{(-V_{ij}/\eta V t_{ij})} - 1\right) \tag{2.43}$$

where $i \in [1 \ldots m]$ and $j \in [1 \ldots n_i]$ The current-voltage expression of the blocking diode in the i^{th} string is as follows:

$$I_i = I_{od_i}\left(e^{(-V_i/\eta V t_i)} - 1\right) \tag{2.44}$$

So, the total number of equations obtained using (2.43) and (2.44) for PV array are $m + \sum_{i=1}^{m} n_i$. Since the voltage across each string is equal, equating the voltage in the i^{th} and the $(i-1)^{th}$ strings, the voltage equation is obtained as follows:

$$V_{(i-1)} + \sum_{j=1}^{n_{(i-1)}} N_{(i-1)j} V_{(i-1)j} = V_i + \sum_{j=1}^{n_i} N_{ij} V_{ij} \tag{2.45}$$

where $i \in [2 \dots m]$ So, the total number of equations obtained using (2.45) for PV array are $m-1$.

The power generated from the PV array using voltage of string 1 is as follows:

$$P = \left(V_1 + \sum_{j=1}^{n_1} N_{1j} V_{1j} \right) \left(\sum_{i=1}^{m} I_i \right) \tag{2.46}$$

In the present analysis, the number of total voltage variables across PV modules in PV array i.e., V_{ij} $(i \in [1 \dots m], j \in [1 \dots n_i])$ are $\sum_{i=1}^{m} n_i$ and the number of total voltage variables across blocking diodes in PV array i.e., V_i $(i \in [1 \dots m])$ are 'm'. Hence, the number of total voltage variables in PV array are $m + \sum_{i=1}^{m} n_i$. However, total number of current variables (i.e., I_1 to I_m) are m. So the number of total variables are $\left(2m + \sum_{i=1}^{m} n_i \right)$. Therefore, the objective function, i.e., P in (2.46) is optimized using $\left(2m - 1 + \sum_{i=1}^{m} n_i \right)$ number of equality constraints obtained from (2.43), (2.44) and (2.45) for $\left(2m + \sum_{i=1}^{m} n_i \right)$ number of variables.

In this chapter, genetic algorithm (GA) is used to optimize the objective function to the GMPP. In this optimization technique, the global V_{mp}, I_{mp}, and P_{mp} are obtained under different shading conditions.

2.5 Results and discussion

2.5.1 MPP estimation of a PV module under uniform irradiance condition

Considering a 250 W DDM PV module, the P-V curves under different values of irradiance such as 200, 400, 600 and 800 W/m^2 at a fixed temperature of 25°C and different values of temperature such as 20, 40, 60 and 80°C at an irradiance of 1000 W/m^2 are plotted in Fig. 2.9 using MATLAB programme.

It is seen from the figure and Table 2.5 that the % error (absolute, with respect to $P_{mp,(simul.)}$) in MPP estimated using the proposed method and obtained using simulation at 200 W/m^2 and 25°C is 0.1252% which decreases to 0.0449% after increase in the irradiance to 800 W/m^2. The % error also decreases from 0.0470% at 20°C to 0.0320% at 80°C for solar irradiance of 1000 W/m^2.

Therefore, the maximum difference between simulated and estimated P_{mp} is within 0.15% under different irradiance and is within 0.05% under different temperature conditions.

Table 2.5: MPP of a 250 W DDM PV module under different environmental conditions

Irradiance variation at 25^{o}C				Temperature variation at 1000 W/m^2			
Irradiation (W/m^2)	% Error of $V_{mp,(est)}$	% Error of $I_{mp,(est)}$	% Error of $P_{mp,(est)}$	Temperature (°C)	% Error of $V_{mp,(est)}$	% Error of $I_{mp,(est)}$	% Error of $P_{mp,(est)}$
200	0.2027	0.0618	0.1252	20	0.2747	0.2955	0.0470
400	0.0331	0.0609	0.1009	40	0.2440	0.2100	0.0470
600	0.1316	0.0405	0.0866	60	0.0085	0.0479	0.0430
800	0.1743	0.2041	0.0449	80	0.0330	0.0112	0.0320

Table 2.6: A comparison of MPP of a 250 W DDM PV module at a temperature of 25°C with varying irradiations

Methods	Irradiation (W/m^2)	V_{mp} (V)	% Error of $V_{mp,(est.)}$	I_{mp} (A)	% Error of $I_{mp,(est.)}$	$P_{mp,(est.)}$ (W)	% Error of $P_{mp,(est.)}$	t_{MPP} (s)
PS	200	29.22	1.2838	1.63	0.6794	47.8610	0.1023	2.791847
	400	29.73	1.5563	3.32	1.1578	98.9262	0.1955	2.78239
	600	29.98	1.3816	4.99	1.0531	149.8886	0.1475	2.603602
Saloux	200	30.95	2.4834	1.74	7.4737	53.85	12.37	0.006411
	400	31.14	3.1126	3.41	3.9001	106.18	7.12	0.006201
	600	31.38	3.2237	5.05	2.2681	158.46	5.56	0.006337
GS	200	28.06	5.2027	1.65	1.9148	46.29	3.38	0.18821
	400	29.52	2.2517	3.33	1.4625	98.30	0.83	0.15336
	600	29.75	2.1382	4.99	1.0531	148.45	1.10	0.17147
NR	200	29.93	1.1148	1.5980	1.2970	47.8362	0.1540	0.225120
	400	31.35	3.8079	3.1071	5.3290	97.4015	1.7238	0.218929
	600	31.57	3.8486	4.6668	5.4921	147.3544	1.8292	0.239564
LM	200	29.30	1.0135	1.62	0.0618	47.46	0.94	0.02006
	400	30.09	0.3642	3.28	0.0609	98.69	0.43	0.01893
	600	30.32	0.2632	4.93	0.1620	149.47	0.42	0.02075
Proposed	200	29.54	0.2027	1.62	0.0618	47.85	0.1252	0.010150
	400	30.19	0.0331	3.28	0.0609	99.02	0.1009	0.011363
	600	30.36	0.1316	4.94	0.0405	150.11	0.0866	0.010380

The estimated MPP of a 250 W DDM PV module using PS, Saloux, GS, NR (Newton Raphson), LM, and the proposed method are compared with the simulated MPP in terms of accuracy and computational time. The simulation results for the MPP estimated using aforementioned methods along with the proposed method at a temperature of 25°C with varying irradiations are presented in Table 2.6. The $P_{mp,(simul.)}$ of 150.11, 99.12, and 47.91 W under different solar irradiations such as, 600, 400, and 200 W/m^2, respectively, are obtained from the P-V characteristics of a DDM PV module at a temperature of 25°C. It is observed from the table that

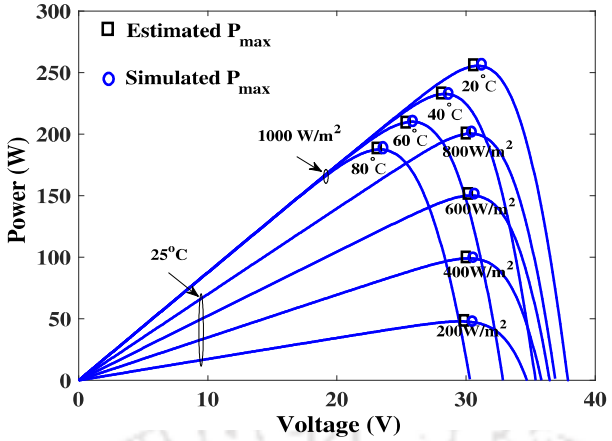

Figure 2.9: MPP comparision of 250 W module at different irradiation and different temperatures.

the % error in $P_{mp,(est)}$ using PS method is very close to the proposed method, but it requires more computational time compared to the proposed method. Although the execution time for Saloux method is less than the proposed method, it shows high % error of $P_{mp,(est)}$. NR method is implemented based on the proposed explicit I-V expression of DDM PV module as given in Table 2.6.

It is observed from the Table that % error in V_{mp}, I_{mp}, P_{mp} and computational time using the proposed method is less as compared to NR method. Therefore, the proposed method for the estimation of MPP of a DDM PV module under different environmental conditions is more accurate and computationally efficient. To obtain the above results, a computer with processor $Intel(R)\ Core(TM)\ i5-6500$ CPU @ 3.20 GHz 3.19 GHz and RAM capacity of 4 GB is used. The errors in GS, NR, and LM could be reduced in Table 2.6. However, for that, the tolerance in the programs of these three must be reduced, which could lead to an increase in computational time. Therefore, in the comparison table for reducing the time consumed by GS, NR, and LM, the tolerance was increased, resulting in higher errors in their results. Additionally, the Saloux method uses an idealized version of the I-V characteristics expression of the PV source, which is the cause of the very high error in the estimated results produced by this method. The low error in the PS method is due to the lower tolerance that was used.

The experimental validation of the proposed method is carried out considering 200 W KC200GT PV module. The measured values of I-V characteristics of the aforementioned module for dif-

ferent irradiances such as 1000, 800 and 600 W/m^2 at a temperature of 25°C are taken from the manufacturer. The P-V curve using experimental values has been plotted along with P-V curve using simulation for different values of irradiance and temperature as shown in Fig. 2.10. The values of MPP calculated using the proposed method for different values of irradiance and temperature are presented in the P-V curves. It is seen from the P-V curve that the estimated MPP using the proposed method closely matches with the MPP obtained experimentally under different environmental conditions.

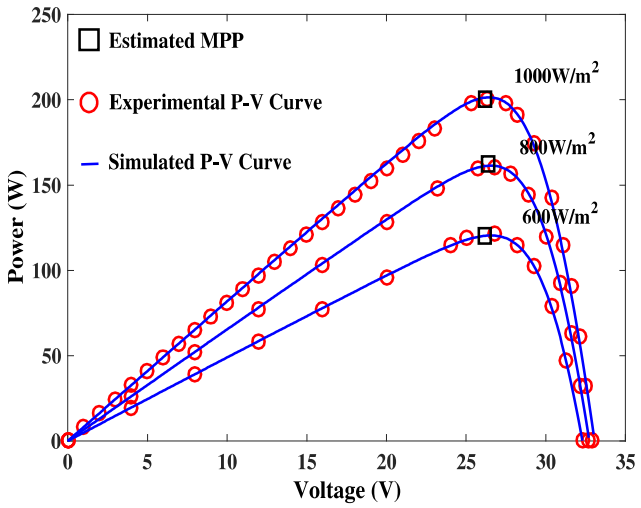

Figure 2.10: MPP comparision of estimated value using the proposed method with experimental value for a 200 W KC200GT module under uniform condition.

2.5.2 Partially shaded PV array

In this study, the GMPP is estimated for three different shading conditions of a string as shown in the Fig. 2.11. In this figure, the shaded modules receive the solar irradiance of 500 W/m^2 while the unshaded modules receive the solar irradiance of 1000 W/m^2 at temperature of 25°C. Temperatures of all four modules are taken as 25°C. Three constraints are obtained in Case-I and Case-II while seven constraints are obtained in Case-III. The optimization function, P given in (2.46) is optimized using GA subjected to the above constraints. The estimated GMPP in this report is obtained by running GA programme for 200 times for better accuracy. The module voltage is taken within the range of -1 to V_{oc} at STC and current through string is taken within range 0 to I_{sc} at standard test condition (STC). However, boundary range can be

decreased wisely for obtaining more accurate result and also GA parameters can be changed for higher accuracy. The I-V and P-V curves of a given string in three different shading patterns are plotted using MATLAB simulation as shown in Fig.(2.12). From this figure, the simulated GMPP values for all the three cases are obtained as Case-I (V_{mp}=90.2 V, I_{mp}=8.223 A, P_{mp}=741.71 W), Case-II (V_{mp}=124.5 V, I_{mp}=4.155 A, P_{mp}=517.30 W) and Case-III (V_{mp}=92.8 V, I_{mp}=12.26 A, P_{mp}=1137.7 W). It is seen that the estimated GMPP closely matches with the simulated GMPP in three different shading patterns.

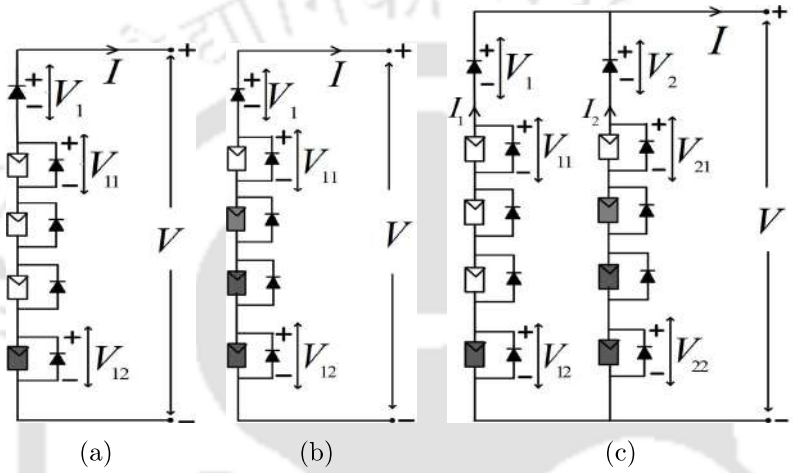

Figure 2.11: Different type of shading conditions (a) Case I, (b) Case II and (c) Case III.

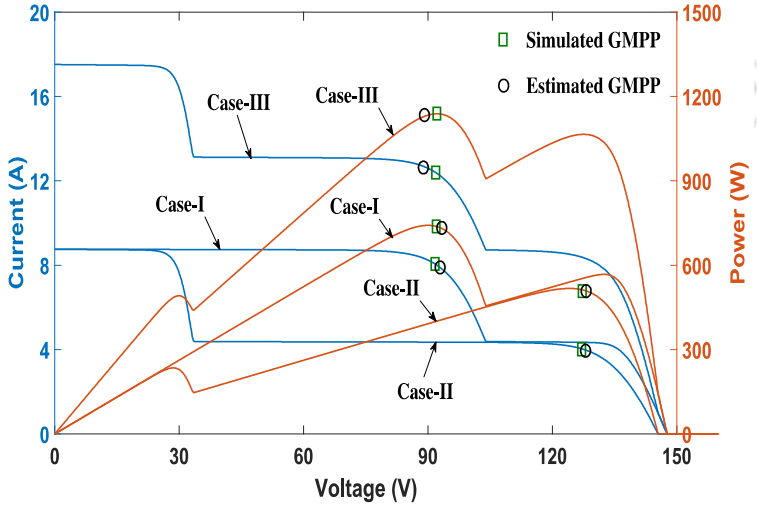

Figure 2.12: Simulated and estimated MPP of a PV system in Case I, Case II and Case III PSCs.

The estimated GMPP values and the absolute % error using [1] and the proposed method

Table 2.7: Estimation of MPP of a PV system of 250W PV module under different shading conditions using [1]

Different shading	$V_{mp,(est.)}$ (V)	% Error of $V_{mp,(est.)}$	$I_{mp,(est)}$ (A)	% Error of $I_{mp,(est.)}$	$P_{mp,(est.)}$ (W)	% Error of $P_{mp,(est)}$
Case-I	91.7	1.6630	8.09	1.6174	741.853	0.0193
Case-II	127.0	2.0080	4.045	2.6474	513.715	0.6930
Case-III	93.554	0.8125	12.135	1.0196	1135.3	0.2110

Table 2.8: Estimation of MPP of a PV system of 250W PV module under different shading conditions using the proposed method

Different shading	$V_{mp,(est.)}$ (V)	% Error of $V_{mp,(est.)}$	$I_{mp,(est)}$ (A)	% Error of $I_{mp,(est.)}$	$P_{mp,(est.)}$ (W)	% Error of $P_{mp,(est)}$
Case-I	90.4476	0.2745	8.200	0.2797	741.67	0.0054
Case-II	125.0074	0.4076	4.1541	0.0217	519.2932	0.3626
Case-III	92.0111	0.8501	12.369	0.8891	1138.1	0.0352

are given in Tables 2.7 and 2.8, respectively. It is observed from the above-mentioned tables, the % error of V_{mp} is less in Case-I and II , the % error in I_{mp} is less in Case-I, II and III, and the % error in P_{mp} is less in Case-I, II and III in the proposed method compared to the ones in [1]. Also, it is observed from Table 2.8 that the maximum absolute percentage error of the estimated P_{mp} in the proposed approach with respect to the actual P_{mp} is around 0.4% under different shading patterns. Therefore, the proposed mathematical modeling approach to estimate the GMPP of any DDM PV array under PSC using GA is more accurate. The execution time to obtain the GMPP in [1] for Case-I, II and III are 0.0124, 0.0119 and 0.0109 s, respectively. However, in the proposed method, the execution time for Case-I, II and III are 3.383, 3.803 and 37.891 s respectively. Eventhough the execution time to obtain the GMPP under PSC using proposed mathematical modeling with GA is higher than [1] method, the proposed method will estimate the GMPP more accurately. The higher error in GMPP estimation using [1] is due to the many simplifications and assumptions made in deriving the expressions for GMPP quantities. In contrast, the proposed estimation technique uses the exact circuit equations obtained from KVL and KCL, as well as the explicit I-V expression of the DDM, which is highly accurate. This results in a lower % error in the estimated GMPP using the proposed method. To validate the proposed method, an experiment is performed using the laboratory scale experimental setup

Figure 2.13: Different components of the experimental setup.

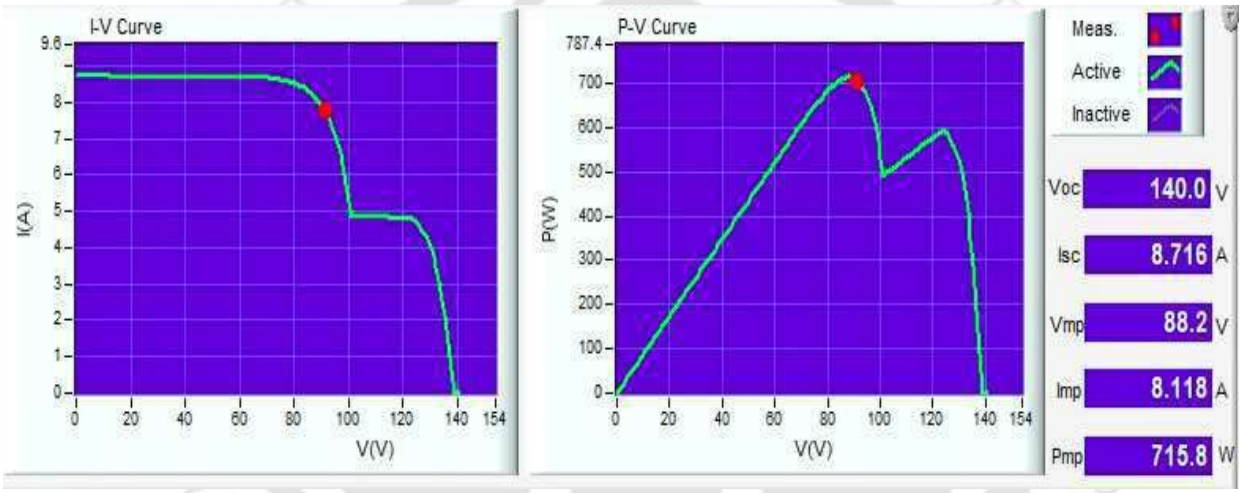

Figure 2.14: Experimentally obtained I-V and P-V curves of a string of four PV modules as in Case I.

shown in Figs. (2.13) which contains a PV simulator (Chroma), a dc-dc boost converter (inductor value of 3 mH and current rating of 10 A, MOSFET of voltage rating 600 V and current rating of 32 A, and capacitor of 4750 μF and voltage rating of 400 V), data acquisition system and controller (sbRIO-9606, NI), personal computer and the dc loads. For dc load, incandescent bulbs of 100 and 200 W ratings are used in the experiment. In the experiment, PV simulator is fed with a string under PSC as described in Case I of Fig. 2.11. It is seen from Fig. (2.14) that the power at MPP of the string is 715.8 W. The estimated power at MPP obtained using the proposed method is 741.67 W as given in Table (2.8). The % error in estimated maximum power using the proposed method with respect to the maximum power obtained experimentally is

3.6141% and which is well within the limit. Therefore, the proposed method for MPP estimation is simple and more accurate.

2.6 Summary of the chapter

This chapter introduces an explicit I-V formula for a PV module to determine its maximum power point (MPP) under different environmental conditions. The explicit I-V formula is compared with the implicit one across three distinct modules to validate its accuracy. Simulation outcomes indicate that the MPP estimation for a DDM PV module using the proposed method is both more precise and faster than five other established techniques, namely PS, Saloux, GS, NR, and LM under DEC. The results of the MPP estimation approach are further corroborated through experiments on a 200W DDM PV module. Moreover, the Global Maximum Power Point (GMPP) of a DDM PV array is deduced from the explicit I-V formula using a mathematical framework under partial shading conditions. This mathematical representation of a special case of series parallel partially shaded DDM PV array is fine-tuned to estimate GMPP using the Genetic Algorithm (GA) optimization method. The findings highlight the accuracy of the estimated GMPP when compared to both simulated and experimental GMPP values. In conclusion, the proposed explicit I-V formula, MPP estimation for uniform irradiance case and the mathematical model for a DDM PV array under partial shading conditions (PSC) are both precise and computationally efficient.

The GMPP estimation algorithm discussed in this chapter is tailored for a specific case of series-parallel PV arrays, utilizing a Genetic Algorithm for GMPP determination under given constraints. However, due to the GA's inherent variability in population-based searches, it yields inconsistent GMPP values for the same partially shaded PV array across different instances. To address these limitations, next chapter introduces a new GMPP estimation technique that is not only accurate, robust, and fast but also applicable to the general case of series-parallel partially shaded PV arrays.

Note: This work, "MPP Estimation of a Double Diode Model PV Module from Explicit I-V Characteristic," has been published in IEEE Transactions on Industrial Electronics, vol. 66, no. 9, pp. 7032-7042, Sept. 2019, doi: 10.1109/TIE.2018.2877116.

Chapter 3

Analysis and GMPP estimation of a generalized model of a series-parallel (S-P) connected partially shaded PV array using implicit double diode model of PV

Contents

3.1 Introduction

Energy received by earth from the sun is highly important to sustain human-life. Solar cell is a device which converts light energy into electric energy. The first usable solar cell was developed in 1954 in Bell labs. Photons of 1.02 electron volts are able to produce electron-hole pairs in silicon. In the presence of a p-n barrier, these electron-hole pairs are separated and made to do work in an external circuit [48]. There are mainly two types of mathematical models such as a SDM [49] and a DDM [50] to represent the current-voltage behavior of a PV cell or module. However, DDM is a more accurate model of the PV cell or module due to consideration of recombination losses [50]. The MPP estimation of a PV system is necessary for its installation and operation. Furthermore, assessing and estimating the MPP of a PV array is crucial for optimizing energy production, reducing operational costs, and thoughtful design, especially in the context of emerging markets. These emerging markets necessitate that PV plants operate in a cost-effective, dependable, and efficient manner. In many such markets, microgrids are common, and their reliable functioning is vital for providing consistent access to electricity. Certain environmental conditions in some of these markets can cause soiling of the PV array modules, leading to an unequal distribution of sunlight across the modules. Other factors, including differing orientations, uneven mounting surface levels, and proximity to buildings, can also cause uneven irradiance or partial shading. The accurate estimation of the GMPP of a PV array in PSC is more challenging than uniform irradiance condition due to the presence of multiple peaks or LMPPs in power-voltage (P-V) curve. Therefore, it is important to accurately analyse the partially shaded PV array. Authors in [51] presented a MATLAB-based simulator cum learning tool, which can be used to enhance the understanding and predict the I-V and P-V characteristics of large PV arrays. Some authors have developed an approximate empirical expression to estimate the GMPP [1, 10, 15] for a PV array in PSC. In [13] authors proposed a novel technique to approximate all the LMMPs of the P-V curve of a partially shaded PV string. However, the robustness and accuracy of these methods depend on shading parameters of partial shading, i.e., irradiance levels and the number of modules in each irradiance level. In [16], authors present a novel Psim-based piece-wise linear macro-model. The new model can be used to predict PV module characteristics for

various operating conditions and understand the behaviours of a long PV string and a large-scale PV array under any PSC patterns on Psim platform. Furthermore, analyses of the I-V and P-V curves of a PV string under PSC of several shading cases were conducted in [17]. These studies have provided significant observations regarding the MPP of a PV string in PSCs. In [18], several rules for general shading patterns of PV array are unveiled. Such insights are crucial for approximating the LMPP and, consequently, the GMPP. However, it should be noted that these methods are not universally robust and may yield incorrect results in different cases of partial shading. In [19], authors propose a field-support vector regression (F- SVR) based MPPE approach for estimating the MPP in PSC. In this, a conventional SVR is applied to study the mapping relationship between PV electrical characteristics and the MPP locus. This technique requires a large amount of data to achieve satisfactory accuracy, thus demanding significant computational resources. Despite these requirements, this method provides only an approximation of the GMPP.

In [52] the concept of inflection point was proposed to fast plotting of the P-V curve and newton-raphson method is applied to calculate the current for a given voltage across PV array. In [53], the authors used the bisection method to calculate the value of array current at given irradiances, temperatures, and array voltage for a PV array in PSC. In [11, 14] authors solved the circuit equations of a partially shaded PV array to get array current at a particular voltage using MATLAB 'fsolve' function. However, in [14] authors used the approximate equations while in [11] authors used exact circuit equations. In [12], authors applied newton-raphson method for solving modified equations of a partially shaded PV array to obtain the value of array current and array voltage at a known load resistance. After obtaining the array current at a known array voltage, the $I-V$ and $P-V$ characteristics are drawn to get the GMPP. However, for estimation of the GMPP, these methods are slow as these first need to plot the curve by varying the array voltage from '0' to V_{oc}. Therefore, these methods require more time depending on the open-circuit voltage of the array. The GMPP can also be obtained without plotting the $P-V$ curve using methods like genetic algorithm (GA) and particle swarm optimisation (PSO). In [50], authors proposed a GA based GMPP estimation technique for the partially shaded PV

array. However, it is less accurate due to randomness factor of GA. Particle swarm optimisation (PSO) [54] can be used to estimate the GMPP of the partially shaded PV array. However, the technique is also based on randomly generated numbers, hence it is less accurate.

Maximum power point tracking (MPPT) algorithms for identifying the GMPP have been proposed in various studies, as referenced in [20], [21] and [22]. These algorithms predominantly use intelligent strategies to decrease the regions of the P-V curve that needs to be investigated for the GMPP. However, even after narrowing down certain regions, these methods still involve small step perturbations in voltage to pinpoint the GMPP. This, in turn, could potentially increase the time required for GMPP estimation if these techniques are employed. The authors in [55] introduce the use of the most valuable player (MVP) based MPPT technique, which is reliant on numerous randomly generated numbers, similar to PSO and GA. Therefore, if this method is used for estimation, it could result in a higher frequency of errors or require more time for the GMPP estimation.

The GMPP estimation algorithm proposed in Chapter 2 was for special case of series parallel PV array. Also in Chapter 2 GA was used for finding the GMPP at given constraints obtained from the PV array. However, the GA ia a population search based method. Therefore, it gives different GMPP values for a same partially shaded PV array at different times when the method is applied. Therefore, there is need of a robust, accurate and fast GMPP estimation method which can also be applied for general case of series parallel partially shaded PV array. In order to overcome above mentioned limitations, an accurate, robust and fast GMPP estimation technique is proposed in this chapter. PV system in the real world has connecting wires which has resistances. Therefore, this chapter proposes a generalized model of PV array and its mathematical modeling. The circuit equations for the detailed model of PV array is developed using set theory based approach. Further, for the GMPP estimation of the PV array, inflection points or zero-voltage points of the power-voltage curve of the generalized array are investigated in this research work. In this chapter, zero-voltage points are used to divide the power-voltage curve of the PV array in multiple sections. The zero-voltage points are managed by a set-theory based approach. Potential section i.e., the sections which have GMPP are identified. Further, the

proposed method is applied to get the GMPP of the partially shaded PV array.The iteration voltage, as discussed later in the paper, divides each potential section into two subsections. Half or more than half of total subsections are simultaneously eliminated by a novel technique described further. In this way after some iterations, iteration points converges at the LMPPs of the non-eliminated section. For GMPP, the LMPP with highest power is selected. The proposed method is found to be best among the other GMPP estimation methods in terms of accuracy and computational complexity.

Section 3.2 presents the detailed model of the PV array and its circuit equations. The description of the proposed GMPP estimation technique is presented in Section 3.3. Results-discussions and Conclusion are presented in Sections 3.4 and 3.5, respectively.

3.2 I-V and P-V characteristics of generalized model of a partially shaded PV array

The electrical equivalent circuit of an extended DDM PV module is given in Fig. 3.1. The I-V expression of an extended DDM PV module is expressed as follows:

$$\begin{aligned} I &= I_{ph} - I_{o1}\left\{\exp\left(\frac{V+IR_s}{A_1N_sV_t}\right)\right\} + I_{o1} - I_{o2}\left\{\exp\left(\frac{V+IR_s}{A_2N_sV_t}\right)\right\} + I_{o2} - \frac{V+IR_s}{R_{sh}} \\ &\quad -\frac{b}{N_s}(V+IR_s)\left(1-\frac{V+IR_s}{V_{br}N_s}\right)^{-r} \end{aligned} \tag{3.1}$$

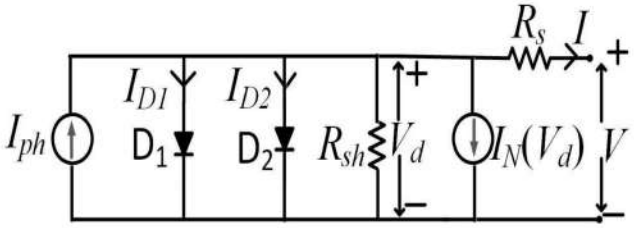

Figure 3.1: Equivalent circuit of an extended DDM PV module.

The variables and parameters of (3.1) have the same meaning as given in [50].

However,$-\frac{b}{N_s}(V+IR_s)\left(1-\frac{V+IR_s}{V_{br}N_s}\right)^{-r}(=I_N)$ term is extra from the usual implicit DDM equation. The extra term becomes significant at negative voltages. The values of parameters b, V_{br}, and r are taken as in [56]: b = 0.002 $\mho$, V_{br} = -21.29 V and r = 3 for a typical PV cell. However, it should be noted that the letter r is used for the letter m of [56]. A proposed

generalized electrical equivalent circuit of a series parallel PV array under PSC is presented in Fig. 3.2. This array has m number of strings, n number of groups in every string, and each group has one bypass diode connected in anti-parallel. Applying KVL and KCL for the i^{th} string of a PV array shown in Fig. 3.2, the expression of current and voltage are as follows:

$$I_{ij} = I_{ph_{ijk}} - I_{o1_{ijk}}\left(e^{\frac{V_{ijk}+I_{ij}R_{s_{ijk}}}{A1_{ijk}Ns_{ijk}Vt_{ijk}}} - 1\right) - I_{o2_{ijk}}\left(e^{\frac{V_{ijk}+I_{ij}R_{s}}{A2_{ijk}Ns_{ijk}Vt_{ijk}}} - 1\right) - \frac{V_{ijk}+I_{ij}R_{s_{ijk}}}{R_{sh_{ijk}}} - \frac{b}{N_{s_{ijk}}}\left(V_{ijk}+I_{ij}R_{s_{ijk}}\right)\left(1 - \frac{V_{ijk}+I_{ij}R_{s_{ijk}}}{V_{br}N_{s_{ijk}}}\right)^{-r} \tag{3.2}$$

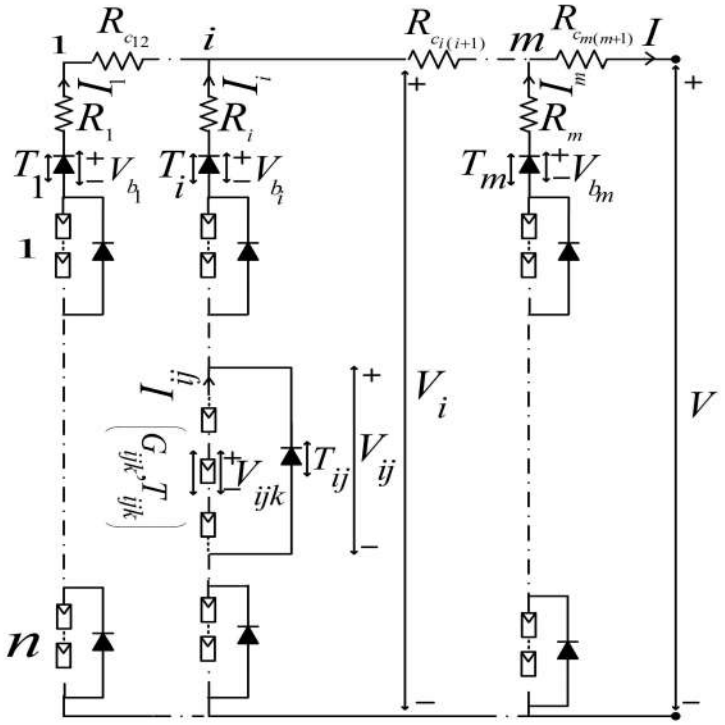

Figure 3.2: Proposed generalized model of a series-parallel PV array under PSC.

$$V_{ij} = \sum_{k=1}^{q_{ij}} \left(N_{ijk}V_{ijk}\right) \tag{3.3}$$

$$I_i = I_{ij} + I_{o_{ij}}\left(e^{\frac{-V_{ij}}{A_{bp_{ij}}Vt_{ij}}} - 1\right) \tag{3.4}$$

$$V_i = V_{b_i} - I_i R_i + \sum_{j=1}^{n} V_{ij} \tag{3.5}$$

$$I_i = I_{o_i} \left(e^{\frac{-V_{b_i}}{A_{bl_i} V_{t_i}}} - 1 \right) \tag{3.6}$$

The current in the j^{th} group of the i^{th} string is denoted by I_{ij}, and V_{ij} represents the voltage of the bypass diode in the same group and string. The photocurrent of a unit PV source, which is a group of series-connected cells or a PV module, in the k^{th} subgroup of the j^{th} group of the i^{th} string, is given by $I_{ph_{ijk}}$. The dark saturation currents of the unit PV source in the k^{th} subgroup of the j^{th} group of the i^{th} string are represented by $I_{o1_{ijk}}$ and $I_{o2_{ijk}}$.

The number of cells in a unit PV source in the k^{th} subgroup of the j^{th} group of the i^{th} string is given by $N_{s_{ijk}}$, and q_{ij} represents the number of subgroups of the j^{th} group in the i^{th} string. V_{b_i} is the voltage across the blocking diode in the i^{th} string, while $A_{bp_{ij}}$ denotes the ideality factor of the bypass diode of the j^{th} group in the i^{th} string. The dark saturation current of the bypass diode of the j^{th} group in the i^{th} string is represented by $I_{o_{ij}}$, and I_{o_i} is the dark saturation current of the blocking diode in the i^{th} string. The ideality factor of the blocking diode of the i^{th} string is denoted by A_{bl_i}.

The voltage of a unit PV source in the k^{th} subgroup of the j^{th} group of the i^{th} string is expressed as V_{ijk}, with I_{ijk} being the corresponding current. G_{ijk} denotes the irradiance of the unit PV source in the same subgroup and group of the i^{th} string, while T_{ijk} denotes its temperature. N_{ijk} indicates the number of unit PV sources within the k^{th} subgroup of the j^{th} group of the i^{th} string. The temperature of the bypass diode of the j^{th} group in the i^{th} string is denoted by T_{ij}, and T_i represents the temperature of the blocking diode of the i^{th} string. The equivalent resistance of the connecting wires between the i^{th} and $(i+1)^{\text{th}}$ string is represented by $R_{c_{i(i+1)}}$.

In Equation (3.2), variables such as $A_{1_{ijk}}$ and $A_{2_{ijk}}$, which are the ideality factors of a unit PV source in the k^{th} subgroup of the j^{th} group of the i^{th} string, are introduced. The series and shunt resistances of the unit PV source in the same subgroup and group of the i^{th} string

are denoted by $R_{s_{ijk}}$ and $R_{sh_{ijk}}$, respectively. $V_{t_{ijk}}$ refers to the thermal voltage of the unit PV source in the k^{th} subgroup of the j^{th} group of the i^{th} string. The current through the i^{th} string is denoted by I_i, and the voltage across the i^{th} string by V_i. The equivalent resistance of the connecting wires in the i^{th} string is denoted by R_i. The thermal voltage of the blocking diode of the i^{th} string is denoted by V_{t_i}.

(3.2) to (3.6) are valid $\forall i \in [1 \ldots m], j \in [1 \ldots n], k \in [1 \ldots q_{ij}]$. Hence, the total number of equations in the equation set of the i^{th} string are $2(n+1) + \sum_{j=1}^{n} q_{ij}$. The equation set for the whole PV array contains the elements of equation set of all m strings and some extra element equations as follow:

$$V_{i+1} = V_i - \sum_{k=1}^{i} I_k R_{c_{i(i+1)}}, \forall i \in [1...m] \tag{3.7}$$

$$V = V_{m+1} \tag{3.8}$$

$$I = \sum_{i=1}^{m} I_i \tag{3.9}$$

Mathematically, equation set, str_eq_i of a string is expressed as:

$$\begin{aligned} str\_eq_i = &\left\{(3.2)_{j=1,k=1}\right\} \cup \ldots \left\{(3.2)_{j=1,k=q_{i1}}\right\} \cup \ldots\ldots \cup \left\{(3.2)_{j=n,k=1}\right\} \cup \ldots \left\{(3.2)_{j=n,k=q_{in}}\right\} \\ &\cup \left\{(3.3)_{j=1}\right\} \cup \ldots \left\{(3.3)_{j=n}\right\} \cup \left\{(3.4)_{j=1}\right\} \cup \ldots \left\{(3.4)_{j=n}\right\} \cup \{(3.5)\} \cup \{(3.6)\} \end{aligned} \tag{3.10}$$

The equation set, Arr_eq for an array is expressed as follows:

$$Arr\_eq = str\_eq_1 \cup str\_eq_2 \cup str\_eq_3 \cup \ldots \cup str\_eq_m \cup \{(3.7)_{i=1}\} \cup \ldots \{(3.7)_{i=m}\} \cup \{(3.8)\} \cup \{(3.9)\} \tag{3.11}$$

The value of the open-circuit voltage, V_{oc_i} of the i^{th} string of a PV array is found by solving the following equation set for variable V_i:

$$str\_eq_i \cup \{I_i = 0\} \tag{3.12}$$

The open-circuit voltage, V_{oc} of the complete PV array is found by solving the following equation-

set for variable V:

$$Arr\_eq \cup \{I = 0\} \tag{3.13}$$

The equation sets (3.14) for string or (3.15) for array are solved for the string current 'I_i' or the array current I at a particular voltage, vol of the string or array:

$$str\_eq_i \cup \{V_i = vol\}, 0 \leq vol \leq V_{oc} \tag{3.14}$$

$$Arr\_eq \cup \{V = vol\}, 0 \leq vol \leq V_{oc} \tag{3.15}$$

The value of array power, $P = vol \times$ value of I is calculated to plot the I-V and P-V characteristics of the PV string or array.

3.3 Proposed technique to estimate the GMPP of a generalized model of a PV array

A flowchart for the proposed GMPP estimation method is shown in Fig. 3.3. The given steps are followed to estimate the GMPP of a generalized model of a PV array:

3.3.1 Finding and storing all the zero points of the PV array in a matrix

In this work, zero voltages are defined as voltage values for the PV array, which encloses the sections.

It could also be said that zero-points approximate the points where the P-V or I-V curve of the array changes its shape due to PSC. However, the majority of the zero-points are found by making the voltages equal to zero (bypass diode voltage or the string voltage). Hence, these are called zero-point voltages. Three types of zero points have been considered in this paper. In the zero point matrix, the first one for any string is assigned as 0. However, the reason behind this is that when the voltage across the groups with the highest short circuit current in a string is made equal to '0', then the voltage appear across the string or array will always be less than or equal to '0'. By taking the first type of zero point voltage as '0', the computational time is saved. The second types are those where the current through any bypass diodes becomes significantly less or comparable to 0. When it occurs, then the diode voltage becomes nearly

0. Therefore, the second zero-voltages are taken as the voltage across string or PV array (for good accuracy) when the voltage across any bypass diode becomes 0. The third type of zero point voltage is defined as the voltage where the current of any string becomes negligible. Short-circuit current, $I_{sc_{ij}}$ of each j^{th} group in the i^{th} string is obtained by solving the equation-set $\{(3.2)_{k=1}\} \cup \ldots \{(3.2)_{k=q_{ij}}\} \cup \{(3.3)\} \cup \{V_{ij} = 0\}$ for the variable I_{ij}. The maximum value of short-circuit current $I_{sc_{\max_i}}$, among all bypass diode groups in the i^{th} string is mathematically written as $I_{sc_{\max_i}} = \max\left(I_{sc_{ij}}, \forall j \in [1 \cdots n]\right)$. For the string having index i and n number of bypass diodes, the zero point voltages $V_{z_{ip}}$, $\forall p \in [1 \ldots n]$ of the PV array for i^{th} string, are obtained as follows:

If $I_{sc_{ip}} = I_{sc_{\max_i}}$, then,

$$V_{z_{ip}} = 0 \tag{3.16}$$

But if $I_{sc_{ip}} < I_{sc_{\max_i}}$, then, $V_{z_{ip}}$ are found by solving the following equation set for variable 'V_i':

$$str\_eq_i \cup \{V_{ip} = 0\} \tag{3.17}$$

if, value of $V_i < 0$ as found from (3.17), Then

$$V_{z_{ip}} = 0 \tag{3.18}$$

For, $p = n + 1$ only, the zero point voltage of the array for the i^{th} string, $V_{z_{i(n+1)}}$ is found by solving following equation for variable V_i:

$$str\_eq_i \cup \{I_i = 0\} \tag{3.19}$$

In the cases when any of the string connecting resistance is non zero, then (3.20)-(3.21) and (3.22)-(3.23) are recommended to solve for variable V instead of (3.17)-(3.18) and (3.19) to solve for variable V_i for estimating the second and third types of zero points, respectively. Also, for high accuracy of the zero-point estimation, in the case of any non-zero resistance between any two strings anywhere or the last string and output, the below mentioned equations are used.

$$Arr\_eq \cup \{V_{ip} = 0\} \tag{3.20}$$

if, value of $V < 0$ as found from (3.20), Then

$$V_{z_{ip}} = 0 \tag{3.21}$$

$$Arr\_eq \cup \{I_i = 0\} \tag{3.22}$$

if, value of $V < 0$ as found from (3.22), Then

$$V_{z_{i(n+1)}} = 0 \tag{3.23}$$

The equations (3.16)-(3.23) are valid $\forall i \in [1 \dots m]$.

All the zero points are stored in a matrix $V_{z_{m\times(n+1)}}$. Here, a row of the matrix stores the zero points related to that string whose index is equal to the index of that row. The matrix formation method can be little modified so that the zero voltages corresponding to the groups of same $I_{sc_{ij}}$ in a string are not required to calculate again by just copying from previously calculated value.

3.3.2 Sorting after merging the elements of all the rows of the matrix containing zero-points in ascending order

Based on the KCL, zero-point voltages of the array current versus voltage is obtained by taking the unrepeated value of the zero-points from all the string current versus array voltage curve. In this approach, the zero-point voltage of the matrix V_z having size $m \times (n+1)$ are arranged in ascending order in a single row without repeating the value of the voltage by utilizing set-theory based operations. Therefore, this row matrix 'A_{V_z}' has a maximum of mn+1 number of elements as the value of the first type of zero point voltages are equal to zero for all strings, i.e., $V_{z_{ij}} = 0$, for at least one value of $j \in [1...n]$ and $\forall i \in [1...m]$.

The arrangement of the elements in A_{V_z} and its length is given below.

$$\mathrm{A_{V_z}} = \text{sort\_in\_ascending}\left([\{\mathrm{V_z}\,(1,:)\} \cup \{\mathrm{V_z}\,(2,:)\} \cup \dots \ \dots \{\mathrm{V_z}\,(m,:)\}]\right) \tag{3.24}$$

and

$$l = \text{length}\left(\mathrm{A_{V_z}}\right) \tag{3.25}$$

Therefore,

$$l \leq mn + 1 \tag{3.26}$$

The A_{I_z} and A_{P_z} defined as the row matrix of the current and power values at every zero point voltage of the finally merged row-matrix, A_{V_z} are obtained as follows:

$$\mathrm{A}_{I_z} = Current\left(\mathrm{A}_{V_z}\right) \tag{3.27}$$

$$\mathrm{A}_{P_z} = \mathrm{A}_{V_z} \circ \mathrm{A}_{I_z} \tag{3.28}$$

Here, *Current* is the function on row-matrix $\mathrm{A}_{\mathrm{V}_z}$, which gives a row-matrix consisting of current values (obtained by (3.15)) of voltages given by elements of $\mathrm{A}_{\mathrm{V}_z}$ and '$\circ$' operation in (3.28) represents the element-wise multiplication of the two matrices. Here, note that whenever in this chapter a middle bracket {} bounds a row matrix it means that it denotes a set whose elements are the elements of the row matrix. Ex- $\{[0,0,2,2,3]\} = \{0,2,3\}$

3.3.3 Elimination of the non-potential sections

Let 'l_{IN}' be the length of row matrix, $\mathrm{A}_{V_{z_{IN}}}$ which contains only the starting voltages of the sections of power-voltage (P-V) or current-voltage (I-V) curve divided between the zero-voltages of the PV array in ascending order. As a result, the number of elements in $\mathrm{A}_{V_{z_{IN}}}$ is one less than A_{V_z}, which is expressed below.

$$l_{IN} = length\left(\mathrm{A}_{V_{z_{IN}}}\right) \tag{3.29}$$

and

$$l_{IN} = l - 1 \Rightarrow l_{IN} \leq mn \tag{3.30}$$

The $Maxpower_{\mathrm{A}_{V_z}}$ is the maximum value of power among the elements of A_{P_z} which is obtained as,

$$Maxpower_{\mathrm{A}_{V_z}} = \max\left(\mathrm{A}_{P_z}\right) \tag{3.31}$$

The $\mathrm{sec}_{s_{pmax}}$ for the s^{th} element of $\mathrm{A}_{V_{z_{in}}}$ is defined such that its value is always greater than all the power values at all voltages between $\mathrm{A}_{V_z}(s)$ and $\mathrm{A}_{V_z}(s+1)$. It is expressed as:

$$\mathrm{sec}_{s_{pmax}} = \mathrm{A}_{I_z}(s)\,\mathrm{A}_{V_z}(s+1) \tag{3.32}$$

The sections having a lesser value of $\mathrm{sec}_{s_{pmax}}$ than $Maxpower_{\mathrm{A}_{V_z}}$ will be eliminated and hence do not contribute to the formation of the row matrix, $\mathrm{A}_{PS_{V_{z_{IN}}}}$, which consists of initial voltages

of only potential sections.

3.3.4 Initialisation of the variable row matrix

$$N_{ES}^{(0)} = length\left(\mathrm{A}_{PS_{V_{z_{IN}}}}\right) \tag{3.33}$$

$$V_S^{(0)}(t) = \mathrm{A}_{PS_{V_{z_{IN}}}(t)} = \mathrm{A}_{V_z}(s) \tag{3.34}$$

$$V_F^{(0)}(t) = \mathrm{A}_{V_z}(s+1) \tag{3.35}$$

$$I_S^{(0)}(t) = \mathrm{A}_{PS_{I_{z_{IN}}}(t)} = \mathrm{A}_{I_z}(s) \tag{3.36}$$

$$I_F^{(0)}(t) = \mathrm{A}_{I_z}(s+1) \tag{3.37}$$

$$P_S^{(0)}(t) = \mathrm{A}_{PS_{P_{z_{IN}}}(t)} = \mathrm{A}_{P_z}(s) \tag{3.38}$$

and

$$P_F^{(0)}(t) = \mathrm{A}_{P_z}(s+1) \tag{3.39}$$

where s^{th} index element in A_{V_z} is same as the t^{th} index element in $\mathrm{A}_{PS_{V_{z_{IN}}}}$ as indicated by (3.34). The '0' super script denotes their initial value or value at the 0^{th} iteration. N_{ES} denotes the number of eligible sections. V_S and V_F represent the starting and final voltages of the current eligible section, respectively. I_S and I_F correspond to the starting and final currents of the current eligible section. Lastly, P_S and P_F indicate the starting and final powers of the current eligible section. The maximum power among the discovered points at the 0^{th} iteration, $M^{(0)}$ is as follow:

$$M^{(0)} = Maxpower_{\mathrm{A}_{V_z}} \tag{3.40}$$

3.3.5 Sub-proposed technique to estimate GMPP

A flowchart for the sub-proposed technique is shown in Fig. 3.3.

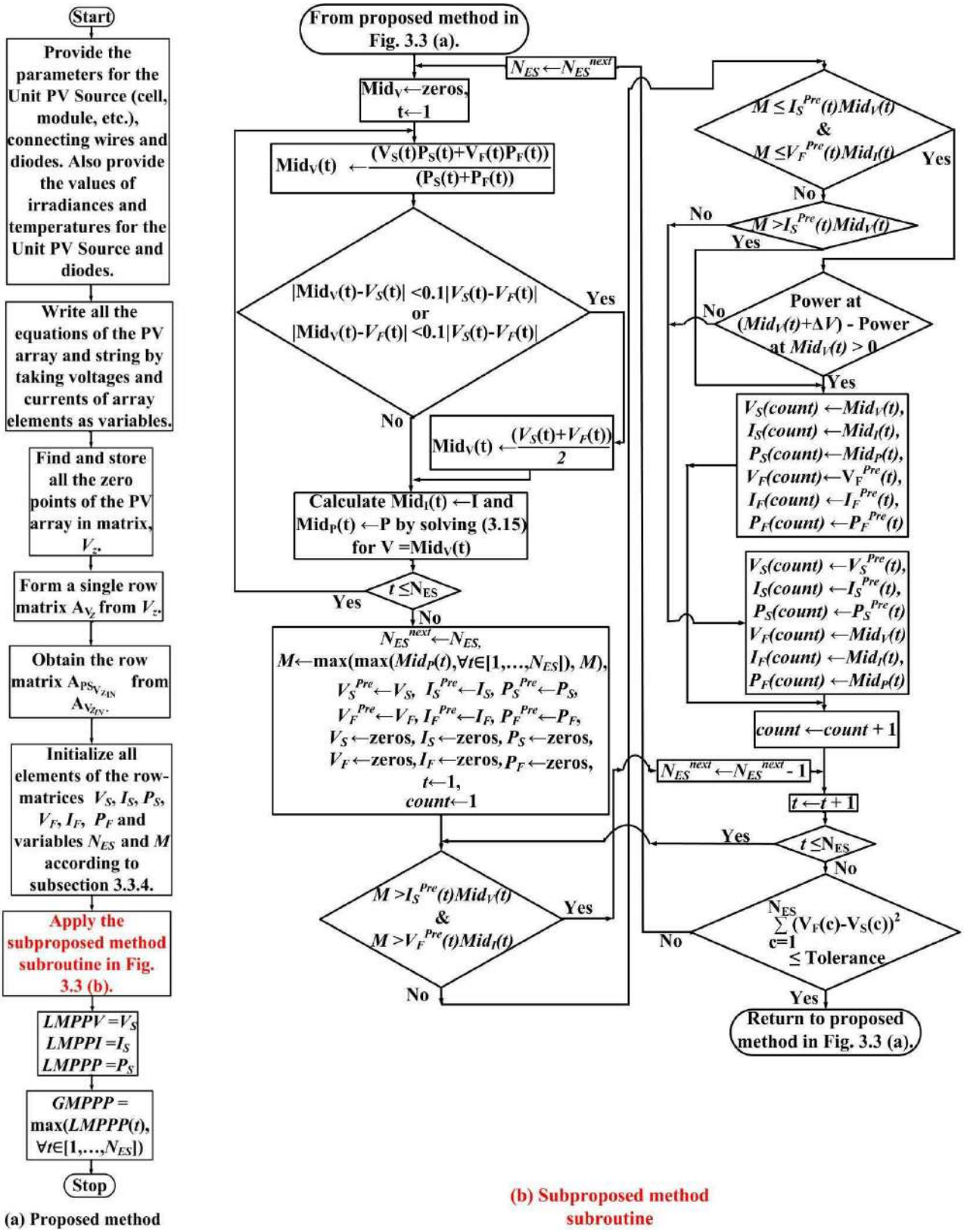

Figure 3.3: Proposed and sub-proposed technique

Derivation of the iteration voltage, $Mid_V(t)$

Fig. 3.4(a) shows two points (x_1, y_1) and (x_2, y_2) in the coordinate axis representing the initial and final boundary points of a section of P-V curve. In general, the LMPP lies near to the boundary point which has higher ordinate value. Hence, in this chapter, the iteration voltage is considered near the boundary point of higher ordinate. Therefore, following mathematical relation is used to derive the iteration voltage:

Ratio of distances of iteration point from the two boundary points = Inverse ratio of ordinates of the boundary points.

Since, $x_1 \leq x \leq x_2$, mathematically the above statement is written as follows:

$$\frac{x - x_1}{x_2 - x} = \frac{y_2}{y_1} \tag{3.41}$$

From (3.41),

$$x = \frac{x_1 y_1 + x_2 y_2}{y_1 + y_2} \tag{3.42}$$

where $y_1 \neq 0$ or $y_2 \neq 0$.

From (3.42), if $y_1 = 0$ then $x = x_2$ also $y_2 = 0$ then $x = x_1$. It is easily seen here that when the ordinate of any of the boundary point is zero or approximately zero, the obtained value of next iteration point is equal or very close to either of the boundary point. This may results in halting or trapping of the iteration point in the crest. Therefore, a modification is added in calculation of next iteration voltage. The modification is given below:

If $|x - x_1| \leq 0.1|x_1 - x_2|$ or $|x_2 - x| \leq 0.1|x_1 - x_2|$,

then, $x = \frac{x_1 + x_2}{2}$.

Now, if $x_1 = V_S(t)$, $x_2 = V_F(t)$, $y_1 = P_S(t)$, $y_2 = P_F(t)$, and $x = Mid_V(t)$,

$$Mid_V(t) = \frac{V_S(t)P_S(t) + V_F(t)P_F(t)}{P_S(t) + P_F(t)} \tag{3.43}$$

and if $|Mid_V(t) - V_S(t)| \leq 0.1|V_S(t) - V_F(t)|$ or $|V_F(t) - Mid_V(t)| \leq 0.1|V_S(t) - V_F(t)|$, then, $Mid_V(t) = \frac{V_S(t) + V_F(t)}{2}$.

3.4 Results and discussion

Three cases of a partially shaded PV array such as Case 1, 2, and 3 shown in Fig. 3.4(b), Fig. 3.4(c) and Fig. 3.4(d) are considered for the comparison of the proposed algorithm with other algorithms. However, 2000 extra cases are considered for the accuracy analysis of the proposed method.

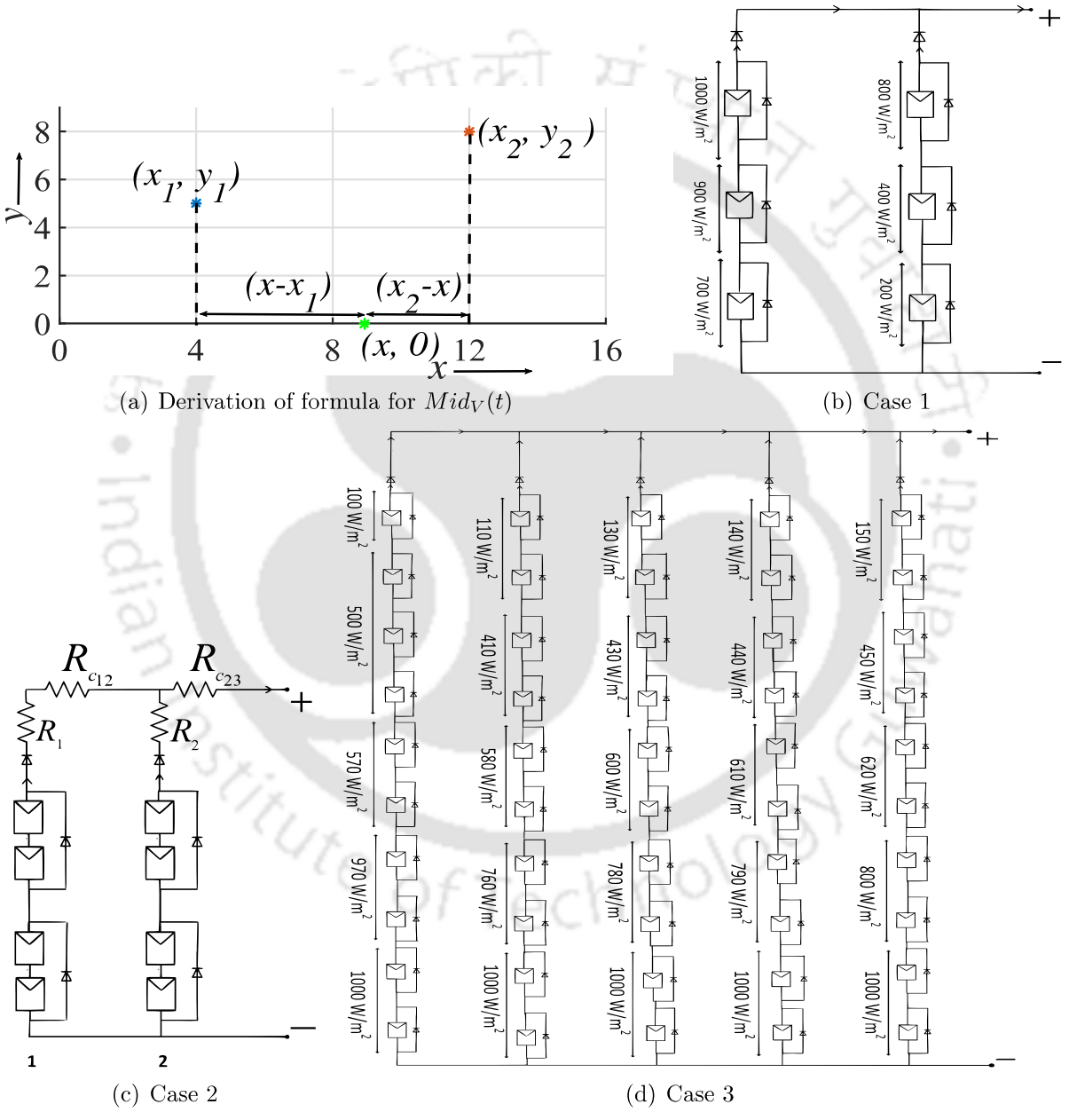

(a) Derivation of formula for $Mid_V(t)$ (b) Case 1

(c) Case 2 (d) Case 3

Figure 3.4: Formula derivation and electrical diagrams with irradiances for the GMPP estimation of Case 1,2 and 3.

The proposed algorithm is validated by estimating the GMPP using (3.15) for the Cases 1, 2, and 3 and performing an experiment in the laboratory scale setup for Case 2. The datasheet values of 3 W (make: Akshaya Solar Pvt. Ltd, India) and 252 W (make: Topsun Energy) PV modules considered for the simulation and experimental analysis are given in TABLE 3.1.

Table 3.1: Datasheet values of the PV modules

PV module	I_{SC} (A)	V_{OC} (V)	V_{MP} (V)	I_{MP} (A)	N_s
3 W	0.37	10.6	8.7	0.34	18
252 W	7.6	44	36	7	72

3.4.1 Simulation results

Case 1 (Fig. 3.4(b)), Case 2 (Fig. 3.4(c)) and Case 3 (Fig. 3.4(d)) are considered for the calculation of results. The proposed method is compared with [1], [50], and PSO[54] for Cases 1 and 3 only. While only PSO method is compared with the proposed method for Case 2 as other methods are not applicable for Case 2. All bypass and blocking diodes have the same diode quality factor and dark saturation current at STC, which are 1.87 and 8.5354 nA, respectively.

Case 1 : Fig. 3.4(b) represents the configuration for Case 1. The values of irradiances of the six 252 W PV modules are also given in the figure. All six modules and diodes are at a common temperature of 25^{o}C. Case 1 is taken as an example to explain the proposed method. Iterations of the proposed method along with the numbers obtained in each iteration of this case are explained with figures in this sub-subsection.

$$V_z \approx \begin{bmatrix} 0 & 34.82 & 77.98 & 125.48 \\ 0 & 39.35 & 81.38 & 130.76 \end{bmatrix}$$

Merging of both rows of V_z gives A_{V_z} as shown in Fig.3.5. After merging,

$$A_{V_z} \approx [0, 34.82, 39.35, 77.98, 81.38, 125.48, 130.76]$$

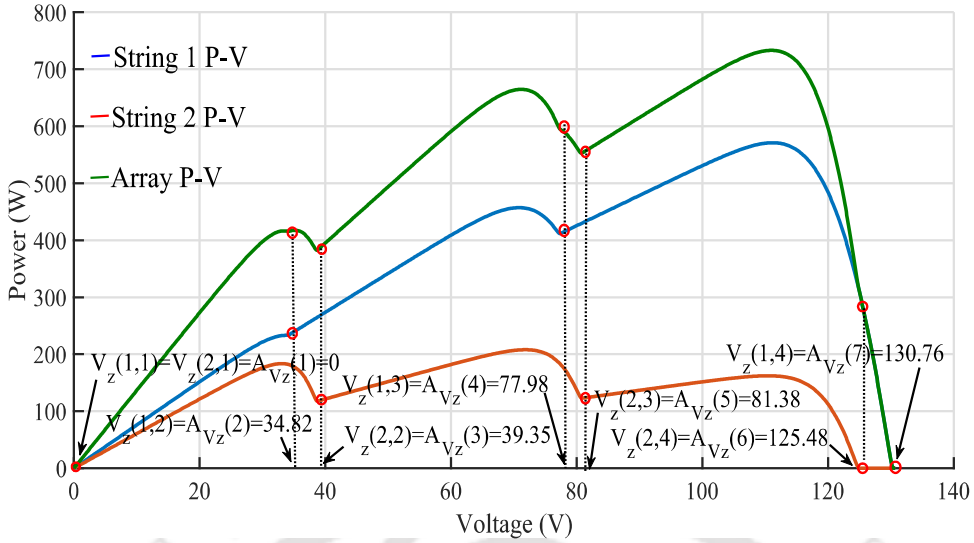

Figure 3.5: Demonstration figure to show formation of A_{V_z} by merging of the two rows of V_z.

Hence,

$$A_{V_{z_{IN}}} \approx [0, 34.82, 39.35, 77.98, 81.38, 125.48]$$

Also,

$$A_{I_z} = \text{Current}(A_{V_z}) \approx [13.68, 11.98, 9.88, 7.56, 6.84, 2.28, 0],$$

$$A_{P_z} = A_{V_z} \circ A_{I_z} \approx [0, 417.32, 388.76, 589.83, 556.60, 285.97, 0],$$

$$\text{Maxpower}_{A_{V_z}} \approx 589.83 \text{ W},$$

$$sec_{1_{pmax}} = A_{I_z}(1) \times A_{V_z}(2) \approx 476.29 \text{ W},$$

$$sec_{2_{pmax}} = A_{I_z}(2) \times A_{V_z}(3) \approx 471.64 \text{ W},$$

$$sec_{3_{pmax}} = A_{I_z}(3) \times A_{V_z}(4) \approx 770.45 \text{ W},$$

$$sec_{4_{pmax}} = A_{I_z}(4) \times A_{V_z}(5) \approx 615.49 \text{ W},$$

$$sec_{5_{pmax}} = A_{I_z}(5) \times A_{V_z}(6) \approx 858.24 \text{ W},$$

$$sec_{6_{pmax}} = A_{I_z}(6) \times A_{V_z}(7) \approx 298.01 \text{ W}.$$

Here, it is observed that $sec_{1_{pmax}}$, $sec_{2_{pmax}}$, and $sec_{6_{pmax}}$ have lesser value than $M^{(0)} = \text{Maxpower}_{A_{V_z}}$ and hence, $N_{ES}^{(0)} = 6 - 3 = 3$ and $A_{PS_{V_{z_{IN}}}} \approx [39.35, 77.98, 81.38]$. The zero

voltage points, '0', '34.82' and '125.48' are not present in $A_{PS_{V_{z_{IN}}}}$ because the section starting with these points are non-potential, as described earlier. Therefore, matrix Mid_V are only obtained from the three sections starting from voltage $A_{PS_{V_{z_{IN}}}}(1) \approx 39.35$ V, $A_{PS_{V_{z_{IN}}}}(2) \approx 77.98$ V and $A_{PS_{V_{z_{IN}}}}(3) \approx 81.38$ V. The index corresponding to $A_{PS_{V_{z_{IN}}}}(1)$, $A_{PS_{V_{z_{IN}}}}(2)$ and $A_{PS_{V_{z_{IN}}}}(3)$ in A_{V_z} are 3, 4 and 5, respectively. Therefore, the eligible boundary pair points corresponding to $A_{PS_{V_{z_{IN}}}}(1)$, $A_{PS_{V_{z_{IN}}}}(2)$ and $A_{PS_{V_{z_{IN}}}}(3)$ are ($A_{V_z}(3) = V_S^{(0)}(1) \approx 39.35$ V, $A_{V_z}(4) = V_F^{(0)}(1) \approx 77.98$ V), ($A_{V_z}(4) = V_S^{(0)}(2) \approx 77.98$ V, $A_{V_z}(5) = V_F^{(0)}(2) \approx 81.38$ V) and ($A_{V_z}(5) = V_S^{(0)}(3) \approx 81.38$ V, $A_{V_z}(6) = V_F^{(0)}(3) \approx 125.48$ V), respectively. Therefore, $V_S^{(0)} \approx$ [39.35 77.98 81.38], $I_S^{(0)} \approx$ [9.88 7.56 6.84], $P_S^{(0)} \approx$ [388.76 589.83 556.60], $V_F^{(0)} \approx$ [77.98 81.38 125.48], $I_F^{(0)} \approx$ [7.56 6.84 2.28], $P_F^{(0)} \approx$ [589.83 556.60 285.97]. $Mid_V^{(0)}$, $Mid_I^{(0)}$, and $Mid_P^{(0)}$ obtained are [62.63 79.63 96.34], [9.82 7.15 6.83] and [614.90 569.14 658.31], respectively. These values are shown in Fig. 3.6. Now, $V_S^{\mathrm{Pre}\,(0)} = V_S^{(0)} \approx [39.35, 77.98, 81.38]$, $I_S^{\mathrm{Pre}\,(0)} = I_S^{(0)} \approx [9.88, 7.56, 6.84]$,

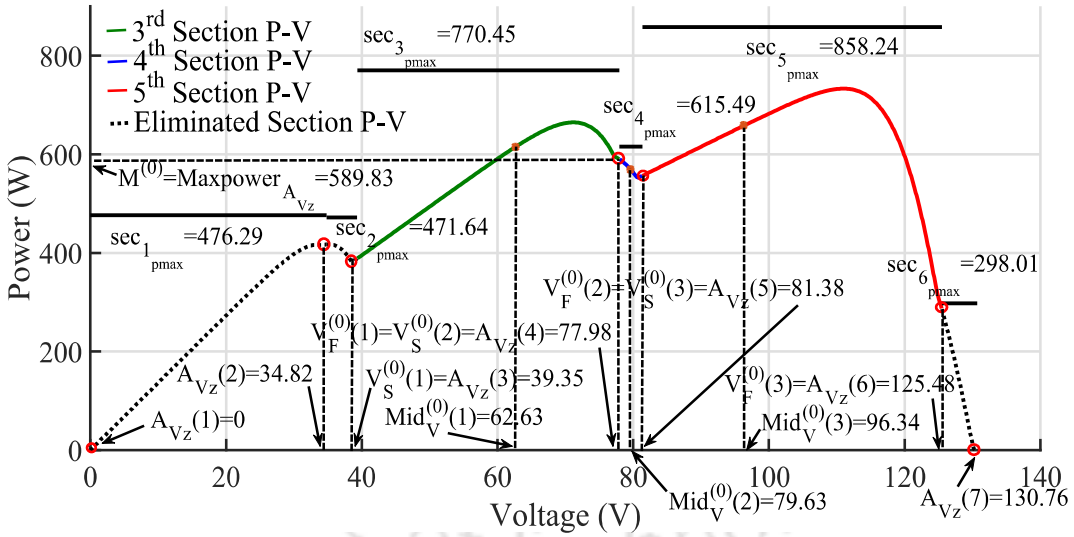

Figure 3.6: Demonstration figure of 0^{th} iteration to determine the GMPP of the P-V curve using the sub proposed method.

$P_S^{\mathrm{Pre}\,(0)} = P_S^{(0)} \approx [388.76, 589.83, 556.60]$,

$V_F^{\mathrm{Pre}\,(0)} = V_F^{(0)} \approx [77.98, 81.38, 125.48]$. $I_F^{\mathrm{Pre}\,(0)} = I_F^{(0)} \approx [7.56, 6.84, 2.28]$,

$P_F^{\mathrm{Pre}\,(0)} = P_F^{(0)} \approx [589.83, 556.60, 285.97]$.

Now, $M^{(1)} = \max(\max(Mid_P^{(0)}), M^{(0)}) \approx 658.31$ W and $N_{ES}^{\mathrm{next}(0)} = N_{ES}^{(0)} = 3$. For the first

eligible section or third section, $I_S^{\text{Pre}\,(0)}(1)Mid_V^{(0)}(1) < M^{(1)}$ and $Mid_I^{(0)}(1)V_F^{\text{Pre}\,(0)}(1) > M^{(1)}$. Therefore, the second part of the first eligible section is eligible for the next iteration. So, $V_S^{(1)}(1) = Mid_V^{(0)}(1)$, $I_S^{(1)}(1) = Mid_I^{(0)}(1)$, $P_S^{(1)}(1) = Mid_P^{(0)}(1)$, $V_F^{(1)}(1) = V_F^{\text{Pre}\,(0)}(1)$, $I_F^{(1)}(1) = I_F^{\text{Pre}\,(0)}(1)$, and $P_F^{(1)}(1) = P_F^{\text{Pre}\,(0)}(1)$.

For the second eligible section or fourth section, $I_S^{\text{Pre}\,(0)}(2)Mid_V^{(0)}(2) < M^{(1)}$ and $Mid_I^{(0)}(2)V_F^{\text{Pre}\,(0)}(2) < M^{(1)}$. Hence no part of the section is eligible for the next iteration. Therefore, due to the ineligibility of the second section, the number of eligible sections is reduced to 2 (= 3 - 1), i.e., $N_{ES}^{\text{next}(1)} = 2$.

For the third eligible section or fifth section, $I_S^{\text{Pre}\,(0)}(3)Mid_V^{(0)}(3) > M^{(1)}$ and $Mid_I^{(0)}(3)V_F^{\text{Pre}\,(0)}(3) > M^{(1)}$. Hence the part eligible for the next iteration is decided by the sign of the slope at $Mid_V^{(0)}(3)$ which is positive. Therefore, the second part of the third eligible section is eligible for the next iteration. Hence, $V_S^{(1)}(2) = Mid_V^{(0)}(3)$, $I_S^{(1)}(2) = Mid_I^{(0)}(3)$, $P_S^{(1)}(2) = Mid_P^{(0)}(3)$, $V_F^{(1)}(2) = V_F^{\text{Pre}\,(0)}(3)$, $I_F^{(1)}(2) = I_F^{\text{Pre}\,(0)}(3)$, and $P_F^{(1)}(2) = P_F^{\text{Pre}\,(0)}(3)$.

Therefore, $V_S^{(1)} \approx$ [62.63 96.34], $I_S^{(1)} \approx$ [9.82 6.83], $P_S^{(1)} \approx$ [614.90 658.31], $V_F^{(1)} \approx$ [77.98 125.48], $I_F^{(1)} \approx$ [7.56 2.28], $P_F^{(1)} \approx$ [589.83 285.97]. $Mid_V^{(1)}$, $Mid_I^{(1)}$, and $Mid_P^{(1)}$ obtained are [70.15 105.17], [9.46 6.79] and [663.61 713.78], respectively. These values are shown in Fig. 3.7.

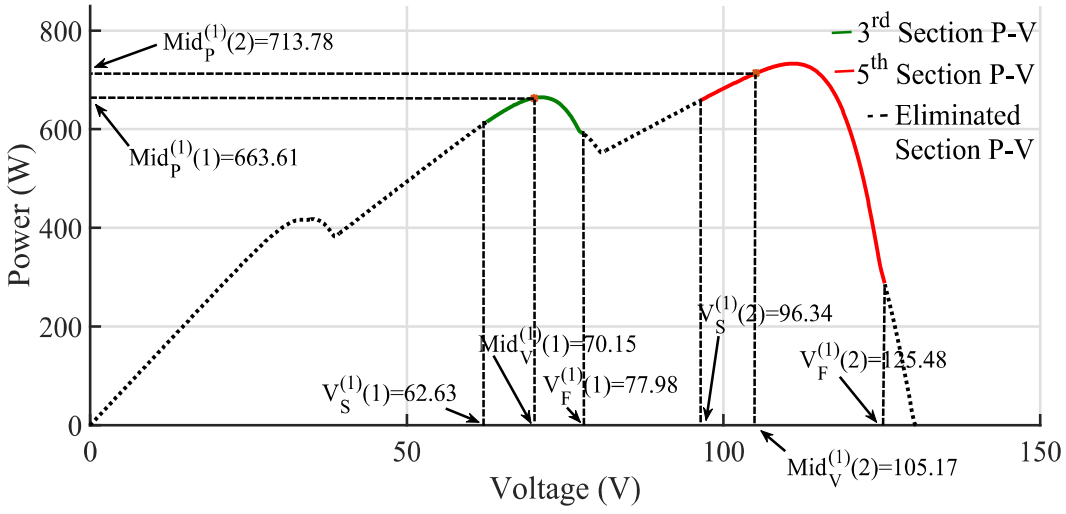

Figure 3.7: Demonstration figure of 1^{st} iteration to determine the GMPP of the P-V curve using the sub proposed method.

Now, $V_S^{\text{Pre}\,(1)} = V_S^{(1)} \approx [62.63, 96.34]$, $I_S^{\text{Pre}\,(1)} = I_S^{(1)} \approx [9.82, 6.83]$, $P_S^{\text{Pre}\,(1)} = P_S^{(1)} \approx [614.90, 658.31]$, $V_F^{\text{Pre}\,(1)} = V_F^{(1)} \approx [77.98, 125.48]$, $I_F^{\text{Pre}\,(1)} = I_F^{(1)} \approx [7.56, 2.28]$, and $P_F^{\text{Pre}\,(1)} = P_F^{(1)} \approx [589.83, 285.97]$.

Now, $M^{(2)} = \max(\max(Mid_P^{(1)}), M^{(1)}) \approx 713.78$ W and $N_{ES}^{\text{next}(1)} = N_{ES}^{(1)} = 2$. For the first eligible section or third section, $I_S^{\text{Pre}\,(1)}(1) Mid_V^{(1)}(1) < M^{(2)}$ and $Mid_I^{(1)}(1) V_F^{\text{Pre}\,(1)}(1) > M^{(2)}$.

Therefore, the second part of the first eligible section is eligible for the next iteration. So, $V_S^{(2)}(1) = Mid_V^{(1)}(1)$, $I_S^{(2)}(1) = Mid_I^{(1)}(1)$, $P_S^{(2)}(1) = Mid_P^{(1)}(1)$, $V_F^{(2)}(1) = V_F^{\text{Pre}\,(1)}(1)$, $I_F^{(2)}(1) = I_F^{\text{Pre}\,(1)}(1)$, and $P_F^{(2)}(1) = P_F^{\text{Pre}\,(1)}(1)$.

For the second eligible section or fifth section, $I_S^{\text{Pre}\,(1)}(2) Mid_V^{(1)}(2) > M^{(2)}$ and $Mid_I^{(1)}(2) V_F^{\text{Pre}\,(1)}(2) > M^{(2)}$. Hence the part eligible for the next iteration is decided by the sign of the slope at $Mid_V^{(1)}(2)$ which is positive. Therefore, the second part of the second eligible section is eligible for the next iteration. Hence, $V_S^{(2)}(2) = Mid_V^{(1)}(2)$, $I_S^{(2)}(2) = Mid_I^{(1)}(2)$, $P_S^{(2)}(2) = Mid_P^{(1)}(2)$, $V_F^{(2)}(2) = V_F^{\text{Pre}\,(1)}(2)$, $I_F^{(2)}(2) = I_F^{\text{Pre}\,(1)}(2)$, and $P_F^{(2)}(2) = P_F^{\text{Pre}\,(1)}(2)$. Therefore, $V_S^{(2)} \approx [70.15, 105.17]$, $I_S^{(2)} \approx [9.46, 6.79]$, $P_S^{(2)} \approx [663.61, 713.78]$, $V_F^{(2)} \approx [77.98, 125.48]$, $I_F^{(2)} \approx [7.56, 2.28]$, $P_F^{(2)} \approx [589.83, 285.97]$. $Mid_V^{(2)}$, $Mid_I^{(2)}$, and $Mid_P^{(2)}$ obtained are [73.84, 110.98], [8.86, 6.61], and [654.34, 733.16], respectively. These values are shown in Fig. 3.8.

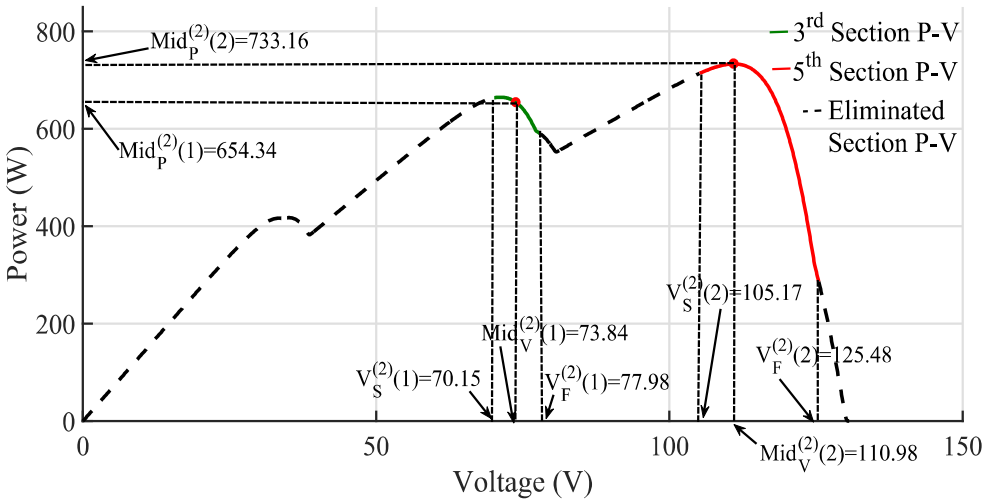

Figure 3.8: Demonstration figure of 2^{nd} iteration to determine the GMPP of the P-V curve using the sub proposed method.

Now, $V_S^{\text{Pre}\,(2)} = V_S^{(2)} \approx [70.15, 105.17]$, $I_S^{\text{Pre}\,(2)} = I_S^{(2)} \approx [9.46, 6.79]$, $P_S^{\text{Pre}\,(2)} = P_S^{(2)} \approx [663.61, 713.78]$, $V_F^{\text{Pre}\,(2)} = V_F^{(2)} \approx [77.98, 125.48]$, $I_F^{\text{Pre}\,(2)} = I_F^{(2)} \approx [7.56, 2.28]$, and $P_F^{\text{Pre}\,(2)} =$

$P_F^{(2)} \approx [589.83, 285.97]$.

Now, $M^{(3)} = \max(\max(Mid_P^{(2)}), M^{(2)}) \approx 733.16$ W and $N_{ES}^{\text{next}(2)} = N_{ES}^{(2)} = 2$.

For the first eligible section or third section, $I_S^{\text{Pre}\,(2)}(1) Mid_V^{(2)}(1) < M^{(3)}$ and $Mid_I^{(2)}(1) V_F^{\text{Pre}\,(2)}(1) < M^{(3)}$. Therefore, no part of the first eligible section is eligible for the next iteration. Due to the ineligibility of the first section, the number of eligible sections is reduced to 1 (= 2 - 1), i.e., $N_{ES}^{\text{next}(3)} = 1$. For the second eligible section or fifth section, $I_S^{\text{Pre}\,(2)}(2) Mid_V^{(2)}(2) > M^{(3)}$ and $Mid_I^{(2)}(2) V_F^{\text{Pre}\,(2)}(2) > M^{(3)}$. The part eligible for the next iteration is decided by the sign of the slope at $Mid_V^{(2)}(2)$, which is negative. Therefore, the first part of the second eligible section is eligible for the next iteration. Hence, $V_F^{(3)}(1) = Mid_V^{(2)}(2)$, $I_F^{(3)}(1) = Mid_I^{(2)}(2)$, $P_F^{(3)}(1) = Mid_P^{(2)}(2)$, $V_S^{(3)}(1) = V_S^{\text{Pre}\,(2)}(2)$, $I_S^{(3)}(1) = I_S^{\text{Pre}\,(2)}(2)$, and $P_S^{(3)}(1) = P_S^{\text{Pre}\,(2)}(2)$.

Therefore,

$$V_F^{(3)} \approx [110.98],$$

$$I_F^{(3)} \approx [6.61],$$

$$P_F^{(3)} \approx [733.16],$$

$$V_S^{(3)} \approx [105.17],$$

$$I_S^{(3)} \approx [6.79],$$

$$P_S^{(3)} \approx [713.78].$$

The values $Mid_V^{(3)}$, $Mid_I^{(3)}$, and $Mid_P^{(3)}$ obtained are [108.11], [6.73], and [727.37], respectively. These values are shown in Fig. 3.9.. Now,

$$V_S^{\text{Pre}\,(3)} \approx [105.17]$$

$$I_S^{\text{Pre}\,(3)} \approx [6.79]$$

$$P_S^{\text{Pre}\,(3)} \approx [713.78]$$

$$V_F^{\text{Pre}\,(3)} \approx [110.98]$$

$$I_F^{\text{Pre}\,(3)} \approx [6.61]$$

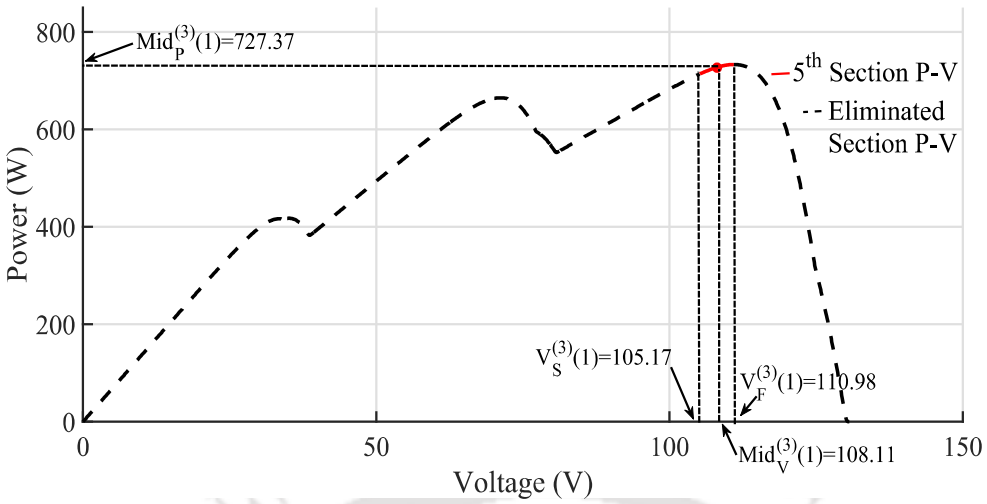

Figure 3.9: Demonstration figure of 3^{rd} iteration to determine the GMPP of the P-V curve using the sub proposed method.

$$P_F^{\text{Pre}\,(3)} \approx [733.16]$$

Furthermore,

$$M^{(4)} = \max\left(\max\left(Mid_P^{(3)}\right), M^{(3)}\right) \approx 733.16\text{W}$$

and

$$N_{ES}^{\text{next}\,(3)} = N_{ES}^{(3)} = 1.$$

After few iterations error reches the desired tolerance and hence the LMPPV and LMPPP obtained for the 5^{th} section are 110.89 V and 733.15 W. Therefore, the GMPP values using the proposed method are GMPPV $\approx$ 110.89 V and GMPPP $\approx$ 733.15 W. All the values in this case is presented in a number of two digits after decimal point. All the required equations in the GMPP estimation process are solved using 'fsolve' function of MATLAB in this and further sections. However, other iterative techniques for solving the equations can be used.

Case 2 : Table 3.2 gives the irradiance and temperature of 3 W PV module. Table 3.3 gives the temperature of the blocking and bypass diodes of the PV array in Fig. 3.4(c).

The resistances in the string-1 (R_1) and 2 (R_2) are 0.5 and 0.3 Ω, respectively. Also, the resistances of the connecting wire between string-1 and 2 ($R_{c_{12}}$) and between string-2 and output ($R_{c_{23}}$) are 0.1 and 0.2 Ω, respectively.

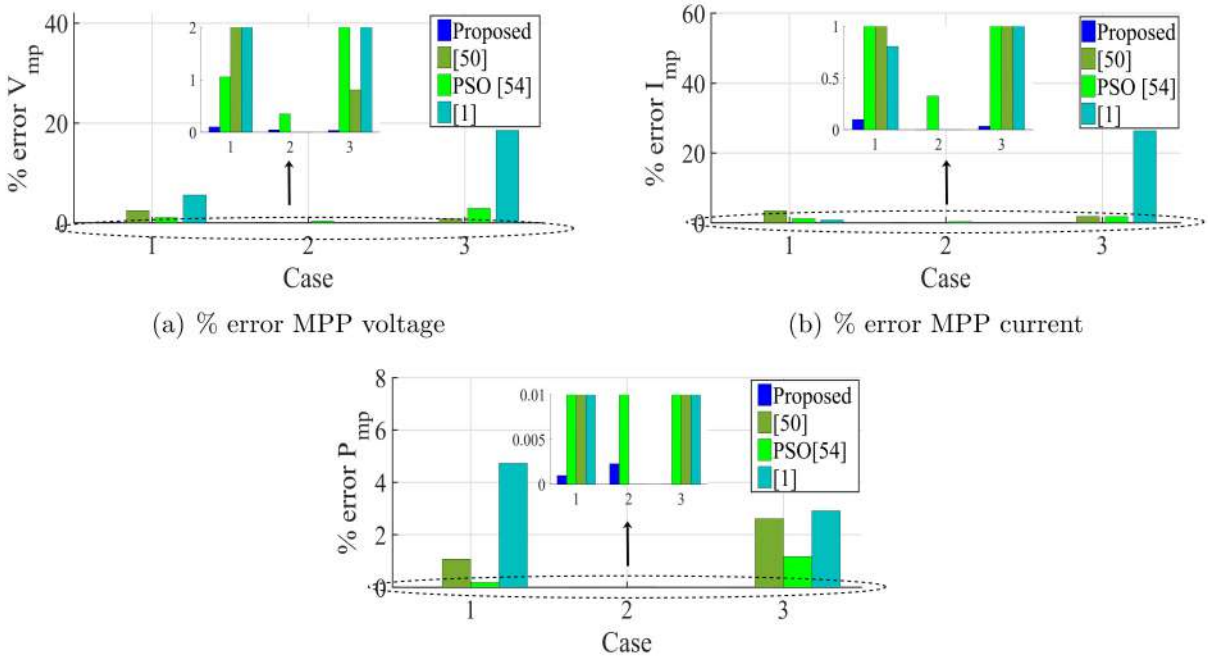

(a) % error MPP voltage

(b) % error MPP current

(c) % error MPP power

Figure 3.10: Comparison of % error in estimated MPP values using bar chart for Cases 1, 2 and 3.

Table 3.2: Irradiances and temperatures of PV modules in the PV array for Case 2

	String-1		String-2	
	Group-1	Group-2	Group-1	Group-2
Irradiances (W/m^2)	$G_{111} = 359.46$, $G_{112} = 381.08$	$G_{121} = 264.86$, $G_{122} = 386.49$	$G_{211} = 248.65$, $G_{212} = 378.38$	$G_{221} = 167.57$, $G_{222} = 386.49$
Temperature ($^\circ C$)	$T_{111} = 58$, $T_{112} = 58$	$T_{121} = 58$, $T_{122} = 58$	$T_{211} = 58$, $T_{212} = 58$	$T_{221} = 58$, $T_{222} = 58$

Table 3.3: Diodes temperatures in the PV array for Case 2

Temperature ($^\circ C$)	String-1	String-2
Bypass diode	$T_{11} = 49$, $T_{12} = 49$	$T_{21} = 51$, $T_{22} = 49$
Blocking diode	$T_1 = 32$	$T_2 = 32$

Following values are obtained during the application of the proposed method for Case 2:

$$V_z = \begin{bmatrix} 0 & 14.4188 & 34.5487 \\ 0 & 14.8622 & 33.9792 \end{bmatrix}$$

By merging the rows $V_z(1,:)$ and $V_z(2,:)$, a single row A_{V_z} is formed as follows, in accordance with the procedure described in Subsection 3.2.

Hence, $A_{V_z} = [0\ 14.4188\ 14.8622\ 33.9792\ 34.5487]$, $A_{PS_{V_{z_{IN}}}} = [0\ 14.4188\ 14.8622]$.

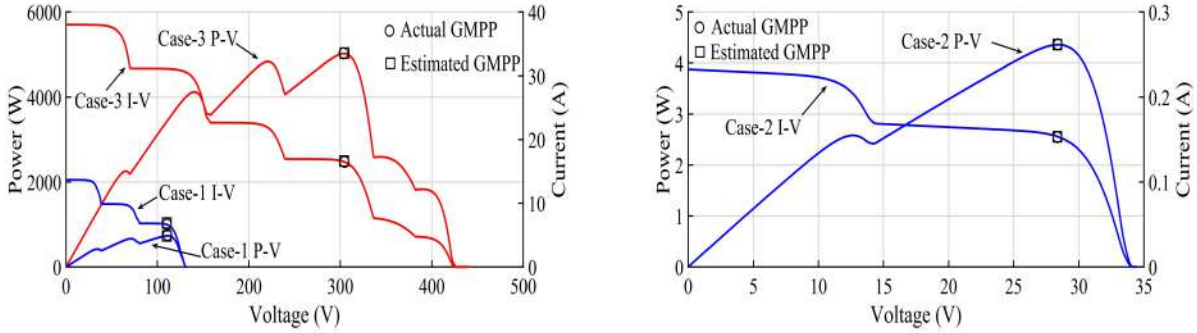

(a) Case-1 and 3 curves

(b) Case-2 curves

Figure 3.11: P-V and I-V curves for Cases 1, 2 and 3 to show accuracy of the proposed technique.

The estimated values of GMPPV and GMPPP are 28.4122 V and 4.3572 W, respectively.

Table 3.4: Comparison of the estimated GMPP using the proposed method with the GMPP using other methods for the partially shaded PV array of Case 3

	Proposed	[50]	[1]	PSO [54]
$GMPPV$ (V)	303.8959	301.5467	247.5996	295.1757
% error GMPPV	0.0342	0.8070	18.5528	2.9027
$GMPPI$ (A)	16.5146	16.2087	20.8600	16.8021
% error GMPPI	0.0339	0.0170	26.3553	1.7754
$GMPPP$ (W)	5018.7	4887.7	5164.9	4959.6
% error GMPPP	0	2.6102	2.9131	1.1776

Case 3 : Fig. 3.4(d) represents the configuration for Case 3. The values of irradiances of the fifty 252 W PV modules are also given in the figure. All the modules and diodes are at a common temperature of 25^{o}C. The estimated value of the GMPPV and GMPPP are 303.8959 V and 5018.7 W, respectively. Table 3.4 shows the comparison of the proposed method with the other methods for Case 3.

Comparisons of voltage, current, power and computational time of all methods in all the three cases : The comparisons of the proposed method with other methods in terms of accuracy are shown in Figs. 3.10(a), 3.10(b), and 3.10(c). It is observed from the figure and Table 3.4 that the % error in accuracy using the proposed method is always less than 1%. Table 3.5 shows the comparison of computational times using different methods. From Table 3.4 and 3.5, it is observed that the proposed method is more accurate and computationally efficient. Accuracy of the proposed method is also validated using the plots in Figs. 3.11(a) and 3.11(b)

for the Case-1, 3 and Case-2, respectively. Both the figures obtained using (3.15) show that the estimated value of GMPP is very close to the actual value of the GMPP.

Table 3.5: Comparison of time (second) to estimate the GMPP for different methods for all the three cases of partially shaded PV array

	Proposed (s)	[50] (s)	[1] (s)	PSO [54] (s)
Case 1	0.556724	10.583991	0.022921	0.841914
Case 2	0.557181	NA*	NA*	1.089763
Case 3	6.262844	1197.330917	0.021107	17.434296

* NA - Not applicable

Study on accuracy and computational time for 2000 random PSCs : The root mean square (RMS) % error and maximum % error of the proposed technique for 2000 randomly generated partially shading cases are shown in Table 3.6. Out of 2000 cases, 1000 cases are for 3×2 PV array of Case-1 while the other 1000 cases are for 4×2 PV array of Case-2 in which 3 W module is replaced by the 252 W module. In 3×2 PV array irradiances of all 6 modules are generated randomly in the range of 100–1100 W/m^2 for every single case of 1000 cases. All the diodes and modules in 3×2 PV array are at the temperature of 25^{o}C. All the parameters of diodes and temperatures of 4×2 PV array are same as in Case-2 however irradiances of 8 modules are randomly generated in the range of 100–1100 W/m^2 for every case of 1000 cases. It is observed from the Table 3.6 that RMS and maximum % error for all 2000 cases are less than 1 %. Average computational time for 1000 cases of 3×2 PV array and for 1000 cases for 4×2 PV array of Case-2 are 0.3398 and 1.2300 s, respectively. Here, RMS $\%error = \sqrt{\frac{\sum_{k=1}^{1000} \%error_k{}^2}{1000}}$ and $\%error_k$ is the % error in the GMPP value of the k^{th} random case.

Table 3.6: Accuracy to estimate the GMPP for the 2000 cases of random irradiances for a partially shaded PV array

	3×2 PV array		**4×2 PV array**	
	RMS (%)	**Maximum (%)**	**RMS (%)**	**Maximum (%)**
GMPPV	0.1107	0.3960	0.0634	0.2455
GMPPI	0.1098	0.3941	0.0631	0.2436
GMPPP	0.0012	0.0065	5.0462×10^{-4}	0.0025

Figure 3.12: Experimental setup

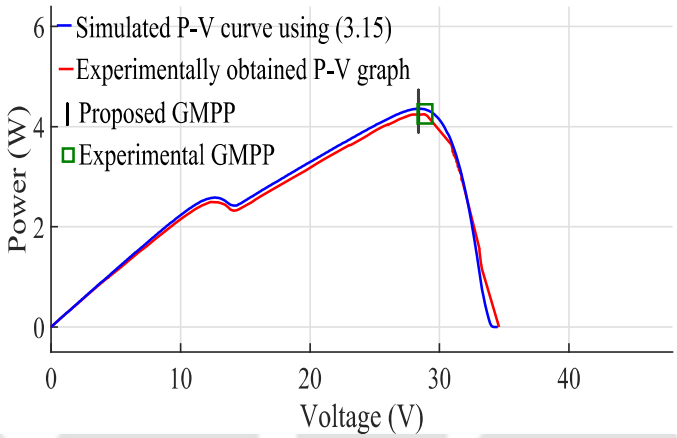

Figure 3.13: Experimental and simulated P-V curve of Case 2

3.4.2 Experimental results

For the validation of the proposed method for GMPP estimation under PSCs for Case 2 (in Fig. 3.4(c)), an experimental setup with wiring resistances is developed in the laboratory as shown in Fig. 3.12. The setup consists of the light source (10 halogen light bulbs) to emulate sun-light, an auto-transformer to control the intensity of halogen light by varying the voltage across bulbs, the PV array whose configuration and module specification is the same as of array in Case 2, a variable resistor (rheostat) to vary operating point and a multimeter to measure the array current and voltage. For emulating shade of different illuminance levels, same-thickness glass slabs of different numbers have been used. Fig. 3.13 shows the comparison of the estimated MPP power with the experimentally obtained value in a P-V curve. The reason for choosing halogen

bulbs is that their spectrum is similar to the solar spectrum. The experimental comparison of the GMPP is shown in Table 3.7. It is seen from the table that the error in the GMPPP obtained using the proposed method is 2.5494 % with respect to the GMPPP obtained experimentally which is well within the limit. The relatively higher % error in the estimated GMPP using the proposed method, compared to the experimental value, may be due to errors in the measurement of irradiance and temperature, as well as changes in parameters caused by the aging of the 3 W PV modules. Another reason could be the discrepancy between the solar and halogen bulb spectra, particularly in the wavelengths at which their spectral irradiance peaks.

Table 3.7: Comparison of the estimated GMPP using proposed method with the experimentally obtained value for Case 2

	Proposed GMPP	Experimental GMPP	% Error
GMPPV (V)	28.4122	28.8200	1.4150
GMPPI (A)	0.1534	0.1474	4.0706
GMPPP (W)	4.3572	4.2480	2.5494

3.5 Summary of the chapter

In this chapter, a novel model was developed for a generallized case of series-parallel (S-P) connected PV arrays. Utilizing set theory, equations were formulated that describe the dynamics of voltages and currents across strings and the entire array. These equations proved to be beneficial for I–V curve representation and GMPP estimation under PSC. A mathematical expression, influenced by the properties of the local maximum power point (LMPP), was also derived to aid the iterative process towards the GMPP.

One notable aspect of this approach is the elimination of non-potential sections from the P–V curve. This strategy enhances the speed of GMPP estimation, which could be particularly beneficial for large PV arrays. When compared to established methods such as those by [1], [50], and the Particle Swarm Optimization (PSO) [54] technique, this method exhibited a more efficient computational performance and improved accuracy.

Experimental validations, conducted using real-world PV modules, provided further support for the method's robustness and accuracy. The findings from this research suggest that the method might offer a reliable and efficient way to estimate GMPP. It is hoped that this approach could be a helpful tool for PV professionals, potentially aiding in the pursuit of optimal energy output from PV arrays.

Chapter 2 and this chapter focused on estimating the maximum power point to enhance the design, maintenance, operation, and power forecasting of PV plants. However, situations arise where maximum power is not harvested from the PV source, underscoring the necessity for a method to accurately calculate output power, voltage, and current under specific load and environmental conditions. Addressing this gap, next chapter introduces a novel method to precisely estimate the operating point, marking a significant advancement in PV system optimization.

Note: This work, "Analysis and GMPP estimation of a generalized model of a series-parallel (S-P) connected partially shaded PV array using Implicit double diode model of PV," has been published in Solar Compass, Volume 7, 2023, 100049, ISSN 2772-9400, DOI: 10.1016/j.solcom.2023.100049, ScienceDirect

Chapter 4

Operating point estimation of a PV plus load system

Contents

4.1 Introduction

Earlier in Chapters 2 and 3, the main emphasis was on the estimation of maximum power point for the design, maintainence, operation and output power forecasting of a PV plant. However, there may be some systems of PV source in which the maximum power is not being harvested from the PV source. In those conditions, it is important to calculate the output power, voltage and current at the given load and environmental condition. Therefore, there is a need to develop a mathematical method to accurately and efficiently estimate the operatimg point at the given load and environmental condition. In this regard, a novel method to estimate the operating point of a PV system with different loading conditions is proposed. The operating point of a PV source connected to a constant voltage load is easily calculated using explicit expression of PV. The DDM and SDM both models provide implicit I-V characteristics. Due to implicit expression, it is difficult to find the operating current of a PV module connected to a constant voltage source. Therefore, some researchers have converted the implicit I-V characteristics into the explicit form. The biggest obstacle to get the Lambert W-function based exact representation of DDM is the presence of two exponential terms [7]. However, researchers in [6] and [7] converted the implicit DDM I-V expression into the Lambert-W function [57] based representation. The proposed explicit expression of DDM PV module based on the Lambert-W function is computationaly less efficient. In case of Lambert-W based function models, series expansion, Pade approximation, and asymptotic expression are considered to estimate the current at various voltage levels, which introduces error in estimation. Some authors have neglected the series and shunt resistances of the PV cell[38]. An explicit expression of the DDM PV module is derived in [50] based on the 2nd order polynomial approximation of the exponential term in implicit I-V DDM equation. Due to approximations in the I-V expression of [38] and [50], the results provided in the literature are less accurate.

Nevertheless, these explicit expressions can only calculate the operating current of a PV module directly connected to a constant voltage source only. However, to estimate the operating voltage and current for other loads (e.g., at a particular resistance) iterative methods such as

Newton-Raphson (NR), Gauss-Siedel, etc., are used. Simulation tools like Spice are generally used to solve the circuits such as PV connected to voltage source or resistor. However, these softwares make circuit equations using the modified nodal analysis (MNA) technique. Thereafter, multi-variable equations are solved using the multidimensional NR method. However, in the process, MNA takes unnecessary variables for forming the equations. Also, the use of multi-dimensional NR increases computational complexity and decreases robustness. In [24], authors used one-dimensional NR to obtain the operating point. Wave digital technique are discussed in [58–63].

Wave digital based method [12] is proposed for the operating point estimation of a PV and resistive load. In [12], authors have applied single dimension NR on a modified function of two extra independent parameters and a single variable i.e., voltage to get the operating point voltage and current for a given load resistance connected to a PV system. Since the modified expression is more complex and requires three manual initialization and derivative calculation, it is computationally more expensive. Further, the Wave method requires a good initial guess for convergence in a reasonable time and it is not applicable to all kinds of loads.

To overcome the aforementioned limitations, a novel method is proposed to estimate the method, the operating point of PV with load system by two processes. The first process is rearranging the circuit into two components such as (i) PV without R_s and (ii) R_s with load. The second process is the characteristics matching between both components using a derivative-free novel method based on the parabolas whose axis of symmetry is parallel to the y-axis while the vertex is lying on the positive x-axis. The main advantage of the proposed method to estimate the operating point is less computationaly complex, in the estimation of the operating point. The complexity reduction is due to the unavailability of load characteristics expression in the exponential terms of the PV without R_s component. The complexity reduction becomes more significant when the operating point is estimated for a large number of cases of PV and load under various environmental conditions. Also, the proposed operating point estimation method is fast because it generally tends to the operating point from one direction only. Hence, it does not deviate much after reaching closer to the operating point. In this chapter, results

with various environmental and loading conditions are presented.

The explicit current expression of R_s with different load combinations in terms of the shunt voltage (V_{sh}) of a PV module in uniform irradiance condition is derived in Section 4.2. The proposed method for the operating point estimation of the PV with load is described in Section 4.3. Results-discussion and conclusion are described in Sections 4.4 and 4.5, respectively.

4.2 Proposed circuit rearrangement of PV plus load circuit

In this section, a novel method to rearrange the circuit of a PV source which is directly connected to an electrical load as shown in Fig. 4.1 is described. The circuit of PV with load system is divided into two components (i) PV without R_s and (ii) R_s with load as shown in the figure. In this chapter, operating point is estimated by the current-voltage characteristics matching of both the components.

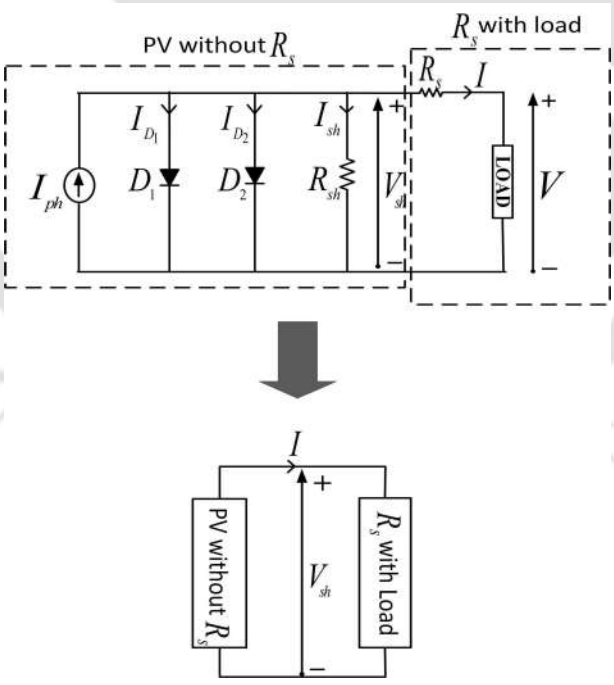

Figure 4.1: Equivalent circuit for PV with the load and the proposed method of circuit rearrangement.

The terminal current of the PV without R_s is given below as a function of V_{sh}.

$$I = I_{ph} - I_{o_1}\left(e^{\frac{V_{sh}}{A_1 N_s V_t}} - 1\right) - I_{o_2}\left(e^{\frac{V_{sh}}{A_2 N_s V_t}} - 1\right) - \frac{V_{sh}}{R_{sh}} = f_{PV}(V_{sh}) \tag{4.1}$$

where I_{ph}, I_{o_1}, I_{o_2}, R_s, R_{sh}, A_1, A_2, V_t and N_s have the same meaning as described in [12].

Function f_{PV} is an explicit expression of V_{sh}. Also from the current-voltage characteristic of the load, the following equation is obtained as follows:

$$I = f_L(V) \tag{4.2}$$

Where, $f_L(V)$ is a function of the load voltage, V only.

From the Ohm's law,

$$V = V_{sh} - IR_s \tag{4.3}$$

For some (resistors, constant voltage loads, combinations of resistors and constant voltage, DC motors, etc.) types of electrical load systems, (4.4) is obtained by combining (4.2) and (4.3).

$$I = F_L(V_{sh}) \tag{4.4}$$

Where $F_L(V_{sh})$ in (4.4) is current-voltage characteristics of R_s with load system and is a function of only variable V_{sh}. Function $F_L(V_{sh})$ for R_s with different loads are derived in further subsections.

4.2.1 Determination of the $F_L(V_{sh})$ of n-parallel $R-E$ loads connected to a DDM PV module

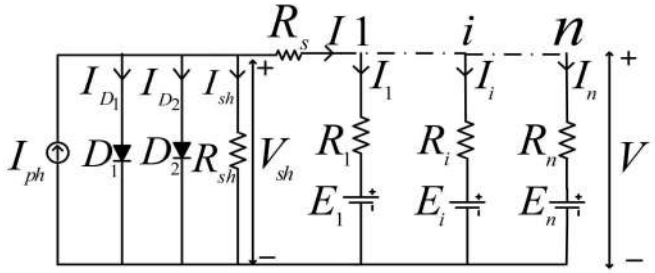

Figure 4.2: Equivalent circuit of PV system with n-parallel R-E loads.

In Fig. 4.2, R_i and E_i, $\forall\ i \in [1..n]$ are the resistance of resistor and voltage of the voltage source of the i^{th} branch of the voltage-source and resistor combination, respectively. Applying KCL and Ohm's law for n-parallel resistor and voltage source connected with PV system as shown in Fig. 4.2, the expression of the terminal current of the PV system is as follows:

$$I = \sum_{i=1}^{n} \frac{V - E_i}{R_i} = V \sum_{i=1}^{n} \frac{1}{R_i} - \sum_{i=1}^{n} \frac{E_i}{R_i} \tag{4.5}$$

Using (4.2) and (4.5), $f_L(V)$ is obtained as follows:

$$f_L(V) = \sum_{i=1}^{n} \frac{V - E_i}{R_i} = V \sum_{i=1}^{n} \frac{1}{R_i} - \sum_{i=1}^{n} \frac{E_i}{R_i} \tag{4.6}$$

Combining (4.5) and (4.3),

$$I = \frac{V_{sh} \sum_{i=1}^{n} \frac{1}{R_i} - \sum_{i=1}^{n} \frac{E_i}{R_i}}{1 + R_s \sum_{i=1}^{n} \frac{1}{R_i}} \tag{4.7}$$

Hence, from (4.4) and (4.7),

$$F_L(V_{sh}) = \frac{V_{sh} \sum_{i=1}^{n} \frac{1}{R_i} - \sum_{i=1}^{n} \frac{E_i}{R_i}}{1 + R_s \sum_{i=1}^{n} \frac{1}{R_i}} \tag{4.8}$$

4.2.2 Determination of the $F_L(V_{sh})$ of PV module connected with n-parallel PMDC motors

This subsection explains the mathematical formulation for PV module directly connected with n parallel PMDC motors.

Case I: When torques applied on different motors are known:

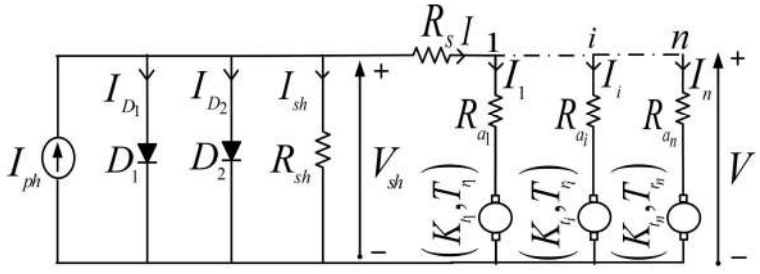

Figure 4.3: Equivalent circuits of a PV system with directly connected to n parallel PMDC motors with known electromagnetic torques.

Fig. 4.3 represents the equivalent circuit of parallel connected n number of permanent magnet DC motors along with known electromagnetic torques. Motor current, armature resistance, and applied electromagnetic torque on the i^{th} DC permanent magnet motor are represented as I_i, R_{a_i}, and T_{r_i}, respectively. Now from the torque equation,

$$I_i = \frac{T_{r_i}}{K_{t_i}}, \forall i \in [1, \ldots, n] \tag{4.9}$$

where K_{t_i} (in NmA^{-1}) is a constant.

Therefore,

$$I = \sum_{i=1}^{n} \frac{T_{r_i}}{K_{t_i}} \tag{4.10}$$

Hence, $f_L(V)$ of (4.2) using (4.10) is as follows:

$$f_L(V) = \sum_{i=1}^{n} \frac{T_{r_i}}{K_{t_i}} \tag{4.11}$$

From (4.4) and (4.10),

$$F_L(V_{sh}) = \sum_{i=1}^{n} \frac{T_{r_i}}{K_{t_i}} \tag{4.12}$$

Case II: **When speeds of different motors are known:** The equivalent circuit for the

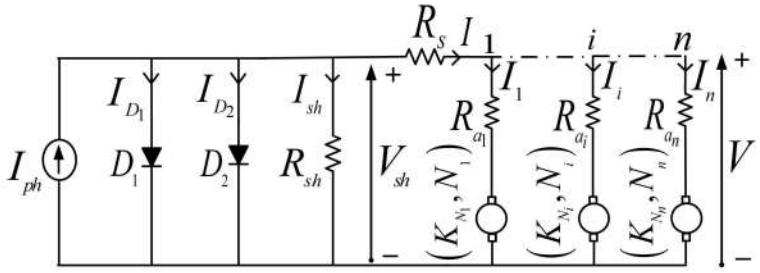

Figure 4.4: Equivalent circuits of a PV system with directly connected to n parallel PMDC motors with known speeds.

parallelly connected n number of PMDC motors with known speeds are presented in Fig. 4.4. Motor current, armature resistance, and speed of the i^{th} permanent magnet DC motors are represented as I_i, R_{a_i}, and N_i, respectively. The expression of the current derived from DC motor emf equation is given below.

$$I_i = \frac{V - K_{N_i} N_i}{R_{a_i}}, \forall i \in [1, \ldots, n] \tag{4.13}$$

where K_{N_i} (in V-min) is a constant.

Therefore, the terminal current of the PV system is as follows:

$$I = \sum_{i=1}^{n} \frac{V - K_{N_i} N_i}{R_{a_i}} \tag{4.14}$$

Hence, $f_L(V)$ of (4.2) using (4.14) is as follows:

$$f_L(V) = \sum_{i=1}^{n} \frac{V - K_{N_i} N_i}{R_{a_i}} \tag{4.15}$$

Substituting (4.3) in (4.14), the expression of I is obtained as follows:

$$I = C_1 V_{sh} - C_2 \tag{4.16}$$

where $C_1 = \frac{\sum_{i=1}^{n} \frac{1}{R_{a_i}}}{1 + R_s \sum_{i=1}^{n} \frac{1}{R_{a_i}}}$ and $C_2 = \frac{\sum_{i=1}^{n} \frac{K_{N_i} N_i}{R_{a_i}}}{1 + R_s \sum_{i=1}^{n} \frac{1}{R_{a_i}}}$

From (4.4) and (4.16),

$$F_L(V_{sh}) = C_1 V_{sh} - C_2 \tag{4.17}$$

4.2.3 Determination of the $F_L(V_{sh})$ of PV module directly connected with n-parallel DC series motors

This subsection explains the mathematical formulation for PV module directly connected with n number of different DC series motor connected in parallel.

Case I: When torques applied on different motors are known:

Fig. 4.5 represents the equivalent circuit for the parallel connected n DC series motors with known electromagnetic torques. Motor current, armature resistance, field resistance, and applied electromagnetic torque on the i^{th} DC series motor are represented as I_i, R_{a_i}, R_{f_i}, and T_{r_i}, respectively. From the torque equation; the derived expression of current is as follows:

$$I_i = \sqrt{\frac{T_{r_i}}{K_{t_i}}}, \forall i \in [1, \ldots, n] \tag{4.18}$$

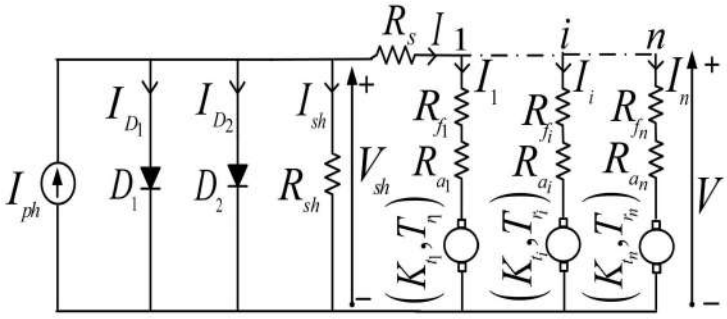

Figure 4.5: Equivalent circuits of a PV system with directly connected to n parallel DC series motors with known electromagnetic torques.

Where K_{t_i} (in NmA^{-2}) is constant.

Therefore, the total current drawn by the load from the PV system is as follows:

$$I = \sum_{i=1}^{n} \sqrt{\frac{T_{r_i}}{K_{t_i}}} \tag{4.19}$$

Since the motor is drawing the power from the PV system, the expression of this current given in (4.19) is taken as positive.

Hence, $f_L(V)$ of (4.2) using (4.19) is as follows:

$$f_L(V) = \sum_{i=1}^{n} \sqrt{\frac{T_{r_i}}{K_{t_i}}} \tag{4.20}$$

From (4.4) and (4.19),

$$F_L(V_{sh}) = \sum_{i=1}^{n} \sqrt{\frac{T_{r_i}}{K_{t_i}}} \tag{4.21}$$

Case II: **When speeds of different motors are known:**

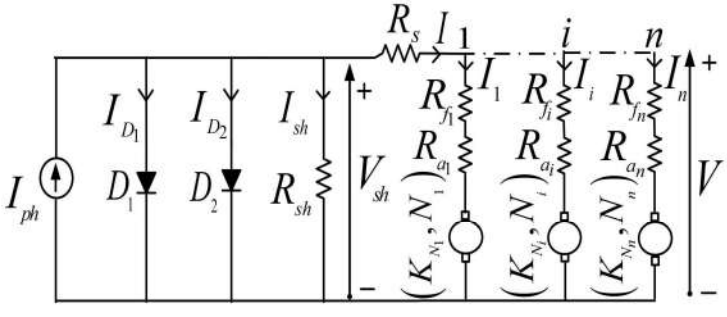

Figure 4.6: Equivalent circuits of a PV system with directly connected to n parallel DC series motors with known speeds.

Fig. 4.6 represents the equivalent circuit for the parallel connected n DC series motors with

known speeds. Motor current, armature resistance, field resistance, and speed of the i^{th} motor are represented as I_i, R_{a_i}, R_{f_i}, and N_i, respectively. The expression of the current from the emf equation of the DC series motor is given below.

$$I_i = \frac{V - I_i\left(R_{a_i} + R_{f_i}\right)}{K_{N_i} N_i}, \forall i \in [1, \ldots, n] \tag{4.22}$$

Where, K_{N_i} (in VA^{-1}-min) used in (4.22) is a constant.

After simplifying (4.22), the expression of I_i is written as:

$$I_i = \frac{V}{K_{N_i} N_i + R_{a_i} + R_{f_i}}, \forall i \in [1, \ldots, n] \tag{4.23}$$

Therefore, the total current drawn by the load from the PV system is as follows:

$$I = \sum_{i=1}^{n} \frac{V}{K_{N_i} N_i + R_{a_i} + R_{f_i}} \tag{4.24}$$

The $f_L(V)$ of (4.2) using (4.24) is as follows:

$$f_L(V) = V \sum_{i=1}^{n} \frac{1}{K_{N_i} N_i + R_{a_i} + R_{f_i}} \tag{4.25}$$

From (4.3) and (4.24),

$$I = \frac{V_{sh} \sum_{i=1}^{n} \frac{1}{K_{N_i} N_i + R_{a_i} + R_{f_i}}}{1 + R_s \sum_{i=1}^{n} \frac{1}{K_{N_i} N_i + R_{a_i} + R_{f_i}}} \tag{4.26}$$

Hence, from (4.4) and (4.26),

$$F_L(V_{sh}) = \frac{V_{sh} \sum_{i=1}^{n} \frac{1}{K_{N_i} N_i + R_{a_i} + R_{f_i}}}{1 + R_s \sum_{i=1}^{n} \frac{1}{K_{N_i} N_i + R_{a_i} + R_{f_i}}} \tag{4.27}$$

Similarly, $F_L(V_{sh})$ can be formulated for various types of loads under different conditions.

4.3 Proposed algorithm for the estimation of operating point of PV module directly connected to load

From Section 4.2, the current expression obtained from the DDM characteristics of the PV module, $f_{PV}(V_{sh})$ and the expression obtained from the electrical characteristics of the load, $F_L(V_{sh})$ as described in (4.4) are explicit expressions of V_{sh}. Let us consider, ΔF as:

$$\Delta F = f_{PV}(V_{sh}) - F_L(V_{sh}) \tag{4.28}$$

and

$$\Delta F_A = |\Delta F| \tag{4.29}$$

For analysis, let us define the operating point voltage of shunt resistance, R_{sh} and current for the combination of PV module with load as $V_{sh_{op}}$ and I_{op} respectively. Mathematically, it can be said that the operating point, ($V_{sh_{op}}$, I_{op}) satisfies both (4.1) and (4.4). Therefore, from (4.1), (4.4), (4.28) and (4.29) the voltage, $V_{sh_{op}}$ will satisfy the following equation:

$$\Delta F_A = 0 \tag{4.30}$$

The main objective of the method proposed in this chapter is to find the value of V_{sh} in power delivering region of PV for which ΔF_A becomes zero. Due to non-linear nature of ΔF_A, it is very difficult to find the V_{sh} which makes ΔF_A equals to zero. However, the proposed method is useful

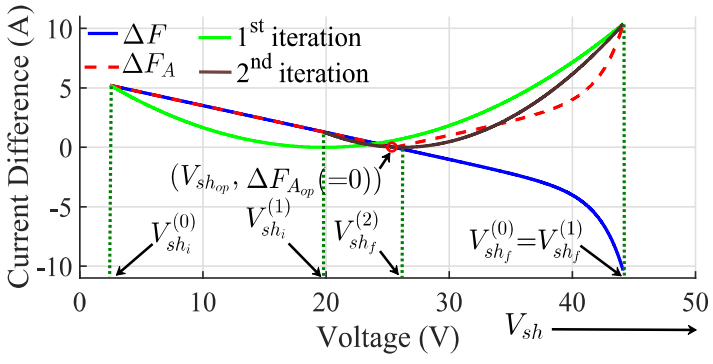

Figure 4.7: Schematic of the proposed algorithm.

to estimate the V_{sh} for which ΔF_A becomes nearly equal to zero. At last, it also checks whether

I_{op} is non-positive or not. If I_{op} is found to be positive then the PV and load combination has the operating point in the power delivering region of PV otherwise it has not. Fig. 4.7 shows the working of the proposed estimation method for the estimation of operating point.

The proposed method is based on the parabola passing through two points of first quadrant whose axis of symmetry is parallel to y-axis while vertex is lying on x-axis. The derivation of vertex position of parabola is given in Subsection 4.3.1.

The steps of the proposed algorithm to determine the operating point are given as:

- $k \leftarrow 0$.

- The initial boundary voltage, $V_{sh_i}^{(0)}$ ($\geq I_{sc}R_s$), should be chosen such that $F_L(V_{sh})$ is real for $V_{sh_i}^{(0)} \leq V_{sh} \leq V_{sh_f}^{(0)}$. Here, I_{sc} is the short circuit current of the PV array at the given environmental condition. However, $V_{sh_i}^{(0)} = I_{ph}R_s$ is valid for many cases. While the final boundary voltage $V_{sh_f}^{(0)}$ is given by $A_1 N_s V_t \ln\left(\frac{I_{ph}}{I_{o_1}} + 1\right)$, which can be assigned to $V_{sh_f}^{(0)}$ instead of actual open-circuit voltage, V_{oc}.

- The value of the vertex voltage of the parabola at the k^{th} iteration is

$$V_{sh_{ver}}^{(k)} = \frac{V_{sh_i}^{(k)}\sqrt{\Delta F_{A_i}^{(k)}} + V_{sh_f}^{(k)}\sqrt{\Delta F_{A_f}^{(k)}}}{\sqrt{\Delta F_{A_i}^{(k)}} + \sqrt{\Delta F_{A_f}^{(k)}}}$$

  Where, functions $\Delta F_{A_i}^{(k)}$ and $\Delta F_{A_f}^{(k)}$ are defined as follows:
  $\Delta F_{A_i}^{(k)} = \Delta F_A|_{V_{sh}=V_{sh_i}^{(k)}}$ and $\Delta F_{A_f}^{(k)} = \Delta F_A|_{V_{sh}=V_{sh_f}^{(k)}}$.
  The derivation of the expression ($V_{sh_{ver}}^{(k)}$) for the vertex position is given in subsection 4.3.1.

- The value of function ΔF and ΔF_A at the k^{th} iteration voltage $V_{sh_{ver}}^{(k)}$ are defined as $\Delta F_{ver}^{(k)}$ and $\Delta F_{A_{ver}}^{(k)}$, respectively. These are found by substituting the value of voltage V_{sh} as $V_{sh_{ver}}^{(k)}$ in (4.28) and (4.29), respectively.

- If $\Delta F_{ver}^{(k)} \geq 0 \Rightarrow V_{sh_{op}} \geq V_{sh_{ver}}^{(k)}$. Hence, $V_{sh_i}^{(k+1)} = V_{sh_{ver}}^{(k)}$ and $V_{sh_f}^{(k+1)} = V_{sh_f}^{(k)}$. Similarly $\Delta F_{A_i}^{(k+1)} = \Delta F_{A_{ver}}^{(k)}$ and $\Delta F_{A_f}^{(k+1)} = \Delta F_{A_f}^{(k)}$.

But if $\Delta F_{ver}^{(k)} < 0 \Rightarrow V_{sh_{op}} \leq V_{sh_{ver}}^{(k)}$. Hence, $V_{sh_f}^{(k+1)} = V_{sh_{ver}}^{(k)}$ and $V_{sh_i}^{(k+1)} = V_{sh_i}^{(k)}$. Similarly $\Delta F_{A_f}^{(k+1)} = \Delta F_{A_{ver}}^{(k)}$ and $\Delta F_{A_i}^{(k+1)} = \Delta F_{A_i}^{(k)}$.

- Check if, $\Delta F_{A_{ver}}^{(k)} \leq \varepsilon$.

  If yes, exit the loop. But if no, k←k+1 and go to step 3. Where, ε is the tolerance which is less for the higher accuracy.

After finding $V_{sh_{op}}$, I_{op} is found using (4.4) or (4.1) by substituting V_{sh}= $V_{sh_{op}}$ and the operating voltage at the output terminal i.e., V_{op} is obtained using (4.3) by substituting V_{sh}= $V_{sh_{op}}$ and I= I_{op}. Also check whether I_{op} is positive. If I_{op} found to be positive then the PV and load combination has the operating point in the power delivering region of PV.

A flowchart of the proposed method is shown in Fig. 4.8. Before applying the proposed method, the condition $\Delta F_i^{(0)} \Delta F_f^{(0)} < 0$ is checked.

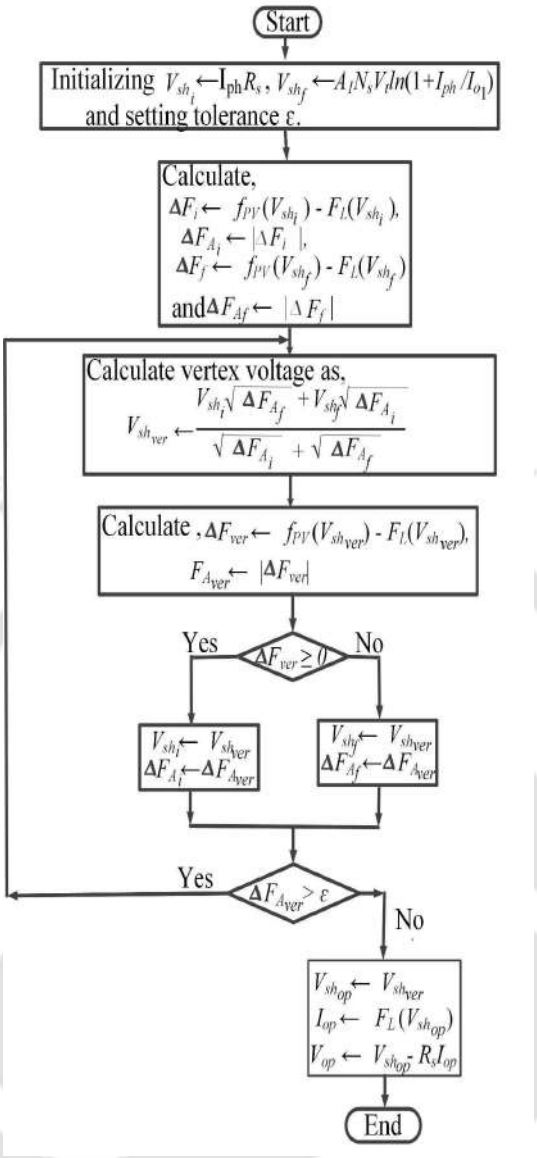

Figure 4.8: Flowchart of the proposed algorithm.

4.3.1 Derivation of the vertex position of the parabola

Let (x_1, y_1) and (x_2, y_2) are two points in the first quadrant and a parabola whose vertex $(c_1, 0)$ lying on x-axis is passing through both the points as shown in Fig. 4.9. Since the axis of symmetry of the parabola is parallel to the y-axis, the equation of the parabola is given below.

$$(x - c_1)^2 = c_2 y \tag{4.31}$$

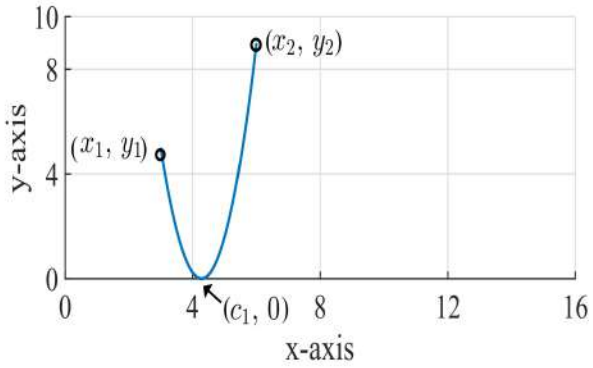

Figure 4.9: Schematic diagram of the parabola to derive its vertex position.

After substituting the points, (x_1, y_1) and (x_2, y_2) in (4.31), following equations are obtained.

$$(x_1 - c_1)^2 = c_2 y_1 \tag{4.32}$$

$$(x_2 - c_1)^2 = c_2 y_2 \tag{4.33}$$

Rearranging (4.33),

$$c_2 y_2 = (x_2 - c_1)^2 \tag{4.34}$$

Multiplying, (4.32) and (4.34),

$$(x_1 - c_1)^2 c_2 y_2 = (x_2 - c_1)^2 c_2 y_1 \tag{4.35}$$

$$\Rightarrow y_2 (x_1 - c_1)^2 = y_1 (x_2 - c_1)^2 \tag{4.36}$$

As $x_1 \leq c_1 \leq x_2$, (4.36) is simplified as follows:

$$(c_1 - x_1)\sqrt{y_2} = (x_2 - c_1)\sqrt{y_1} \tag{4.37}$$

$$\Rightarrow c_1 = \frac{x_1\sqrt{y_2} + x_2\sqrt{y_1}}{\sqrt{y_1} + \sqrt{y_2}} \tag{4.38}$$

Where, $y_1 \neq 0$ or $y_2 \neq 0$.

4.4 Results and discussion

4.4.1 Simulation results

In the present analysis, three types of loads are directly connected to 195.5 W (make: Topsun) PV module. The datasheet values of modules are given in Table 4.1. The comparison of the operating points for Wave and the proposed techniques in terms of computational time and % errors for resistive load (R = 60 Ω), PMDC motor (K_t = 0.0047 NmA^{-1}, $K_N = 4.9218 \times 10^{-4}$ V-min/A, R_a = 4.2 Ω) and DC series motor (K_t = 0.1511 NmA^{-2}, K_N = 0.0158 V-min/A, R_a = 0.6 Ω, R_f = 0.4 Ω) are given in Table-4.2.

Table 4.1: Datasheet values of the PV modules

PV module	I_{SC} (A)	V_{OC} (V)	V_{MP} (V)	I_{MP} (A)	N_s
250 W	8.76	37.7	30.9	8.09	60
195.5 W	5.77	44	36	5.43	72
10 W	0.63	21.07	17.03	0.59	36

Table 4.2: Comparison of estimated operating points for different loads

Methods	V_{op} (V)	% Error of V_{op}	I_{op} (A)	% Error of I_{op}	P_{op} (W)	% Error of P_{op}	t_{op} (s)
Resistive load, $R = 60\Omega$							
Wave [12]	41.7293	≈ 0	0.6955	≈ 0	29.0222	≈ 0	0.0251
Proposed	41.7293	≈ 0	0.6955	≈ 0	29.0222	≈ 0	0.0131
PMDC motor, $T = 0.0017$ Nm							
Proposed	42.0021	≈ 0	0.3617	≈ 0	15.1923	≈ 0	0.0137
PMDC motor, $N = 15000$ rpm							
Proposed	30.8930	≈ 0	5.5977	≈ 0	172.9294	≈ 0	0.0137
DC series motor, $T = 1$ Nm							
Proposed	39.9754	≈ 0	2.5725	≈ 0	102.8360	≈ 0	0.0122
DC series motor, $N = 300$ rpm							
Proposed	31.8828	≈ 0	5.5545	≈ 0	177.0924	≈ 0	0.0139

In first case, the PV module of 195.5 W at the irradiance of 980 W/m^2 and temperature of 36 ^{o}C is connected to a resistive load of 60 Ω. The actual operating point calculated from Figure 4.10 is 41.7293 V, 0.6955 A, and 29.0222 W.

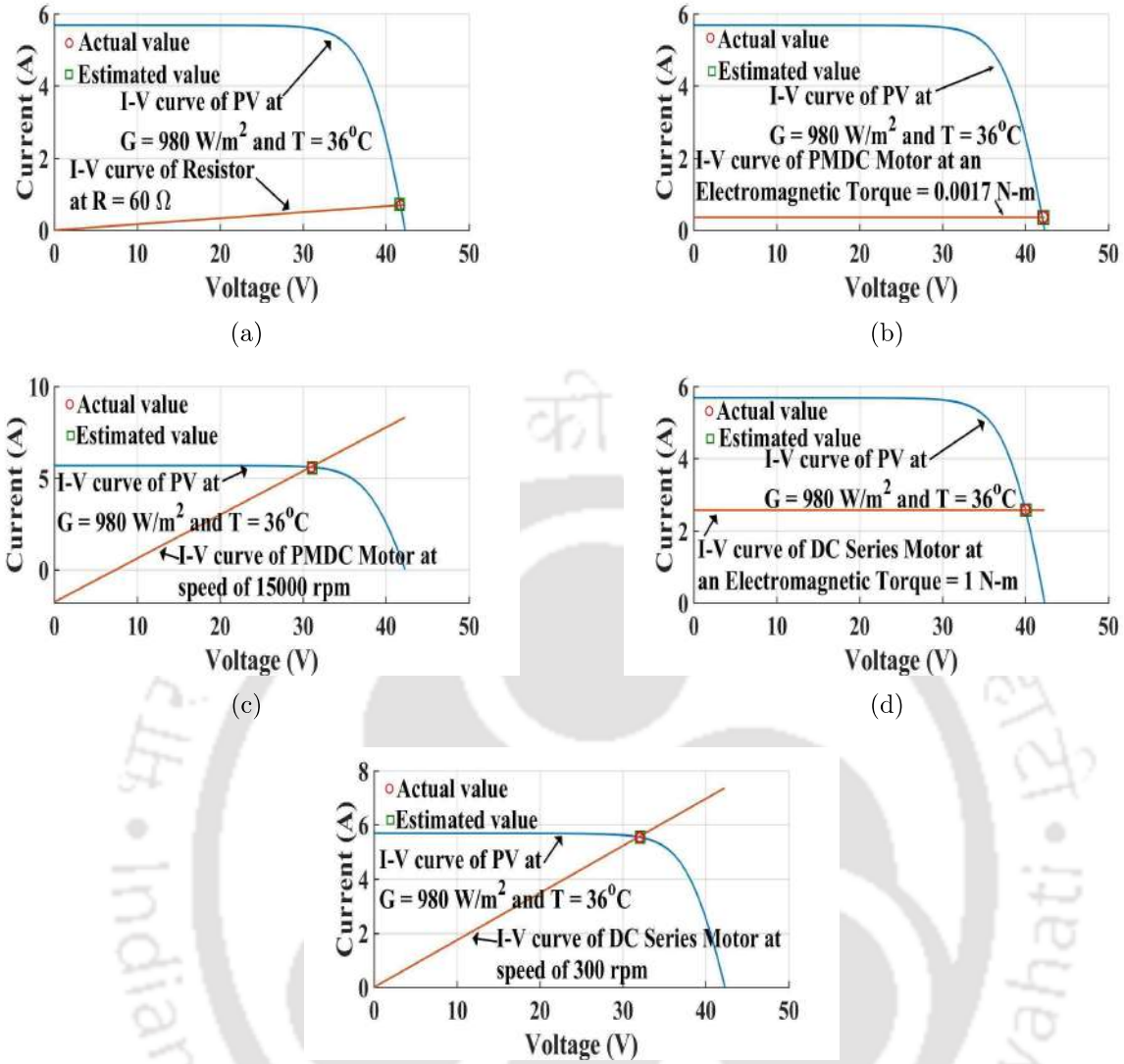

Figure 4.10: Operating points of PV system with directly connected to (a) resistive load, (b) PMDC motor with known torque, (c) PMDC motor with known speed, (d) DC series motor with known torque, and (e) DC series motor with known speed.

In second, third, fourth and fifth cases, 195.5 W PV module at the irradiance of 980 W/m^2 and temperature of 36 ^{o}C is connected to a PMDC motor applying an electromagnetic torque of 0.0017 N-m, a PMDC motor rotating at a speed of 15000 rpm, a DC series motor applying an electromagnetic torque of 1 N-m and a DC series motor rotating at the speed of 300 rpm, respectively. The actual operating point for the second case is 42.0021 V, 0.3617 A, and 15.1923 W, for the third case is 30.8930 V, 5.5977 A, and 172.9294 W, for the fourth case is 39.9754 V, 2.5725 A, and 102.8360 W, and for the fifth case is 31.8828 V, 5.5545 A and 177.0924 W. The

results obtained using the proposed method are compared with the results obtained using Wave method. It is observed from Table 4.2 that the proposed method is computationally more efficient for all the five cases. Since the Wave method is only applicable for resistive load, the comparison between the proposed and Wave method is not presented for PMDC and series motors in Table 4.2.

Table 4.3 presents the comparison between the proposed and Wave method in terms of % error in operating power and computational time varying irradiance from 500 to 1000 W/m^2 for R = 50 Ω, temperature of 20 ^{o}C and R = 75 Ω, temperature of 40 ^{o}C. It is observed from the table that the proposed method is more computationally efficient than the Wave method. The operating point of a PV module connected to the resistance from 125 to 9600 Ω with stepsize of 1 Ω estimated using proposed and Wave method are presented in Table 4.4. The simulation results for three different PV modules under two different cases such as Case A (G = 980 W/m^2 and T = 36 ^{o}C) and Case B (G = 500 W/m^2 and T = 10 ^{o}C) are depicted in this table.

Table 4.3: Detailed comparison between Wave and the proposed method

	Irradiance (W/m^2)	500	600	700	800	900	1000
		$R = 50\ \Omega$ and $T = 20°C$					
Wave [12]	% P_{op}	≈ 0	≈ 0	≈ 0	≈ 0	≈ 0	≈ 0
	t_{op} (s)	0.0252	0.0244	0.0228	0.0236	0.0256	0.0258
Proposed	% P_{op}	≈ 0	≈ 0	≈ 0	≈ 0	≈ 0	≈ 0
	t_{op} (s)	0.0130	0.0137	0.0126	0.0126	0.0149	0.0129
		$R = 75\ \Omega$ and $T = 40°C$					
Wave [12]	% P_{op}	≈ 0	≈ 0	≈ 0	≈ 0	≈ 0	≈ 0
	t_{op} (s)	0.0273	0.0226	0.0255	0.0256	0.0232	0.0227
Proposed	% P_{op}	≈ 0	≈ 0	≈ 0	≈ 0	≈ 0	≈ 0
	t_{op} (s)	0.0127	0.0126	0.0145	0.0124	0.0161	0.0142

It is observed from the table computational time in the proposed method compared to Wave method decreases when the operating points are calculated for a large number of cases of PV and load or when the $f_L(V)$ of given load combination connected to the PV unit is very complex.

The root mean square of percentage error in operating voltage, current and power and total computation time (s) using Wave and proposed method are presented in this table. It is observed

Table 4.4: Comparison between Wave and the proposed method

PV module	Case	% RMSE for V_{op}	% RMSE for I_{op}	% RMSE for P_{op}	Total time (s)
			Wave		
10 W	Case A	≈ 0	≈ 0	≈ 0	0.7217
	Case B	≈ 0	≈ 0	≈ 0	0.7676
195.5 W	Case A	≈ 0	≈ 0	≈ 0	0.5881
	Case B	≈ 0	≈ 0	≈ 0	0.6835
250 W	Case A	≈ 0	≈ 0	≈ 0	0.4891
	Case B	≈ 0	≈ 0	≈ 0	0.5838
			Proposed		
10 W	Case A	≈ 0	≈ 0	≈ 0	0.0932
	Case B	≈ 0	≈ 0	≈ 0	0.0812
195.5 W	Case A	≈ 0	≈ 0	≈ 0	0.0904
	Case B	≈ 0	≈ 0	≈ 0	0.0824
250 W	Case A	≈ 0	≈ 0	≈ 0	0.0964
	Case B	≈ 0	≈ 0	≈ 0	0.0931

from the table that the proposed method is more computationally efficient compared to Wave method. And Wave method requires a good initial guess for the convergence which proposed method does not require.

Wave method exploits the characteristics matching between load and PV whereas the proposed method matches the characteristics of PV without R_s and R_s with load system. Accuracy of the proposed method is depicted in Fig.4.10. From the Figure, it is observed that % errors in the estimated values of the operating point parameters are very less.

The processor, Intel(R) core(TM) i5-3210M CPU @ 2.50 GHz with 4 GB of RAM and 64-bit Windows operating system is used to run the MATLAB program to obtain the simulation results.

4.4.2 Experimental validation

For experimental validation of the results obtained using proposed algorithm, a controlled experimental setup is developed in the laboratory considering the PV modules 195.5 W (make: Topsun) loaded with three parallel-connected immersion rods (each of rating 1500 W, 230 V) with equivalent resistance (R) of 14.0383 Ω as shown in Fig. 4.11. The datasheet values of the PV module are provided in Table 4.1.

As seen in Fig. 4.11, all three immersion rods are dipped in a bucket filled with water. The

Figure 4.11: Experimental setup of PV module connected to resistive load, R = 14.0383 Ω

Table 4.5: Experimental comparison of the estimated operating point for three immersion rods of resistance 14.0383 Ω

	Estimated result	Experimental results	% error
Resistive load, $R = 14.0383\Omega$			
V_{op} (V)	23.2055	22.7	2.2269
I_{op} (A)	1.6530	1.617	2.2263
P_{op} (W)	38.3589	36.7059	4.5034

195.5 W module is operating at the irradiance of 285.7 W/m^2 and temperature of 36 °C. The comparison of the operating point obtained using the proposed method and experimentally is provided in Table 4.5. It is observed from the table that the % error is less than 5%.

4.5 Chapter summary

In this chapter, a novel methodology is introduced to determine the operating point of a PV-load system. The system is dissected into two primary components: the PV without R_s and R_s coupled with the load. Subsequent to this, explicit expressions for the series combination of R_s and various loads are derived. The results obtained using the proposed is compared with the results obtained using Wave method. Proposed approach consistently showcased, a significantly diminished computational time in comparison to Wave method. The estimations derived from the proposed algorithm are juxtaposed against empirical data from laboratory scale experiments,

revealing a % error that is consistently below 5%. This methodology is poised to significantly influence the planning, operation, and maintenance of standalone PV systems.

The preceding Chapters 2, 3, and this chapter concentrated on analyzing the performance of PV sources and their connection to loads under specific environmental conditions. However, the absence of PV parameter values at STC limits the applicability of these methods. Recognizing this, the next chapter proposes a parameter estimation technique essential for accurately simulating a PV model across diverse environmental conditions, bridging a critical methodological gap.

Chapter 5

Parameter estimation of a DDM PV module

Contents

5.1 Introduction

The solar photovoltaic (PV) has shown the great potential for the replacement fossil fuels to meet the energy demand in many countries globally especially in the area of distributed electric power generation. Appropriate modelling of PV cells is crucial for simulation, design, evaluation, control and optimisation of solar PV system [64]. The characteristics of a PV module are mainly studied by using two types of models: single diode model (SDM) and double diode model (DDM). Single diode model is simpler due to least number of parameters involved and only one exponential term in current equation. However, the DDM is more accurate than SDM due to consideration of recombination losses. The difference in accuracy is more visible at low irradiance condition. Some researchers also studies a three diode model of PV module to account for the effect of the leakage current and call the model as TDM [65]. Earlier in chapter 2, 3 and 4 the main focus was on the performance analysis of a PV source and PV source connected to load at given environmental condition. However, without the parameter values of PV at STC, it is not possible to utilize the methods provided in these earlier chapters. Therefore, parameter estimation is necessary to accurately simulate a PV model at varying environmental condition. Parameter estimation algorithms can be devided into three main category: analytical, itterative and population search based method. Analytical methods utilize extra equations, approximations, and information to estimate parameters. For example, the analytical methods in [29] use datasheet information.

Iterative algorithms, such as nonlinear least squares (NLS) [30], essentially solve the error minimization problem. In [26], a Levenberg-Marquardt (LM) based iterative method is used for parameter estimation. A pattern search-based algorithm is proposed in [31] for parameter estimation of PV modules. On the other hand, population search-based methods for parameter estimation start with many sets of randomly generated parameters and use various techniques to find the optimal set. Differential evolution algorithm is a type of population-based method [32]. Many nature inspired algorithms are reviewed in [33]. In [34,35] population based methods which utilize GA are used. However, population-based methods produce different values in each run and is not very reliable.

A separable non-linear least square search (SNLSS) is proposed in [36] to estimate the PV parameters. For a fixed value of R_s, the least square algorithm is applied to minimize the error and determine the other four linear parameters. The parameter R_s is optimized using the Nelder-Mead algorithm, which is an iterative method.

However in this chapter, a itterative parameter estimation technique is proposed which does not require any manual initialization. The proposed techique uses bisection based MPP estimation technique to get error between estimated MPP and datasheet MPP.

5.2 Derivation of equations for I_{o1}, I_{o2} and R_{sh} in terms of R_s and I_{ph}

The electrical equivalent circuit of a DDM PV module is given in Fig. 5.1. The I-V characteristic

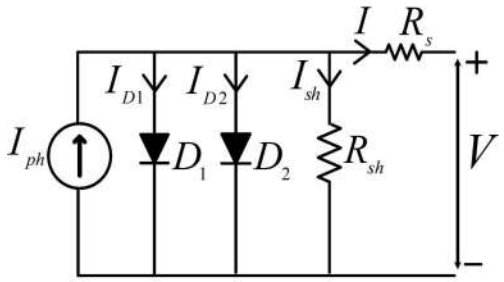

Figure 5.1: Equivalent circuit of a DDM PV module.

of a DDM PV module is expressed as follows:

$$I = I_{ph} - I_{o1}\left\{e^{\left(\frac{V+IR_s}{A_1 N_s V_t}\right)} - 1\right\} - I_{o2}\left\{e^{\left(\frac{V+IR_s}{A_2 N_s V_t}\right)} - 1\right\} - \frac{V + IR_s}{R_{sh}} \tag{5.1}$$

The maximum power point voltage, maximum power point current, open circuit voltage and short circuit current at STC are V_{MP}, I_{MP}, V_{OC} and I_{SC}, respectively. As the points (V_{MP}, I_{MP}), (V_{OC}, 0) and (0, I_{SC}) are the points on current-voltage (I-V) curve at STC, the following equations are obtained by putting these points in (5.1) for (V, I).

$$I_{MP} = I_{ph} - I_{o1}\left\{e^{\left(\frac{V_{MP}+I_{MP}R_s}{A_1 N_s V_t}\right)} - 1\right\} - I_{o2}\left\{e^{\left(\frac{V_{MP}+I_{MP}R_s}{A_2 N_s V_t}\right)} - 1\right\} - \frac{V_{MP} + I_{MP}R_s}{R_{sh}} \tag{5.2}$$

$$I_{ph} - I_{o_1}\left(e^{\frac{V_{OC}}{A_1 N_s V_t}} - 1\right) - I_{o_2}\left(e^{\frac{V_{OC}}{A_2 N_s V_t}} - 1\right) - \frac{V_{OC}}{R_{sh}} = 0 \tag{5.3}$$

$$I_{ph} - I_{o_1}\left(e^{\frac{I_{SC}R_s}{A_1 N_s V_t}} - 1\right) - I_{o_2}\left(e^{\frac{I_{SC}R_s}{A_2 N_s V_t}} - 1\right) - \frac{I_{SC}R_s}{R_{sh}} = I_{SC} \tag{5.4}$$

In (5.1), the parameters I_{ph}, I_{o1}, I_{o2}, R_s, R_{sh}, A_1, A_2, V_t and N_s have the same meaning as given in [50]. Now, using (5.3),

$$I_{o_1} = \frac{I_{ph} - I_{o_2}\left(e^{\frac{V_{OC}}{A_2 N_s V_t}} - 1\right) - \frac{V_{OC}}{R_{sh}}}{\left(e^{\frac{V_{OC}}{A_1 N_s V_t}} - 1\right)} \tag{5.5}$$

Putting I_{o1} from (5.5) in (5.4),

$$R_{sh} = \frac{I_{SC}R_s - V_{OC}\frac{\left(e^{\frac{I_{SC}R_s}{A_1 N_s V_t}} - 1\right)}{\left(e^{\frac{V_{OC}}{A_1 N_s V_t}} - 1\right)}}{I_{ph}\left(1 - \frac{\left(e^{\frac{I_{SC}R_s}{A_1 N_s V_t}} - 1\right)}{\left(e^{\frac{V_{OC}}{A_1 N_s V_t}} - 1\right)}\right) - I_{SC} + c_1} \tag{5.6}$$

where

$$c_1 = I_{o_2}\left(\frac{\left(e^{\frac{V_{OC}}{A_2 N_s V_t}} - 1\right)\left(e^{\frac{I_{SC}R_s}{A_1 N_s V_t}} - 1\right)}{\left(e^{\frac{V_{OC}}{A_1 N_s V_t}} - 1\right)} - \left(e^{\frac{I_{SC}R_s}{A_2 N_s V_t}} - 1\right)\right) \tag{5.7}$$

Now, from (5.2), (5.5), and (5.6),

$$I_{o_2} = \frac{(E - F)}{(G + H)} \tag{5.8}$$

where

$$E = \frac{I_{MP} - I_{ph} + I_{ph}\frac{\left(e^{\frac{V_{MP}+I_{MP}R_s}{A_1 N_s V_t}} - 1\right)}{\left(e^{\frac{V_{OC}}{A_1 N_s V_t}} - 1\right)}}{V_{OC}\frac{\left(e^{\frac{V_{MP}+I_{MP}R_s}{A_1 N_s V_t}} - 1\right)}{\left(e^{\frac{V_{OC}}{A_1 N_s V_t}} - 1\right)} - (V_{MP} + I_{MP}R_s)} \tag{5.9}$$

$$F = \frac{I_{ph} - I_{SC} - I_{ph}\frac{\left(e^{\frac{I_{SC}R_s}{A_1 N_s V_t}} - 1\right)}{\left(e^{\frac{V_{OC}}{A_1 N_s V_t}} - 1\right)}}{-V_{OC}\frac{\left(e^{\frac{I_{SC}R_s}{A_1 N_s V_t}} - 1\right)}{\left(e^{\frac{V_{OC}}{A_1 N_s V_t}} - 1\right)} + I_{SC}R_s} \tag{5.10}$$

$$G = \frac{\frac{\left(e^{\frac{V_{OC}}{A_2 N_s V_t}} - 1\right)\left(e^{\frac{I_{SC}R_s}{A_1 N_s V_t}} - 1\right)}{\left(e^{\frac{V_{OC}}{A_1 N_s V_t}} - 1\right)} - \left(e^{\frac{I_{SC}R_s}{A_2 N_s V_t}} - 1\right)}{I_{SC}R_s - V_{OC}\frac{\left(e^{\frac{I_{SC}R_s}{A_1 N_s V_t}} - 1\right)}{\left(e^{\frac{V_{OC}}{A_1 N_s V_t}} - 1\right)}} \tag{5.11}$$

$$H = \frac{\frac{\left(e^{\frac{V_{OC}}{A_2 N_s V_t}} - 1\right)\left(e^{\frac{V_{MP}+I_{MP}R_s}{A_1 N_s V_t}} - 1\right)}{\left(e^{\frac{V_{OC}}{A_1 N_s V_t}} - 1\right)} - \left(e^{\frac{V_{MP}+I_{MP}R_s}{A_2 N_s V_t}} - 1\right)}{V_{OC}\frac{\left(e^{\frac{V_{MP}+I_{MP}R_s}{A_1 N_s V_t}} - 1\right)}{\left(e^{\frac{V_{OC}}{A_1 N_s V_t}} - 1\right)} - (V_{MP} + I_{MP}R_s)} \tag{5.12}$$

5.3 Parameter estimation algorithm

A flowchart for the parameter estimation method is preseted in Fig. 5.2.

Steps to find the parameters of a DDM PV module are as follow:

- Update the variables V_{OC}, I_{SC}, I_{MP}, V_{MP} and N_s from the datasheet value of the PV module.
- Update A_1=1, A_2=2, V_t=0.0257 V, $miner$ = 1000 and tol=0.01.
- Initialize I_{ph}=I_{SC}.
- Increase I_{ph} as I_{ph}=I_{ph}+0.001.
- Check if I_{ph}< I_{SC}+0.5.

- Initialize R_s=0.
- Increase R_s as R_s=R_s+0.01.
- Check if $R_s < 1$.

  if true go to next step.

  otherwise go to step 4.
- Find the values of I_{o2}, R_{sh} and I_{o1} using equations (5.8), (5.6) and (5.5).
- Check if I_{o1}, I_{o2} and $R_{sh} > 0$.

  if true go to next step, otherwise goto step 7.
- Apply the bisection method to get the maximum power point voltage V_{mp}.
- Find err=abs(V_{mp}-V_{MP}).
- Check if $err < miner$

  if true go to next step.

  if false go to step 7.
- Update variables $miner = err$, $minI_{ph} = I_{ph}$, $minI_{o1} = I_{o1}$, $minI_{o2} = I_{o2}$, $minR_{sh} = R_{sh}$ and $minR_s = R_s$.
- Check if $err < tol$.

  If true go to next step.

  If false go to step 7.
- Update the estimated values of parameters to variables $I_{ph} = minI_{ph}$, $I_{o1} = minI_{o1}$, $I_{o2} = minI_{o2}$, $R_{sh} = minR_{sh}$ and $R_s = minR_s$.

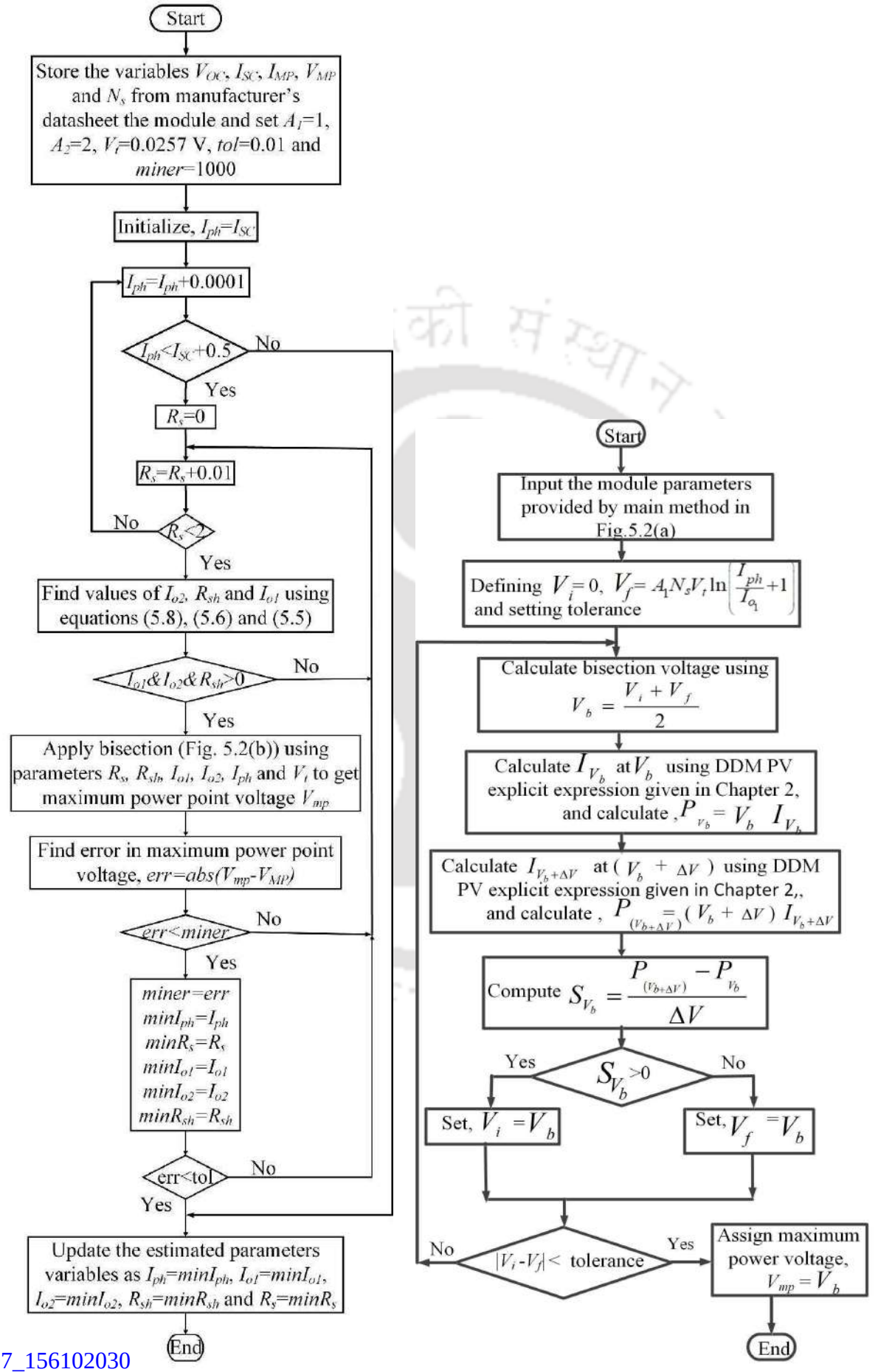

(a) Parameter estimation algorithm (b) Bisection method

Figure 5.2: Flowcharts of parameter estimation algorithm.

5.4 Results and discussion

In this section, two parameter estimation techniques LM and SNLLS [36] are compared with the proposed method. Datasheet values and estimated DDM parameters using proposed method for five different ratings of PV modules of 140, 250, 252, 335 and 545 W are given in Table 5.1 and 5.2, respectively. Computation time and RMS error of the proposed method with LM and SNLLS methods are compared. Further, experimental validation of proposed method is done. The I-V curves of DDM of a PV modules are plotted under DEC using the estimated parameters. Then, the plotted I-V curves matches with measured I-V curve provided by the manufacturer under same environmental condition. The measured data provided in the datasheet of manufacturer is generally obtained using photovoltaic module testing facility which uses flash of artificial light. Also, two bar charts are used to show the RMS error of the simulated curve with respect to (w.r.t) experimental data. Here, RMS error is calculated using following formula:
RMS $error = \sqrt{\frac{\sum_{k=1}^{N} {error_k}^2}{N}}$. where, $error_k$ is the absolute difference between the estimated current value and the experimental value of current of the k^{th} sample point on the current-voltage curve and N is total number of sample points.

Table 5.1: Datasheet values of the PV modules

Modules	I_{SC} (A)	V_{OC} (V)	V_{MP} (V)	I_{MP} (A)	N_s
545 W	13.9	49.76	41.9	13.02	72
335 W	9.49	46.5	38.2	8.77	72
252 W	7.6	44	36	7	72
250 W	8.76	37.7	30.9	8.09	60
140 W	8.30	22.2	18.10	7.73	36

Table 5.2: Estimated parameters of the PV modules

Modules	I_{ph} (A)	I_{o_1} (nA)	I_{o_2} (μA)	R_s (Ω)	R_{sh} (Ω)
545 W	13.9002	0.021590	4.8133	0.1000	7027.2
335 W	9.4902	0.074275	11.312	0.1900	9347.8
252 W	7.6002	0.23372	17.250	0.2200	8793.6
250 W	8.7601	0.13906	13.966	0.1700	16307
140 W	8.3013	0.26057	7.7939	0.1500	963.2416

The RMS error and computation time in the parameter estimation using LM, SNLLS and the

proposed methods are given in Table 5.3 for PV modules of rating 335, 252, 250, and 140 W. From the table, it is observed that RMS error and computation time using the proposed method are less than LM and SNLLS methods. In a solar plant, PV modules are continuously used, leading to changes in their parameters over time due to environmental effects. Therefore, it is important to estimate these parameters while the plant is operational to account for the changes in module characteristics. Minimizing the computational time of the parameter estimation technique would be beneficial for efficient plant operation. Thus, a comparison of computational times among different techniques is required.

Table 5.3: Comparison of different parameter estimation techniques

Modules	LM		SNLSS		Proposed	
	RMSE	Time (s)	RMSE	Time (s)	RMSE	Time (s)
140 W	3.4897×10^{-6}	0.106765	2.0031×10^{-16}	0.161220	9.7981×10^{-15}	0.080385
250 W	5.9890×10^{-6}	0.127060	1.3628×10^{-15}	0.209466	5.1288×10^{-15}	0.090075
252 W	6.8724×10^{-6}	0.122507	6.4099×10^{-16}	0.155993	3.0772×10^{-15}	0.083964
335 W	5.3614×10^{-6}	0.105862	1.0498×10^{-15}	0.162020	1.0314×10^{-14}	0.086878

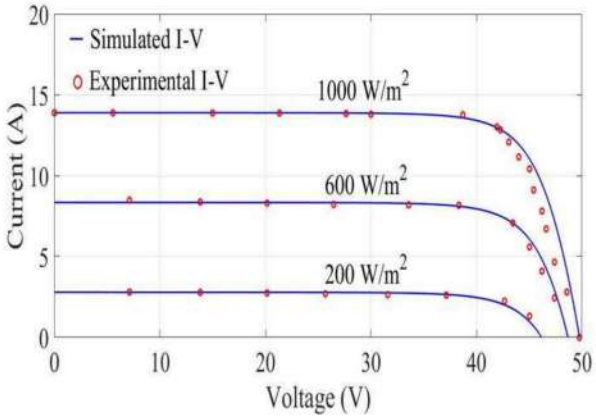

Figure 5.3: Experimental validation of proposed parameter estimation technique through I-V curves of a 545 W PV module for varying irradiance.

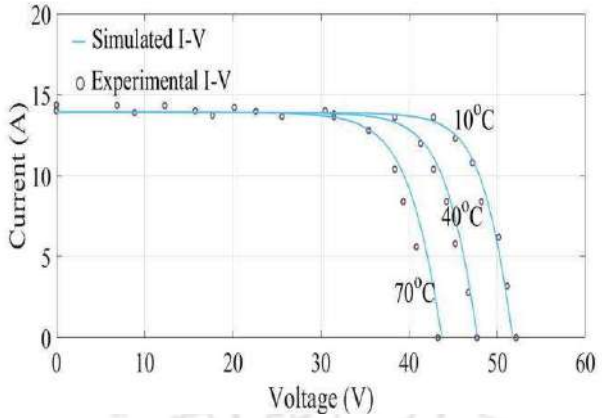

Figure 5.4: Experimental validation of proposed parameter estimation technique through I-V curves of a 545 W PV module for varying temperature.

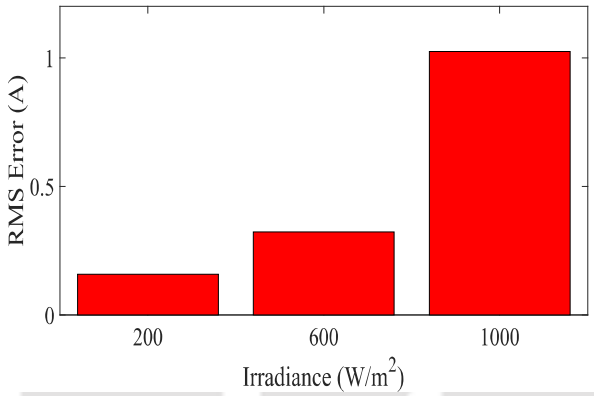

Figure 5.5: Barchart for RMSE in parameter estimation of 545 W PV module at varrying irradiances.

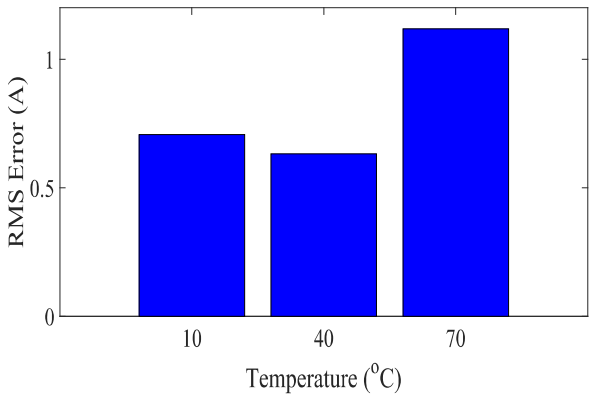

Figure 5.6: Barchart for RMSE in parameter estimation of 545 W PV module at varrying temperatures.

The I-V curves by estimated value of parameters using the proposed method and using ex-

perimental data obtained from the manufacturer's datasheet of 545 W PV module for irradiances 1000, 600 and 200 W/m^2 at a temperature of 25^{o}C are shown in Fig. 5.3. Also, the I-V curves for temperatures 10^{o}C, 40^{o}C and 70^{o}C at irradiance of 1000 W/m^2 are shown in Fig. 5.4. It is seen from the figures that the error between simulated and the experimental curve is minimal. Further, two bar charts as shown in Figs. 5.5 and 5.6 presents the RMS error in current w.r.t experimental value for varying irradiances and temperatures. It is observed from both bar charts that the RMS error under varying environmental conditions are below 1.5 A which is well within the limit. The maximum RMS error of approximately 1 A in both Figs. 5.5 and 5.6 is primarily due to errors in the I-V data provided in the manufacturer's datasheet of 545 W PV module, as well as errors during data recording for comparison.

5.5 Summary of the chapter

In this chapter, a novel and streamlined approach was introduced for the parameter estimation of the DDM of a PV module utilizing datasheet values. Expressions for three dependent parameters, based on two independent parameters, are formulated. Subsequently, a technique for parameter estimation is proposed.

Comparative analysis is conducted between the LM and SNLLS methods in terms of RMS error and computational time, juxtaposed against the proposed methodology. The findings reveal that the proposed method consistently outperformed in terms of reduced RMS error and computational time.

Furthermore, the estimated parameters of the DDM for a PV module are rigorously validated using empirical data sourced from the manufacturer's datasheet, spanning various environmental conditions. Examination of the resultant curves and bar-charts underscore that the curves, derived using the estimated parameters, exhibited a high degree of congruence with the datasheet curves.

Given its simplicity and precision, this methodology is poised to be a valuable for PV professionals.

Note: This work, "Parameter estimation of a DDM PV module," has been published in 2022 IEEE 2nd International Conference on Sustainable Energy and Future Electric Transportation (SeFeT), Hyderabad, India, 2022, pp. 1-6, doi: 10.1109/SeFeT55524.2022.9908938.

Chapter 6

Conclusion and future work

Contents

6.1 Summary of the present work

This comprehensive thesis comprises meticulous research on photovoltaic (PV) modules, focusing primarily on the development and validation of novel models and methodologies to enhance PV performance and estimation accuracy. Chapter 2 introduces and validates an explicit I-V formula for optimal power estimation under varying environmental conditions. The subsequent chapter delves into a unique model for series-parallel connected PV arrays, emphasizing rapid and accurate GMPP estimation. In Chapter 4, a novel technique is unveiled to discern the PV-load system's operating point, showcasing notable computational efficiency. Finally, Chapter 5 introduces a streamlined approach for the parameter estimation of PV modules, demonstrating superior precision and congruence with manufacturer data. Chapter 2 of this thesis introduces an explicit I-V formula for a PV module to determine its maximum power point (MPP) under different environmental conditions. The explicit I-V formula is compared with the implicit one across three distinct modules to validate its accuracy. Simulation outcomes indicate that the MPP estimation for a DDM PV module using the proposed method is both more precise and faster than five other established techniques, namely PS, Saloux, GS, NR, and LM under different environmental conditions. The results of the MPP estimation approach are further corroborated through experiments on a 200W DDM PV module. Moreover, the global maximum power point (GMPP) of a DDM PV array is deduced from the explicit I-V formula using a mathematical framework under partial shading conditions. This mathematical representation of a special case of series parallel partially shaded DDM PV array is fine-tuned to estimate GMPP using the Genetic Algorithm (GA) optimization method. The findings highlight the accuracy of the estimated GMPP when compared to both simulated and experimental GMPP values. In conclusion, the proposed explicit I-V formula, MPP estimation for uniform irradiance case and the mathematical model for a DDM PV array under partial shading conditions (PSCs) are both precise and computationally efficient.

In Chapter 3 of this thesis, a novel model is developed for a generallized case of series-parallel (S-P) connected PV arrays. Utilizing set theory, equations are formulated that describe the

dynamics of voltages and currents across strings and the entire array. These equations prove to be beneficial for I–V curve representation and GMPP estimation under PSC. A mathematical expression, influenced by the properties of the local maximum power point (LMPP), is also derived to aid the iterative process towards the GMPP.

One notable aspect of this approach is the elimination of non-potential sections from the P–V curve. This strategy enhances the speed of GMPP estimation, which could be particularly beneficial for large PV arrays. When compared to established methods such as those by [1], [50], and the Particle Swarm Optimization (PSO) [54] technique, this method exhibits a more efficient computational performance and improved accuracy.

Experimental validations, conducted using real-world PV modules, provides further support for the method's robustness and accuracy. The findings from this research suggest that the method might offer a reliable and efficient way to estimate GMPP. It is hoped that this approach could be a helpful tool for PV professionals, potentially aiding in the pursuit of optimal energy output from PV arrays.

In Chapter 4 of this thesis, a novel methodology is introduced to determine the operating point of a PV-load system. The system is dissected into two primary components: the PV without R_s and R_s coupled with the load. Subsequent to this, explicit expressions for the series combination of R_s and various loads are derived.

This novel approach is compared with another method. Proposed approach consistently showcases a significantly diminished computational time in comparison to other method. The estimations derived from the proposed algorithm are juxtaposed against empirical data from laboratory experiments, revealing a % error that is consistently below 5%. This methodology is poised to significantly influence the planning, operation, and maintenance of standalone PV systems.

In Chapter 5 of this thesis, a novel and streamlined approach is introduced for the parameter estimation of the DDM of a PV module utilizing datasheet values. Expressions for three dependent parameters, based on two independent parameters, are formulated. Subsequently, a technique for parameter estimation is proposed.

Comparative analysis is conducted between the LM and SNLLS methods in terms of RMS error and computational time, juxtaposed against the proposed methodology. The findings reveal that the proposed method consistently outperformed in terms of reduced RMS error and computational time.

Furthermore, the estimated parameters of the DDM for a PV module are rigorously validated using empirical data sourced from the manufacturer's datasheet, spanning various environmental conditions. Examination of the resultant curves and bar-charts underscored that the curves, derived using the estimated parameters, exhibits a high degree of congruence with the datasheet curves.

Given its simplicity and precision, this methodology is poised to be a valuable for PV professionals.

6.2 Future work suggestions

- Investigate various explicit current expressions as functions of voltage considering higher order polynomial expression of current.
- Enhancement of the computational efficiency of MPP estimation of a PV system under uniform and PSC by using the modified ITM.
- Formulate an explicit expression for GMPP specifically designed for the special case of series parallel partially shaded PV arrays.
- Development of an efficient general algorithm for estimation of GMPP of a series-parallel partially shaded PV array.
- Development of a control algorithm tailored to optimize the combination of load and battery connected to PV source under uniform and partial shading conditions.
- Development of a robust and efficient MPPT algorithm of a PV array under PSCs.

Chapter 7

Publications

7.1 Publications

7.1.1 Journal Papers

- **Shashank Kumar**, Himanshu Sekhar Sahu and Sisir Kumar Nayak, "Estimation of MPP of a Double Diode Model PV Module From Explicit I–V Characteristic," in *IEEE Transactions on Industrial Electronics*, vol. 66, no. 9, pp. 7032-7042, Sept. 2019, doi: 10.1109/TIE.2018.2877116. [Chapter 2]

- **Shashank Kumar**, Sisir Kumar Nayak, Himanshu Sekhar Sahu, "A novel GMPP estimation technique for series parallel connected partially shaded PV array," in *Solar Compass*, Volume 7, 2023, 100049, ISSN 2772-9400, DOI: 10.1016/j.solcom.2023.100049, ScienceDirect. [Chapter 3]

- Shivam Tripathi, Himanshu Sekhar Sahu, **Shashank Kumar**, Sisir Kumar Nayak and Mahesh Kumar Mishra, "Maximum Energy Harvest From a TCT Connected PV Array Under Nonhomogeneous Irradiation Conditions," in *IEEE Journal of Emerging and Selected Topics in Power Electronics*, vol. 11, no. 5, pp. 5441-5453, Oct. 2023, doi: 10.1109/JESTPE.2023.3307734

- Shivam Tripathi, Sarthak Chopra, Himanshu Sekhar Sahu, Mahesh Kumar Mishra, **Shashank Kumar** and Sisir Kumar Nayak, "A Novel MPP Estimation Technique for DDM PV Array Under Different Solar Irradiance Conditions," in *IEEE Transactions on Sustainable*

Energy, vol. 14, no. 4, pp. 2177-2191, Oct. 2023, doi: 10.1109/TSTE.2023.3294809

- Papul Changmai, **Shashank Kumar**, Sisir Kumar Nayak and Sanjeev Kumar Metya, "Maximum Power Estimation of Total Cross-Tied Connected PV Cells in Different Shading Conditions for High Current Application," in *IEEE Journal of Emerging and Selected Topics in Power Electronics*, vol. 10, no. 4, pp. 3883-3894, Aug. 2022, doi: 10.1109/JESTPE.2021.3105808

- Himanshu Sekhar Sahu, Mahesh Kumar Mishra, **Shashank Kumar** and Sisir Kumar Nayak, "A Novel Approach for Direct MPP Estimation of a PV Module Under Different Irradiation Conditions," in *IEEE Transactions on Energy Conversion*, vol. 36, no. 4, pp. 3127-3136, Dec. 2021, doi: 10.1109/TEC.2021.3072453

7.1.2 Conference Papers

- **Shashank Kumar**, Himanshu Sekhar Sahu, Sisir Kumar Nayak and Papul Changmai, "Parameter Estimation of a DDM PV Module Using a Simplistic Novel Method," in *2022 IEEE 2nd International Conference on Sustainable Energy and Future Electric Transportation (SeFeT)*, Hyderabad, India, 2022, pp. 1-6, doi: 10.1109/SeFeT55524.2022.9908938. [Chapter 5]

- Himanshu Sekhar Sahu, **Shashank Kumar**, Papul Changmai and Sisir Kumar Nayak, "Peak Power Extraction from a PV System for Various DC and AC Loads," *2024 Third International Conference on Power, Control and Computing Technologies (ICPC2T)*, Raipur, India, 2024, pp. 259-264, doi: 10.1109/ICPC2T60072.2024.10475038

- Himanshu Sekhar Sahu, **Shashank Kumar**, and Sisir Kumar Nayak, "Maximum Power Point Estimation of a PV Array by Using Improve Bisection Method," *2018 IEEE Transportation Electrification Conference and Expo, Asia-Pacific (ITEC Asia-Pacific)*, Bangkok, Thailand, 2018, pp. 1-5, doi: 10.1109/ITEC-AP.2018.8432595

Bibliography

[1] G. N. Psarros, E. I. Batzelis, and S. A. Papathanassiou, "Partial shading analysis of multistring PV arrays and derivation of simplified MPP expressions," *IEEE Trans. Sustain. Energy*, vol. 6, no. 2, pp. 499–508, April 2015.

[2] K. Ishaque, Z. Salam, and A. Syafaruddin, "A comprehensive MATLAB simulink PV system simulator with partial shading capability based on two-diode model," *Sol. Energ.*, vol. 85, no. 9, pp. 2217 – 2227, Sept. 2011.

[3] L. H. I. Lim, Z. Ye, J. Ye, D. Yang, and H. Du, "A linear identification of diode models from single I-V characteristics of PV panels," *IEEE Trans. Ind. Electron.*, vol. 62, no. 7, pp. 4181–4193, July 2015.

[4] D. Chan and J. Phang, "Analytical methods for the extraction of solar-cell single- and double-diode model parameters from I-V characteristics," *IEEE Trans. Electron Devices,*, vol. 34, no. 2, pp. 286–293, Feb 1987.

[5] J. P. Charles, I. M. Alaoui, G. Bordure, and P. Mialhe, "A critical study of the effectiveness of the single and double exponential models for I-V characterization of solar cells," *Solid-State Electron.*, vol. 28, no. 8, pp. 807 – 820, 1985.

[6] S. xian Lun, S. Wang, G. hong Yang, and T. ting Guo, "A new explicit double-diode modeling method based on Lambert W-function for photovoltaic arrays," *Sol. Energ.*, vol. 116, pp. 69 – 82, June 2015.

[7] X. Gao, Y. Cui, J. Hu, G. Xu, and Y. Yu, "Lambert W-function based exact representation for double diode model of solar cells: Comparison on fitness and parameter extraction," *Energ. Convers. Manage.*, vol. 127, pp. 443–460, Nov. 2016.

[8] M. Masoum, H. Dehbonei, and E. Fuchs, "Theoretical and experimental analyses of photovoltaic systems with voltage and current-based maximum power-point tracking," *IEEE Trans. Energy Convers.*, vol. 17, no. 4, pp. 514–522, Dec 2002.

[9] H. S. Sahu and S. K. Nayak, "Estimation of maximum power point of a double diode model photovoltaic module," *IET Power Electron.*, vol. 10, no. 6, pp. 667–675, 2017.

[10] S. Moballegh and J. Jiang, "Modeling, prediction, and experimental validations of power peaks of PV arrays under partial shading conditions," *IEEE Trans. Sustain. Energy*, vol. 5, no. 1, pp. 293–300, Jan 2014.

[11] J. D. Bastidas-Rodriguez, J. M. Cruz-Duarte, and R. Correa, "Mismatched series-parallel photovoltaic generator modeling: An implicit current-voltage approach," *IEEE J. Photovolt.*, vol. 9, no. 3, pp. 768–774, May 2019.

[12] A. Bernardini, P. Maffezzoni, L. Daniel, and A. Sarti, "Wave-based analysis of large nonlinear photovoltaic arrays," *IEEE Trans. Circuits Syst. I, Reg. Papers*, vol. 65, no. 4, pp. 1363–1376, April 2018.

[13] A. Xenophontos and A. M. Bazzi, "Model-based maximum power curves of solar photovoltaic panels under partial shading conditions," *IEEE J. Photovolt.*, vol. 8, no. 1, pp. 233–238, Jan 2018.

[14] M. Arjun, V. V. Ramana, R. Viswadev, and B. Venkatesaperumal, "An iterative analytical solution for calculating maximum power point in photovoltaic systems under partial shading conditions," *IEEE Trans. Circuits and Syst. II, Exp. Briefs*, vol. 66, no. 6, pp. 973–977, June 2019.

[15] E. I. Batzelis, G. E. Kampitsis, S. A. Papathanassiou, and S. N. Manias, "Direct MPP calculation in terms of the single-diode PV model parameters," *IEEE Trans. Energy Convers.*, vol. 30, no. 1, pp. 226–236, March 2015.

[16] Z. Mao, Z. Sunan, M. Peng, S. Yanlong, and Z. Weiping, "Macro-model of PV module and its application for partial shading analysis," *IET Renew. Power Gener.*, vol. 12, no. 15, pp. 1748–1754, 2018.

[17] J. Ma, X. Pan, K. L. Man, X. Li, H. Wen, and T. On Ting, "Detection and assessment of partial shading scenarios on photovoltaic strings," *IEEE Trans. Ind. Appl.*, vol. 54, no. 6, pp. 6279–6289, Nov 2018.

[18] Z. Mao, Z. Sunan, M. Peng, S. Yanlong, and Z. Weiping, "Modelling of PV module and its application for partial shading analysis - part II: partial shading analysis and simulation approach of large-scale PV array," *J. Eng.*, vol. 2017, no. 13, pp. 1316–1320, 2017.

[19] J. Ma, H. Jiang, Z. Bi, K. Huang, X. Li, and H. Wen, "Maximum power point estimation for photovoltaic strings subjected to partial shading scenarios," *IEEE Trans. Ind. Appl.*, vol. 55, no. 2, pp. 1890–1902, March 2019.

[20] M. Aquib, S. Jain, and S. Ghosh, "A technique for tracking the global peak of PV arrays during partially shaded conditions using the detection of current source and voltage source regions of I–V curves," *IEEE J. Emerg. Selec. Topics Ind. Electron.*, vol. 3, no. 4, pp. 1096–1105, 2022.

[21] S. Xu, Y. Gao, G. Zhou, and G. Mao, "A global maximum power point tracking algorithm for photovoltaic systems under partially shaded conditions using modified maximum power trapezium method," *IEEE Trans. Ind. Electron.*, vol. 68, no. 1, pp. 370–380, 2021.

[22] M. A. Ghasemi, H. M. Foroushani, and F. Blaabjerg, "Marginal power-based maximum power point tracking control of photovoltaic system under partially shaded condition," *IEEE Trans. Power Electron.*, vol. 35, no. 6, pp. 5860–5872, 2020.

[23] T. Yamamoto, "Historical developments in convergence analysis for newton's and newton-like methods," *J. Comput. Appl. Math.*, vol. 124, no. 1, pp. 1–23, Dec. 2000.

[24] M. Uoya and H. Koizumi, "A calculation method of photovoltaic array's operating point for MPPT evaluation based on one-dimensional newton–raphson method," *IEEE Trans. Ind. Appl.*, vol. 51, no. 1, pp. 567–575, Jan./Feb. 2015.

[25] K. Levenberg, "A method for the solution of certain non-linear problems in least squares," *Q. Appl. Math.*, vol. 2, no. 2, pp. 164–168, 1944.

[26] H. S. Sahu and S. K. Nayak, "Numerical approach to estimate the maximum power point of a photovoltaic array," *IET Gener. Transm. Dis.*, vol. 10, no. 11, pp. 2670–2680, Aug. 2016.

[27] B. Alajmi, K. Ahmed, S. Finney, and B. Williams, "Fuzzy-logic-control approach of a modified hill-climbing method for maximum power point in microgrid standalone photovoltaic system," *IEEE Trans. Power Electron.*, vol. 26, no. 4, pp. 1022–1030, April 2011.

[28] Syafaruddin, E. Karatepe, and T. Hiyama, "Artificial neural network-polar coordinated fuzzy controller based maximum power point tracking control under partially shaded conditions," *IET Renew. Power Gener.*, vol. 3, no. 2, pp. 239–253, June 2009.

[29] H. Ibrahim and N. Anani, "Evaluation of analytical methods for parameter extraction of PV modules," *Energy Procedia*, vol. 134, pp. 69–78, 2017, sustainability in Energy and Buildings 2017: Proceedings of the Ninth KES International Conference, Chania, Greece, 5-7 July 2017. [Online]. Available: https://www.sciencedirect.com/science/article/pii/S1876610217347355

[30] B. K. Nayak, A. Mohapatra, and K. B. Mohanty, "Parameters estimation of photovoltaic module using nonlinear least square algorithm: A comparative study," Dec. 2013, pp. 1–6.

[31] M. AlHajri, K. E. Naggar, M. AlRashidi, and A. Al-Othman, "Optimal extraction of solar cell parameters using pattern search," *Renew. Energy*, vol. 44, pp. 238 – 245, Aug. 2012.

[32] C. Chellaswamy and R. Ramesh, "Parameter extraction of solar cell models based on adaptive differential evolution algorithm," *Renew. Energ.*, vol. 97, pp. 823–837, 2016. [Online]. Available: https://www.sciencedirect.com/science/article/pii/S0960148116305456

[33] I. F. Jr., X. Yang, I. Fister, J. Brest, and D. Fister, "A brief review of nature-inspired algorithms for optimization," *CoRR*, vol. abs/1307.4186, 2013. [Online]. Available: http://arxiv.org/abs/1307.4186

[34] Y. Zhang, S. Lyden, B. Len de la Barra, and M. Haque, "A genetic algorithm approach to parameter estimation for PV modules," in *2016 IEEE Power and Energy Society General Meeting (PESGM)*, 2016, pp. 1–5.

[35] X. Lingyun, S. Lefei, H. Wei, and J. Cong, "Solar cells parameter extraction using a hybrid genetic algorithm," in *2011 Third International Conference on Measuring Technology and Mechatronics Automation*, vol. 3, 2011, pp. 306–309.

[36] J. Xu, "Separable nonlinear least squares search of parameter values in photovoltaic models," *IEEE J. Photovolt.*, pp. 1–9, 2021.

[37] H. S. Sahu, S. K. Nayak, and S. Mishra, "Maximizing the power generation of a partially shaded PV array," *IEEE J. Emerg. Sel. Topics Power Electron.*, vol. 4, no. 2, pp. 626–637, June 2016.

[38] E. Saloux, A. Teyssedou, and M. Sorin, "Explicit model of photovoltaic panels to determine voltages and currents at the maximum power point," *Sol. Energ.*, vol. 85, no. 5, pp. 713 – 722, May 2011.

[39] F. Ghani, M. Duke, and J. Carson, "Numerical calculation of series and shunt resistances and diode quality factor of a photovoltaic cell using the Lambert W-function," *Sol. Energ.*, vol. 91, pp. 422 – 431, 2013. [Online]. Available: http://www.sciencedirect.com/science/article/pii/S0038092X12003295

[40] G. Araujo, E. Sanchez, and M. Martf, "Determination of the two-exponential solar cell equation parameters from empirical data," *Sol. Cells*, vol. 5, no. 2, pp. 199 – 204, 1982.

[41] A. Hovinen, "Fitting of the solar cell I-V curve to the two diode model," *Physica Scripta*, vol. vol. 54, no. T54, pp. 175–176, 1994.

[42] T. Esram and P. Chapman, "Comparison of photovoltaic array maximum power point tracking techniques," *IEEE Trans. Energy Convers.*, vol. 22, no. 2, pp. 439–449, June 2007.

[43] D. Sera, R. Teodorescu, J. Hantschel, and M. Knoll, "Optimized maximum power point tracker for fast-changing environmental conditions," *IEEE Trans. Ind. Electron.*, vol. 55, no. 7, pp. 2629–2637, July 2008.

[44] Y. C. Kuo, T. J. Liang, and J. F. Chen, "Novel maximum-power-point-tracking controller for photovoltaic energy conversion system," *IEEE Trans. Ind. Electron.*, vol. 48, no. 3, pp. 594–601, Jun 2001.

[45] V. Salas, A. Barrado, Lazaro, and A. E. Olias, "Review of the maximum power point tracking algorithms for stand-alone photovoltaic systems," *Sol. Energy Material. Sol. Cells*, vol. 90, pp. 1555 – 1578, 2006.

[46] S. Tripathi, S. Chopra, H. S. Sahu, M. K. Mishra, S. Kumar, and S. K. Nayak, "A novel MPP estimation technique for DDM PV array under different solar irradiance conditions," *IEEE Trans. Sustain. Energy*, vol. 14, no. 4, pp. 2177–2191, 2023.

[47] A. Chatterjee, A. Keyhani, and D. Kapoor, "Identification of photovoltaic source models," *IEEE Trans. Energy Convers.*, vol. 26, no. 3, pp. 883–889, Sept 2011.

[48] D. M. Chapin, C. S. Fuller, and G. L. Pearson, "A new silicon p-n junction photocell for converting solar radiation into electrical power," *J. Appl. Phys.*, vol. 25, no. 5, pp. 676–677, May 1954.

[49] H. S. Sahu, M. K. Mishra, S. Kumar, and S. Kumar Nayak, "A novel approach for direct MPP estimation of a PV module under different irradiation conditions," *IEEE Trans. Energy Convers.*, vol. 36, no. 4, pp. 3127–3136, 2021.

[50] S. Kumar, H. S. Sahu, and S. K. Nayak, "Estimation of MPP of a double diode model PV module from explicit I-V characteristic," *IEEE Trans. Ind. Electron.*, vol. 66, no. 9, pp. 7032–7042, Sep. 2019.

[51] H. Patel and V. Agarwal, "MATLAB-based modeling to study the effects of partial shading on PV array characteristics," *IEEE Trans. Energy Conver.*, vol. 23, no. 1, pp. 302–310, 2008.

[52] G. Petrone and C. Ramos-Paja, "Modeling of photovoltaic fields in mismatched conditions for energy yield evaluations," *Electric Power Systems Research*, vol. 81, no. 4, pp. 1003–1013, 2011. [Online]. Available: https://www.sciencedirect.com/science/article/pii/S0378779610003317

[53] X. Qing, H. Sun, X. Feng, and C. Y. Chung, "Submodule-based modeling and simulation of a series-parallel photovoltaic array under mismatch conditions," *IEEE J. Photovolt.*, vol. 7, no. 6, pp. 1731–1739, 2017.

[54] J. Kennedy and R. Eberhart, "Particle swarm optimization," in *Proceedings of ICNN'95 - International Conference on Neural Networks*, vol. 4, 1995, pp. 1942–1948 vol.4.

[55] I. Pervez, I. Shams, S. Mekhilef, A. Sarwar, M. Tariq, and B. Alamri, "Most valuable player algorithm based maximum power point tracking for a partially shaded PV generation system," *IEEE Trans. Sustain. Energy*, vol. 12, no. 4, pp. 1876–1890, 2021.

[56] E. I. Batzelis, I. A. Routsolias, and S. A. Papathanassiou, "An explicit PV string model based on the Lambert W function and simplified MPP expressions for operation under partial shading," *IEEE Trans. Sustain. Energy*, vol. 5, no. 1, pp. 301–312, 2014.

[57] R. M. Corless, G. H. Gonnet, D. E. G. Hare, D. J. Jeffrey, and D. E. Knuth, "On the LambertW function," *Adv. Comput. Math.*, vol. 5, no. 1, pp. 329–359, Nov. 1996.

[58] A. Sarti and G. De Sanctis, "Systematic methods for the implementation of nonlinear wave-digital structures," *IEEE Trans. Circuits Syst. I: Regular Papers*, vol. 56, no. 2, pp. 460–472, Feb. 2009.

[59] A. Bernardini, K. J. Werner, A. Sarti, and J. O. Smith, III, "Modeling nonlinear wave digital elements using the Lambert function," *IEEE Trans. Circuits Syst. I: Regular Papers*, vol. 63, no. 8, pp. 1231–1242, Aug. 2016.

[60] T. Schwerdtfeger and A. Kummert, "Newton's method for modularity-preserving multidimensional wave digital filters," in *2015 IEEE 9th Int. Workshop on Multidimensional (nD) Syst. (nDS)*, Sep. 2015, pp. 1–6.

[61] A. Bernardini, K. J. Werner, A. Sarti, and J. O. Smith, "Multi-port nonlinearities in wave digital structures," in *2015 Int. Symp. Signals, Circuits Syst. (ISSCS)*, Jul. 2015, pp. 1–4.

[62] A. Bernardini and A. Sarti, "Dynamic adaptation of instantaneous nonlinear bipoles in wave digital networks," in *2016 24th Eur. Signal Process. Conf. (EUSIPCO)*, Aug. 2016, pp. 1038–1042.

[63] L. Lombardi, P. Belforte, and G. Antonini, "Digital wave simulation of quasi-static partial element equivalent circuit method," *IEEE Trans. Electromagn. Compat.*, vol. 59, no. 2, pp. 429–438, Apr. 2017.

[64] A. R. Jordehi, "Parameter estimation of solar photovoltaic (PV) cells: A review," *Renewable and Sustainable Energy Reviews*, vol. 61, pp. 354–371, 2016. [Online]. Available: https://www.sciencedirect.com/science/article/pii/S1364032116300016

[65] S. A. Mahmoud, M. M. Alsari, E. I. Reda, and R. M. Alhammadi, "Matlab modeling and simulation of photovoltaic modules," in *2012 IEEE 55th International Midwest Symposium on Circuits and Systems (MWSCAS)*, 2012, pp. 786–789.